2017

Exosomes From The Tumor Microenvironment Promote Breast Cancer Progression And Therapy Resistance Through Unshielded Non-Coding Rna

Barzin Y. Nabet
University of Pennsylvania, barzin.nabet@gmail.com

Exosomes From The Tumor Microenvironment Promote Breast Cancer Progression And Therapy Resistance Through Unshielded Non-Coding Rna

Abstract
Breast cancer is the most common cancer type amongst women in the United States and will account for approximately 7% of all cancer-related deaths each year. For most breast cancer patients, conventional genotoxic therapy is the standard of the care. Unfortunately, as breast cancer progresses it becomes treatment resistant and incurable. Therefore, understanding mechanisms of treatment response and resistance are of paramount importance. Stromal communication with cancer cells is a major determinant of progression and treatment response. We show that stromal and breast cancer (BrCa) cells utilize paracrine and juxtacrine signaling to drive progression and conventional therapy resistance. Upon heterotypic interaction, exosomes are unidirectionally transferred from stromal to breast cancer cells. Breast cancer cells stimulate stromal cell upregulation of RNA polymerase III through activation of stromal NOTCH1 and MYC. This results in a subsequent increase in stromal 5'triphosphate RN7SL1, an SRP RNA, in exosomes. Unlike cytoplasmic RN7SL1 that is shielded by RNA binding proteins (RBPs), RN7SL1 in exosomes produced after breast cancer cell interaction lack RBPs like SRP9 and SRP14. Consequently, unshielded stromal RN7SL1 in exosomes, which is also found in cancer patients, is transferred to breast cancer cells to stimulate the pattern recognition receptor RIG-I and activate STAT1-dependent anti-viral signaling.

In parallel, stromal cells also activate NOTCH3 on breast cancer cells. The paracrine anti-viral and juxtacrine NOTCH3 pathways converge as STAT1 facilitates transcriptional responses to NOTCH3 and expands therapy resistant tumor-initiating cells. Primary human and mouse breast cancer analysis support the role of anti-viral and NOTCH3 pathway crosstalk in maximal activation of NOTCH signaling and stromal-mediated resistance. Stromal-mediated therapy resistance can be overcome by combination of conventional therapy with γ-secretase inhibitors. Thus, RBPs shield endogenous POL3-driven RNA from RIG-I, a process circumvented when breast cancer cells coerce stromal cells to propagate anti-viral signaling through exosomes. Anti-viral and NOTCH3 signaling then converge to enhance tumor growth, metastasis, and therapy resistance.

Degree Type
Dissertation

Degree Name
Doctor of Philosophy (PhD)

Graduate Group
Cell & Molecular Biology

First Advisor
Andy J. Minn

Keywords
breast cancer, exosomes, non-coding RNA, stroma, tumor microenvironment, unshielded RNA

Subject Categories
Cell Biology | Molecular Biology | Oncology

EXOSOMES FROM THE TUMOR MICROENVIRONMENT PROMOTE BREAST CANCER PROGRESSION AND THERAPY RESISTANCE THROUGH UNSHIELDED NON-CODING RNA

Barzin Y. Nabet

A DISSERTATION

in

Cell and Molecular Biology

Presented to the Faculties of the University of Pennsylvania

in

Partial Fulfillment of the Requirements for the

Degree of Doctor of Philosophy

2017

Supervisor of Dissertation

_____

Andy J. Minn, M.D., Ph.D., Assistant Professor of Radiation Oncology

Graduate Group Chairperson

_____

Daniel S. Kessler, Ph.D., Associate Professor of Cell and Developmental Biology

Dissertation Committee

Eric S. Witze, Ph.D., Assistant Professor, Department Cancer Biology

Roger A. Greenberg, M.D., Ph.D., Associate Professor, Department of Cancer Biology

Ellen Puré, Ph.D., Professor and Chair, Department of Biomedical Sciences, School of Veterinary Medicine

Brian D. Gregory, Ph.D., Associate Professor, Department of Biology

EXOSOMES FROM THE TUMOR MICROENVIRONMENT PROMOTE BREAST CANCER PROGRESSION AND THERAPY RESISTANCE THROUGH UNSHIELDED NON-CODING RNA

ACKNOWLEDGEMENT

I would like to thank my advisor Andy Minn for his fantastic mentorship and support throughout my thesis work. I would also like to thank the other members of the laboratory for their technical assistance, feedback, hard work, and friendship. I would like specifically thank Tony Wu, Bihui Xu, Yu Qiu, and Taewon Yoon for their contributions to the work presented here, it would not have been possible without them. I would like to further thank my thesis committee (Eric Witze, Roger Greenberg, Ellen Puré, and Brian Gregory), their feedback and mentorship have been invaluable. I would also like to thank Sandra Ryeom for her advice and suggestions, as well as members of the broader AFCRI and UPENN community.

I would especially like to thank my family. To my mother, Zohreh, my father, Bahram, my brothers, Behnam and Bardia, and my sister-in-law, Suzanne, for being the smartest, hardest working, and most supportive people I know. I would also like to thank my fiancée, Amber, for her support, virology knowledge, and friendship.

ABSTRACT

EXOSOMES FROM THE TUMOR MICROENVIRONMENT PROMOTE BREAST CANCER PROGRESSION AND THERAPY RESISTANCE THROUGH UNSHIELDED NON-CODING RNA

Barzin Y. Nabet

Andy J. Minn

Breast cancer is the most common cancer type amongst women in the United States and will account for approximately 7% of all cancer-related deaths each year. For most breast cancer patients, conventional genotoxic therapy is the standard of the care. Unfortunately, as breast cancer progresses it becomes treatment resistant and incurable. Therefore, understanding mechanisms of treatment response and resistance are of paramount importance. Stromal communication with cancer cells is a major determinant of progression and treatment response. We show that stromal and breast cancer (BrCa) cells utilize paracrine and juxtacrine signaling to drive progression and conventional therapy resistance. Upon heterotypic interaction, exosomes are unidirectionally transferred from stromal to breast cancer cells. Breast cancer cells stimulate stromal cell upregulation of RNA polymerase III through activation of stromal NOTCH1 and MYC. This results in a subsequent increase in stromal 5'triphosphate RN7SL1, an SRP RNA, in exosomes. Unlike cytoplasmic RN7SL1 that is shielded by RNA binding proteins (RBPs), RN7SL1 in exosomes produced after breast cancer cell interaction lack RBPs like SRP9 and SRP14. Consequently, unshielded stromal RN7SL1 in exosomes, which is also found in cancer patients, is transferred to breast cancer cells to stimulate the pattern recognition receptor RIG-I and activate STAT1-dependent anti-viral signaling.

In parallel, stromal cells also activate NOTCH3 on breast cancer cells. The paracrine anti-viral and juxtacrine NOTCH3 pathways converge as STAT1 facilitates transcriptional responses to NOTCH3 and expands therapy resistant tumor-initiating cells. Primary human and mouse breast cancer analysis support the role of anti-viral and NOTCH3 pathway crosstalk in maximal activation of NOTCH signaling and stromal-mediated resistance. Stromal-mediated therapy resistance can be overcome by combination of conventional therapy with γ-secretase inhibitors. Thus, RBPs shield endogenous POL3-driven RNA from RIG-I, a process circumvented when breast cancer cells coerce stromal cells to propagate anti-viral signaling through exosomes. Anti-viral and NOTCH3 signaling then converge to enhance tumor growth, metastasis, and therapy resistance.

TABLE OF CONTENTS

LIST OF TABLES

LIST OF FIGURES

CHAPTER 1: INTRODUCTION

Breast Cancer is the Leading Cause of Female Cancer-Related Deaths

Cancer is a significant global public health problem and is the leading cause of death for adults aged 40 to 79[1]. As populations age, it is increasingly important to understand mechanisms of cancer treatment resistance and develop novel tools to meet these challenges. In the United States, breast cancer is the most common cancer type amongst women and will account for approximately of 15% of all new cancer cases and 7% of all cancer-related deaths each year. One in eight women will be diagnosed with breast cancer in her lifetime, meaning over three million women will be living with breast cancer each year. Advances in the implementation of screening technologies has resulted in earlier detection of disease; thus, relative survival rates for breast cancer are high for early stage disease. However, advanced breast cancer can be treatment resistant and incurable[2]. Conventional therapies are the current standards of care for the large majority of breast cancers[3].

Breast cancer is classified into three heterogeneous subtypes: hormone receptor (HR) positive, epidermal growth factor (HER2) positive, and triple negative breast cancer (TNBC), which lacks estrogen receptor (ER), progesterone receptor (PR), and HER2 expression. These subtypes currently form the basis for diagnosing and treating the disease[4]. Targeted therapies have allowed for incremental advances in the treatment of HR and HER2 positive breast cancers. In the case of ER positive breast cancers, adjuvant therapies targeting either ER itself, or effector pathways such as mTOR and CDK4/6 have demonstrated significant advances in treatment[5–7]. For HER2 positive disease, a monoclonal antibody approach has resulted in significant improvements in patient survival[8,9]. Unfortunately, the majority of patients treated with these targeted therapies will develop resistance. Basal-like and TNBC are the most heterogeneous subtype of breast

cancer with the highest rate of relapse and shortest overall survival[4]. Further, no targeted therapy has been approved for its treatment and conventional treatments remain the only viable options. Therefore, elucidation of conventional therapy resistance mechanisms in TNBC and biomarkers to classify this heterogeneous disease is of chief importance.

The Tumor Microenvironment is a Major Determinant of Cancer Progression and Treatment Resistance

The tumor microenvironment is an active participant of all stages of cancer initiation and progression. All hallmarks of cancer such as sustaining proliferative signals, evading growth suppression, avoiding immune recognition, activation of the invasion and metastatic cascades, resisting cell death, inducing angiogenesis, and deregulation of cellular energetics are directly and indirectly influenced by the tumor microenvironment[10]. Further, the tumor microenvironment is being increasingly appreciated to participate in therapy resistance. For example, conventional chemo- and radiation therapy induce stromal cells to increase production of canonical Wnt ligands. These Wnt ligands can then signal in a paracrine fashion to cancer cells to promote their survival and ultimate disease progression[11]. Similar resistance mechanisms have been identified in response to targeted therapies. For example, tumor and stromal production of distinct growth factors that bypass the initial target have been demonstrated to overcome initial sensitivity to inhibitors targeting a wide range of receptor tyrosine kinases[12–14]. In total, the tumor microenvironment can amplify critical oncogenic pathways in cancer cells to promote tumor progression, metastasis, and resistance[15]. Thus, it is imperative to account for stromal contribution to therapy resistance in the design of novel and combinatorial strategies to target tumors.

The tumor microenvironment is a complex ecosystem of several cell types. A dominant component of the cancer microenvironment are fibroblasts, known as cancer-

associated fibroblasts (CAFs)[16]. Fibroblasts are well-suited to actively supporting cancer cells due to their resistance to stress, plasticity, and function in wound healing and fibrosis. In the context of wound healing, fibroblasts function in concert with immune cells to implement an inflammatory response to promote angiogenesis and deposition of extracellular matrix (ECM)[17]. Should these insults be prolonged, this repair response may continue unabated and result in tissue fibrosis. The role of fibroblasts in these processes is remarkably similar in the initiation and progression of cancer. In cancer, fibroblasts can be tumor-promoting as well as tumor-restrictive. Fibroblasts can promote tumorigenesis by altering the microenvironmental secretome[18,19]. The CAF secretome can mediate immune reprogramming to suppress immune activation, sustain fibroblast activation, and directly engage cancer cells sustain their proliferation and enhance their invasiveness. Moreover, CAFs promote invasiveness of cancer cells by producing matrix metalloproteinases that reshape the ECM of the tumor microenvironment[20]. The tumor-restrictive properties of fibroblasts are less understood, but they may function by reducing hypoxia and modulating the innate and adaptive immune system[21,22]. Moreover, fibroblasts critically influence cancer therapy response and resistance. CAFs can alter therapy response by directly altering cancer cell-ECM interactions, stromal cell-ECM interactions, cytokine and chemokine release, enhancement of cancer cell resistance pathways, and indirectly by increasing intratumoral interstitial fluid pressure to such a high degree that drugs can no longer be delivered effectively[23]. Specifically in the case of TNBC, a gene signature indicative of fibroblast activation is predictive of tumor relapse after conventional therapy[24]. In total, CAFs are a crucial component of both tumorigenesis and resistance to conventional and targeted therapies.

Notch Pathway Activation Underlies Breast Cancer Tumorigenesis and Progression

One pathway that allows for breast cancer cells to survive in harsh environments is the Notch pathway. Originally discovered in *Drosophila melanogaster*, the mammalian Notch receptor family consists of four type I transmembrane receptors (NOTCH1-4)[25]. This family of proteins are synthesized and activated in a similar fashion. First, Notch proteins are synthesized in a precursor form that are cleaved to generate the mature receptor, which is comprised of two subunits, an extracellular domain and an intracellular domain. The extracellular domains prevent ligand-independent signaling. Generally, Notch signaling is initiated by engagement of a Notch ligand to a Notch receptor in the event of cell-to-cell contact[26]. Notch ligands include jagged 1 (JAG1), JAG2, Delta-like 1 (DLL1), DLL3, and DLL4. Once bound to the Notch receptor, the ligand induces a conformational change, exposing a cleavage site in the extracellular domain to for cleavage by the metalloproteinase tumor necrosis factor-α-converting enzyme (ADAM17). After this cleavage, the intracellular domain of Notch is cleaved by the presenilin-γ-secretase complex. This final cleavage allows for the release of the intracellular domain of Notch and subsequent nuclear translocation. There, Notch recruits its transcriptional co-activator protein mastermind-like 1 (MAML1). Notch proteins exert their wide-ranging functions by initiating a transcriptional cascade. Notch transcriptional targets include Notch receptors, Notch ligands, cyclins, and MYC. In total, Notch activation regulates tumorigenesis, progression, and therapy resistance in a context and cell-type dependent manner.

In different cancers, Notch pathway activation can have oncogenic or tumor suppressive roles[27]. In breast cancer, Notch pathway activation has long been implicated as an oncogenic driver. Early work found that the Notch locus is a common integration site in MMTV-induced tumors and expression of Notch4 in the mammary epithelium results in mammary tumor formation[28]. Notch activation in breast cancer has been further implicated

in various stages of tumor progression. Notch signaling can promote transformation of mammary epithelial cells by transcriptionally regulating Cyclin D1[29]. Similar to the role of the Notch pathway in stem cell maintenance, it has been demonstrated that Notch signaling can regulate the stemness of breast cancer tumors and result in therapy resistance[30–32]. Interestingly, Notch can also cooperate with other oncogenic signaling pathways such as RAS to enhance proliferative capacity and transformation[33]. Expression of active forms of Notch results in the activation of the phosphoinositide 3-kinase/Protein kinase B (PI3K-AKT) signaling axis, to further amplify tumorigenic capacity by suppressing apoptosis[34]. Interestingly, in developmental systems, crosstalk between Notch signaling and janus kinase signal transducer and activator pathway (JAK-STAT) results in a proliferative response that is responsible for stem cell self-renewal and differentiation[35]. Therefore, we hypothesize that in breast cancer cells, Notch pathway activation by the tumor microenvironment may cooperate with existing oncogenic pathways to maximize their oncogenic potential. Due to the necessity for proteolytic cleavage for activation, inhibition of the presenilin-γ-secretase complex with small molecule inhibitors (GSI) is an attractive therapeutic target for Notch-driven cancers[36]. However, clinical application of GSIs has yet to find success due to a lack of a companion biomarker that would identify patients that would benefit from Notch pathway inhibition[37]. Therefore, we expect that in certain conditions, treatment with GSIs will be able to reverse the oncogenic potential conferred by Notch pathway activation.

Interferon-Stimulated Genes Are Effectors of Cancer Progression and Viral Defense

Another pathway that has been implicated in tumorigenesis, progression, and therapy resistance in a variety of cancers are interferon-stimulated genes (ISGs). ISGs are best studied in the context of viral infection; however, cancer therapies induce ISGs through previously undefined mechanisms. Conventional radiation therapy is known to

induce ISGs in many cancers, including breast cancer, and contribute to resistance. Previously, through *in vivo* selection for resistance to radiation therapy, our lab demonstrated the biological relevance of an experimentally derived gene program. This gene network consists of a network of ISGs that clinically predict chemotherapy and radiation resistance across multiple human cancers[38,39]. Functionally, several of these ISGs were shown to influence treatment resistance in cell lines and mouse tumor models. For breast cancer, high ISG expression is the strongest predictor of resistance to chemotherapy or RT. These results suggest that ISGs may be a major determinant of clinical breast cancer treatment resistance. Further, chemotherapy[40] and DNA methylation inhibitors also induce ISGs in cancer and stromal cells[41,42]. In these studies, it is suggested that DNA methylation inhibitors can de-repress endogenous double-stranded RNA (dsRNA) species that are recognized by cellular pathogen-sensing machinery to activate an ISG response. In addition to therapy resistance, ISG induction in breast cancer cells and the brain metastatic microenvironment aids in the establishment of metastases by enhancing colonization capabilities[43]. Here, breast cancer cells that are colonizing the brain transfer cyclic GMP-AMP (cGAMP) to resident astrocytes via connexion junctions. cGAMP can then directly activate stimulator of interferon genes (STING) in the recipient astrocytes, which leads to tumor necrosis factor (TNF) and interferon production, which then activate ISGs in the breast cancer cells in a paracrine fashion. While the induction of ISGs in breast cancer cells appears to be a crucial element of cancer progression and therapy resistance, both the mechanisms of their activation and their effector functions in cancer have remained elusive.

Activation of ISGs is best studied in the context of viral infection. The first line of defense to any pathogen is detection. In mammalian cells this is accomplished by pattern recognition receptors (PRRs) that are fine-tuned to detect pathogen-associated molecular patterns (PAMPS) and trigger intracellular signaling cascades that result in the

upregulation of ISGs[44]. PRRs include Toll-like receptors (TLRs), RIG-I-like receptors (RLRs), NOD-like receptors (NLRs), and C-type lectin receptors (CLRs). Toll-like receptors include 12 transmembrane receptors that localize to either the plasma membrane or endolysome and can detect lipoproteins, lipopolysaccharides, flagellin, DNA, and RNA of viral, bacterial, protazoal, and self-origin. NOD-like receptors are cytoplasmic and recognize bacterial peptidoglycans, while CLRs are plasma membrane localized and recognize microorganismal carbohydrates. RLRs are near-ubiquitously expressed in all cell types, localize to the cytoplasm, and include RIG-I, MDA-5, and LGP2. RLRs are canonically activated by viral RNA originating from DNA and RNA viruses. RIG-I is best characterized to be activated by short, double-stranded, 5'triphosphorylated RNA of viral origin[45]. Pathogenic DNA has been implicated to indirectly activate RIG-I by is transcription by RNA polymerase III[46,47]. In this context, viral DNA can be recognized by RNA polymerase III and transcribed. Based on its sequence, these transcripts will form double-stranded structure, and consistent with all RNA polymerase III transcripts, maintain a 5'triphosphorylated (5'ppp) moiety. Therefore, this endogenously-produced RNA can activate RIG-I and ISGs.

Interferon-stimulated genes include PRRs, interferon regulator factors (IRFs), and several signal transducing proteins involved in the JAK-STAT signaling pathway[48]. These proteins are present as baseline, but their expression markedly enhances upon pathogenic insult. Downstream of JAK-STAT signaling, many ISGs function to restrict viral activity, reinforce ISG expression, and promote cell survival. ISGs such as the interferon-induced Mx family of proteins restrict viral entry[49], while interferon-induced proteins with tetratricopeptide proteins (IFITs) and protein kinase R (PKR) can directly inhibit viral translation. Furthermore, the ubiquitin-like protein, interferon-stimulated gene 15 (ISG15), can function to both directly destabilize viral proteins while also promoting or repressing other ISG expression and function[50]. Other ISGs such as the OAS/RNaseL pathway can

function to amplify ISG expression by nondiscriminate cleavage of endogenous RNAs to serve as RIG-I ligands and further enhance RIG-I activation[51]. Collectively, in the case of viral infection, a multi-tiered signaling cascade that initiates with nucleic acid recognition by PRRs, such as RIG-I, and results in the enhanced expression of effector ISGs culminates in the restriction of viral activity and cell survival.

RIG-I Discrimination of Self from Non-Self RNA

The initiators of any host response to pathogenic insults are PRRs. RIG-I and other PRRs are maintained in an inactive state until contact with a ligand[52]. For maximal activation, a strict set of requirements must be met for sensing of a nucleic acid as foreign, or non-self. Broadly, these requirements include availability of the ligand, localization of the ligand, and the structure of potential nucleic acid ligands. All three aspects contribute to the reliable recognition of pathogenic nucleic acids as foreign and restrict inappropriate recognition of self nucleic acids. In the context of RIG-I, many of these aspects are well studied. First, RIG-I is exclusively localized to the cytoplasm; therefore, any nucleic acid ligand must also be present in the cytoplasm[53]. Other cytoplasmic RNA sensors include melanoma differentiation-associated protein 5 (MDA5), IFIT1, PKR, and 2'-5'-oligoadenylate synthase (OAS) family members, which can recognize discrete and overlapping structural RNA elements[54]. Endosomal RNA sensors include the TIR-domain-containing adapter-inducing interferon-β (TRIF) dependent TLR, TLR3, and the myeloid differentiation primary response gene 88 (MYD88) dependent TLRs, TLR7 and TLR8. Second, for RIG-I activation after encountering an RNA ligand in the cytoplasm, the ligand must be present at a high local concentration. Many endogenous nucleic acid ligands can be present at high levels, but are recognized and degraded by endogenous nucleases to prevent inappropriate activation of anti-viral signaling[55,56]. RIG-I and other PRRs recognize a restricted set of structural features to discriminate self from non-self RNA. RIG-I is best

characterized to recognize short, dsRNA, with a 5'ppp end. However, recent quantitative structural studies have demonstrated that RIG-I can recognize a wide array of end modifications, albeit with lower affinity. For example, RNA modifications such as 2-O-methylation are determinants of RIG-I recognition, irrespective of a 5'ppp or capped ends[57,58]. These structural preferences illuminate the necessity for a variety of RNA PRRs. In the cytoplasm, RIG-I and MDA5 function in concert to recognize short (<300bp) and long (>300bp) dsRNA, respectively, with similar downstream ISG outcomes. In endosomes, TLR3 largely recognizes dsRNA, while TLR7 and TLR8 recognize ssRNA. In total, these guiding principles allow for efficient recognition of non-self RNA, while restricting inappropriate immune activation.

While studies assessing RNA features and requirements for optimal RIG-I activation have been extensive, they are based on synthetic and/or artificial RNAs. Therefore, the requirements for sensing endogenous RNA may be more nuanced. Various cellular RNA transcripts are present in the cytoplasm, at high levels, and have all the structural features capable inducing RIG-I. However, these transcripts do not ubiquitously induce ISG responses. These potential RIG-I ligands are largely RNA polymerase III transcripts which are generally short, double stranded, and contain 5'ppp moieties[59,60] and include SRP RNAs, Y RNAs, tRNAs, and certain snRNA species. Therefore, other characteristics must govern their relative innocuousness. Similar to shielding of viral genomes by viral RNA binding proteins (RBPs) is shielding of endogenous RNA by cellular RBPs. The vast majority of RNA polymerase III transcripts that are best suited to act as endogenous RIG-I ligands function in ribonucleoprotein (RNP) complexes; thus, they are likely entirely shielded from recognition by RIG-I[61]. Whether protein shielding of RNA is a major determinant of PRR activation remains unclear. While PRRs can recognize a wide-array of distinct nucleic acid ligands, their purpose remains unified, to serve as the initiators of an anti-viral response within infected cells.

Exosomes are Mediators of Cell-Cell Communication

Recent evidence reveals that in addition to cell intrinsic anti-viral responses that occur after viral infection, mechanisms exist to propagate an anti-viral response from infected to uninfected cells via exosomal transfer of anti-viral cargo[62,63]. Exosomes are small (<150nm), extracellular vesicles of endosomal origin that are implicated in a myriad of biological and pathological processes[64]. Exosomes form by a dynamic endocytic process. First, early endosomes mature into late endosomes and begin accumulating intraluminal vesicles (ILVs) via ESCRT-dependent and independent processes. These late endosomes containing ILVs are referred to as multivesicular endosomes, or MVBs. The ILVs that form from this double invagination are lipid-bilayered in the same orientation as the plasma membrane and contain directly sorted and stochastically acquired cytoplasmic contents. Under most cellular contexts, MVBs will fuse with lysosomes and their contents will be degraded and/or recycled. Some MVBs will fuse with the plasma membrane and release their vesicular content. These vesicles are known as exosomes. The processes that regulate this secretion are not well understood; however, several exosome secretion-stimulating conditions have been identified. For example, dendritic cells increase exosome secretion after interaction CD4 T lymphocytes[65]. Neurons will secrete exosomes after depolarization and stimulation by neurotransmitters[66,67]. Exogenous stimuli such as irradiation can also stimulate exosome release[68,69]. Once secreted, exosomes are stable both *in* and *ex vivo* and can then be internalized by recipient cells by endocytosis, phagocytosis, or fusion to the plasma membrane[70]. Several receptor-ligand pairings have been implicated in the targeting of exosomes to recipient cells such as cell adhesion molecules, integrins, and tetraspanins. Exosomes can then elicit responses in recipient cells simply by their adherence to recipient cells or transference of their cellular content after endocytosis or fusion.

Exosomes contain DNA, RNA, lipids, and proteins and harbor evidence of directed sorting of their contents[64]. Exosomes are classically identified by their protein markers of their biogenesis such as endosomal tetraspanins such as CD9, CD81, and TSG101. Beyond exosome proteins that result from their shared origins, cell-type specific exosomal proteins of largely cytoplasmic origins can also be found, including adhesion molecules, cytoskeletal proteins, enzymes, and other transmembrane proteins. Lipids are also a key component of exosomes. Specifically, sphingomyelin, phosphatidylserine, cholesterol, and saturated fatty acids have been demonstrated to be enriched in exosomes when compared to cells[71–73]. Collectively, the enrichment of specific lipid and protein contents in exosomes suggests a targeted mechanism of content sorting.

Exosomes are also enriched in nucleic acids. While, genomic and mitochondrial DNA has been reported to be found in exosomes[74–76], best characterized are the vast complexity of RNA species in exosomes. Exosomal RNA differs from cellular RNA in that is largely bereft of full-length ribosomal RNA (rRNA) that makes up greater than 95% of the human transcriptome[77]. While functional mRNAs are present in exosomes, they make a small fraction of the total exosomal RNA contents, which are largely non-coding RNA (ncRNA). These RNAs are resistant to RNase digestion, suggesting they are contained within exosomes, rather than on the surface. The advent of next-generation sequencing (NGS) technologies has allowed for an explosion of reports of exosomal RNA contents, but, few unifying properties other than a general enrichment for ncRNA have been identified to date. In total, the functional of content of exosomes is context specific and remains unclear.

Exosomes in Viral Infection and Cancer

In the context of propagation of anti-viral signals and amplification of ISG responses, exosomal RNA is crucial to this process. Secretion and transfer of exosomes

to uninfected bystander cells can result in exosome-transferred viral RNA by PRRs. For example, in cells infected with an Hepatitis C virus (HCV) strain that is incapable of producing virions, HCV genomic RNA is transferred via exosomes to uninfected cells[78]. This HCV RNA is then recognized as PAMP by recipient cells and ISGs are activated in the absence of direct virus infection. Similarly, adenoviruses can cause an increase in exosome transfer containing PRR activating cargo that results in ISG upregulation and a short-range anti-viral response[79]. In the case of latent Epstein-Barr virus (EBV) infection, exosomal transfer of EBV RNA can alert neighboring cells of an infection[80]. Here, latent-infected cells can trigger an anti-viral ISG response in neighboring cells by the transfer of EBV 5'ppp RNA that is bereft of any shielding RNA-binding proteins. Together, these studies demonstrate that exosomes can mediate ISG induction within uninfected cells and tissue-level amplification of the anti-viral response.

Exosomes and exosomal contents have been implicated in a host of processes related to the progression of various cancer types. In the initial stages of glioma tumorigenesis, cells bearing the activated EGFRvIII receptor can transfer this protein to wild-type cells to aid in their transformation[81]. Notably, exosomes derived from patients and breast cancer cell lines containing RNA-induced silencing complex-associated (RISC-associated) miRNAs can also induce tumor formation by the non-tumorigenic mouse mammary cells[82]. In established tumors, glioblastoma exosomes can transport functional mRNA that are able enhance tumor growth[83]. Exosomes have been best characterized to enhance the metastatic potential of cancer cells by various mechanisms. First, exosomes reshape the pre-metastatic niche through mobilization of various stromal subtypes at distant metastatic sites[84,85]. Moreover, these processes can specify organ-specific metastatic potential through integrin interactions[86]. Exosomes can also enhance invasion of cells into vasculature by destruction of endothelial cell junctions[87]. Stromal-derived exosomes can also increase breast cancer cell invasion by activating Wnt-planar cell

polarity signaling to dramatically induce metastases[88]. Lastly, exosomes can enhance colonization of distant sites after extravasation by augmenting the surrounding ECM to better support metastatic outgrowth[89]. Exosomes of stromal and cancer origin have been implicated in resistance to conventional therapies, largely by transfer of functional miRNAs[90,91]. Further, exosomes can also impact therapy response by shuttling chemotherapeutics out of target cells[92,93]. In total, exosomes of cancer and stromal origin can have profound impacts on all stages of cancer progression.

Host Mimicry in Viral Infection and Virus Mimicry in Cancer

Besides transferring viral RNA, the ability to horizontally transfer damage-associated molecular patterns (DAMPs) may also be an important feature of virus infection. As described, host cells utilize exosomal machinery to transport viral nucleic acids to propagate anti-viral signals. Virions have also been described to contain an abundance of host RNA polymerase III transcripts in the absence of canonical RBP partners[94–97]. The role of these non-viral RNAs in virions has not been well characterized; however, it has been postulated that they might stimulate innate immune signaling[98]. Therefore, whether in virions or in exosomes, cells under viral attack ensure a broad anti-viral response by packaging endogenous DAMPs alongside viral RNA PAMPs. In support of this concept, recent studies show that cells infected by certain viruses can package the nucleoside second-messenger cGAMP into secreted virions and extracellular vesicles to trigger a STING-dependent ISG response in recipient cells[99,100]. Altogether, these observations suggest that horizontal transfer of DAMPs to promulgate anti-viral signaling as a means of host mimicry by virions.

Cancer cells may also utilize a process of virus mimicry, whereby they can provoke an anti-viral response in surrounding cancer and stromal cells. For example, stromal PRRs have been demonstrated to recognized exosomal RNA (exoRNA) in the tumor

microenvironment[101,102]. Here, exosome-derived miRNAs can function as PRR ligands and help establish pre-metastatic and maintain post-metastatic niches. Moreover, under stress conditions such as chemo and radiation therapy, it has been demonstrated that endogenous nucleic acids can act as endogenous PRR ligands and elicit an ISG response. As described, DNA methylation inhibitors can de-repress endogenous dsRNA species to activate stromal and cancer cell PRRs[41,42]. Chemotherapeutic anthracyclines may also induce endosomal localization of dsRNA for recognition by TLR3[40]. Radiation therapy may also induce endogenous RNA for PRR recognition[103,104]. Finally, in autoimmune states, endogenous RNAs are also de-repressed and recognized as foreign, further amplifying autoimmunity[55,105]. These studies have illuminated a common theme of virus mimicry and ISG activation across multiple cancer types; however, the nature and identity of the PRR activating nucleic acid ligand, functional consequences of ISG activation, and the mechanisms by which endogenous DAMPs are mobilized have yet to be delineated.

Project Aims and Summary

The central aims of this project were to demonstrate why and how the tumor microenvironment propagates anti-viral signaling in cancer cells and to further elucidate how anti-viral signaling influences cancer progression and response to therapies. We hypothesized that stromal cells could be responsible for ISG activation in breast cancer cells by the transfer of exosomes containing endogenous ncRNA that act as RIG-I ligands. In turn, activation of ISGs can then aid in tumor progression and therapy resistance. While others have demonstrated that endogenous RNA can act as DAMPs, the identity of specific RNA and mechanism by which they are available for recognition is unknown. Further, there has been extensive work characterizing the functional effects of exosomes; however, few studies have identified a specific mechanism by which exosomal cargo

exerts its effects in recipient cells. In total, our work aimed to understand specific mechanisms for tumor-stromal signaling cascades initiated by exosomal contents that result in cancer progression and therapy resistance.

In Chapter 2, we examined the role of fibroblasts in inducing anti-viral responses in a subset of basal-like and triple negative breast cancers. Utilizing *in vitro* and *in vivo* breast cancer models as well as primary patient data, we identified a complex signaling cascade that was reminiscent of tissue-level propagation of anti-viral signals in viral infection. To do so, breast cancer cells induce exosome secretion by stromal fibroblasts. These exosomes are enriched in 5'ppp RNA, which when taken up by breast cancer cells, activate RIG-I and induce ISGs. In parallel, this heterotypic interaction induces a juxtacrine signaling pathway centering on NOTCH3. These pathways converge, as STAT1 and NOTCH3 transcriptionally cooperate to achieve maximal activation of NOTCH target genes that mediate stemness capabilities in breast cancer cells. In total, activation of the paracrine anti-viral and juxtacrine NOTCH pathways results in breast cancer progression and therapy resistance. In Chapter 3, we delved deeper into the virus mimicry occurring in the breast cancer tumor microenvironment. Here, we identified an abundant RNA polymerase III transcript, RN7SL1, as a potent RIG-I ligand that is transferred from stromal cells to breast cancer cells via exosomes. The major determinant of RN7SL1 function as a DAMP in stroma-derived exosomes was its relative lack of shielding; whereas, in all cells examined, RN7SL1 is entirely shielded as part of the signal recognition particle (SRP). Moreover, we demonstrate that deployment of RN7SL1 as an unshielded RNA DAMP results from breast cancer mediated activation of stromal NOTCH1 and subsequent MYC and RNA polymerase III activation. *In vivo*, unshielded RN7SL1 can function to enhance tumor progression and metastasis. Further, many of the above findings were validated with human breast tumor-derived CAFs and found in patient-derived exosomes harvested

from serum. In total, our work delineates a mechanism and function of endogenous RNAs as DAMPs in the breast cancer tumor microenvironment.

CHAPTER 2: EXOSOME TRANSFER FROM STROMAL TO BREAST CANCER CELLS REGULATES THERAPY RESISTANCE PATHWAYS

Sections of this chapter have been adapted from the following manuscript with permission from Elsevier: Boelens, M.C.*, Wu, T.J*, Nabet, B.Y.*, Xu, B., Qiu, Y., Yoon, T., Azzam, D.J., Twyman-Saint Victor, C., Wiemann, B.Z., Ishwaran, H., ter Brugge, P.J., Jonkers, J., Slingerland, J., Minn, A.J. Exosome Transfer from Stromal to Breast Cancer Cells Regulates Therapy Resistance Pathways. *Cell* **159,** 499–513 (2014).

*Co-first author

Author Contributions: M.C.B., T.J.W., and B.Y.N. contributed equally as co-first authors, and their names were ordered arbitrarily. M.C.B. and T.J.W. initiated the project and performed the initial characterzations of the stromal protective effect. T.J.W. characterized the NOTCH pathway. B.Y.N. performed the exosomes, exosomal RNA, and RIG-I studies. T.J.W. and B.Y.N. performed the xenograft experiments. T.J.W. and B.Y.N. performed the mammosphere studies. B.Y.N. prepared the RNA-sequencing libraries and aided in the analysis. M.C.B. performed protein analysis of human and mouse tumors. B.X. performed STAT1 and NOTCH3 transcriptional studies. Y.Q. and A.J.M. analyzed the sequencing studies. A.J.M., B.Y.N, and T.J.W. wrote the manuscript.

Introduction

The elucidation of resistance mechanisms to chemotherapy and radiation is an important goal in improving cancer survival. Previously, we characterized a gene signature for radiation (RT) and chemotherapy (chemo) resistance that was discovered through *in vivo* selection for RT resistant tumors[38,39]. Because the majority of the genes identified were interferon-stimulated genes (ISGs), which normally are activated as part of an anti-viral response, we termed this signature the Interferon-Related DNA Damage Resistance Signature (IRDS). Several IRDS genes, including the transcription factor *STAT1*, influence RT/chemo resistance in cell lines and mouse tumor models. Interrogation across the most common human cancers revealed that a large proportion of untreated primary tumors express the IRDS. In breast cancer, IRDS expression measured by a clinical classifier comprised of seven IRDS genes (*STAT1*, *MX1*, *ISG15*, *OA2*, *IFIT1*, *IFIT3*, *IFI44*) identifies patients whose cancers are resistant to chemo and RT. Thus, the IRDS may represent a common and inherent mechanism of resistance across various human cancers. How the IRDS is regulated and how ISGs can protect against RT/chemo is unclear.

A common way that ISGs are activated is through pattern recognition receptors (PRRs) that are triggered by pathogen-associated molecular patterns such as viral nucleic acids[44]. PRRs include toll-like receptors (TLRs) and RIG-I-like receptors. Typically, RIG-I is activated by 5'-triphosphate viral RNA after viruses gain entry into immune and non-immune cells. However, PRRs can also be activated through alternative routes by exosomes, which are small membrane vesicles capable of transferring contents between cells to function in cell-cell communication[106]. Exosomes can transfer viral RNA from infected cells to trigger an interferon response in immune cells, presumably through TLRs, to enhance viral suppression[78,79]. In cancer, exosomes secreted by tumor cells can increase metastasis through interaction with cells of the microenvironment[84,101].

Alternatively, exosomes from mesenchymal cells can be transferred to cancer to promote metastasis[88]. Thus, these recent data suggest that PRRs and exosomes orchestrate heterotypic cell-cell communication to regulate anti-viral responses or to aid cancer progression. Whether cross-talk between cancer and the tumor microenvironment can use exosomes and PRRs to similarly control ISG/IRDS expression or influence treatment resistance is unknown.

The importance of the tumor microenvironment in dictating treatment response is increasingly evident. Stromal cells, which are primarily fibroblasts but can also be other cell types, can promote survival after genotoxic and targeted therapy through the secretion of paracrine factors[13]. Many of these interactions between stromal cells and tumor cells may support the maintenance of cancer stem-like cells (i.e., tumor-initiating cells) analogously to how normal stem cells depend on a niche[107]. Since tumor-initiating cells are resistant to RT/chemo, and their survival would allow efficient tumor regrowth, understanding how the stromal microenvironment can influence these therapy resistant cells may provide promising new drug targets.

The NOTCH family of receptors activates developmental signaling pathways that have multiple roles in cancer, including drug resistance[108,109] and the regulation of tumor-initiating cells[110]. Activation requires cell-cell contact and engagement of NOTCH ligands, such as JAGGED proteins. Given the properties of the NOTCH pathway in cancer, there is a significant interest in targeting the pathway as a cancer therapeutic. Activation of NOTCH occurs through the cleavage of its intracellular domain and can be blocked by a gamma secretase inhibitor (GSI). Currently, there are multiple clinical trials testing GSIs combined with other targeted agents and conventional chemotherapy[37]. However, challenges exist that include lack of a companion biomarker to identify patients who will benefit from NOTCH inhibition. Understanding how NOTCH can be activated in subsets of cancers may facilitate their utilization as drug targets.

In this study, we integrate experimental and computational models to investigate how stromal cells communicate with breast cancer to regulate expression of ISGs. In so doing, we define an anti-viral pathway that is activated by exosomes and RIG-I, and cooperates with NOTCH3 to regulate stroma-mediated expansion of therapy resistant cells.

Results

Stromal cells induce the IRDS and increase breast cancer radiation resistance

Previous reports indicate that ISGs can be modulated by the microenvironment[111]. To examine if the microenvironment can influence IRDS expression and contribute to RT/chemo resistance, we utilized metastatic MDA-MB-231 breast cancer cells (1833)[112] expressing a GFP-luciferase reporter and xenografted them with or without non-transformed MRC5 human diploid fibroblasts used as stromal cells. Tumors containing admixed fibroblasts exhibited high expression of several IRDS genes including *STAT1* (Figure 1A), particularly from breast cancer cells (Figure 1B). In contrast, tumors arising from breast cancer cells alone had lower STAT1/ISG expression and remained primarily comprised of human breast cancer cells, suggesting poor stromalization by mouse cells. The presence of admixed fibroblasts enhanced the growth rate of breast cancer cells (Figure 1C), which is a defining property of carcinoma-associated fibroblasts (CAFs), as measured by the rate of change in bioluminescence signal at each time point. After RT, breast cancer cells from tumors without admixed fibroblasts promptly stopped growing and showed regression by day 24. In contrast, breast cancer admixed with fibroblasts showed dramatically reduced cell death (Figure 1D) and maintained significant growth even after RT (Figure 1C). In total, these observations suggest a relationship between tumor and stromal cell interaction, anti-viral signaling, and survival of cells adept at resisting DNA damage and sustaining tumor growth.

Table 1: IRDS Responder (IRDS-R) and IRDS Nonresponder (IRDS-NR) Breast Cancer Cells and Stromal Cell Lines

Cell Line	Subtype	ER	HER2	IRDS Induction	Stromal Protection	Microarray
IRDS-R						
MDA-MB-231 (1833)	Basal B	(-)		+	+	+
MDA-MB-231	Basal B	(-)		+	+	+
HS578T	Basal B	(-)		+	ND	
MDA-MB-436	Basal B	(-)		+	+	
MDA-MB-157	Basal B	(-)		+	+	
HCC1937	Basal A	(-)		+	+	+
IRDS-NR						
SKBR3	Luminal	(-)	(+)	-	-	
T47D	Luminal	(+)		-	-	
MCF7	Luminal	(+)		-	-	+
HCC70	Basal A	(-)		-	-	
MDA-MB-468	Basal A	(-)			-	+
Cell Line	**Type**			**IRDS Induction**	**Stromal Protection**	**Microarray**
Stroma						
MRC5				+	+	+
CAF61a				+	+	
BJ				+	+	
Hs27a				+	+	
Hs5				+	ND	
THP-1				-	-	

Subtype, ER, and HER2 status were determined by other groups[113]. ND refers to not determined. In the case of Hs578T, difficulty separating breast cancer from stromal cells did not allow for accurate measurements of breast cancer cell death. Cell lines used for microarray and microarray-based studies are also indicated.

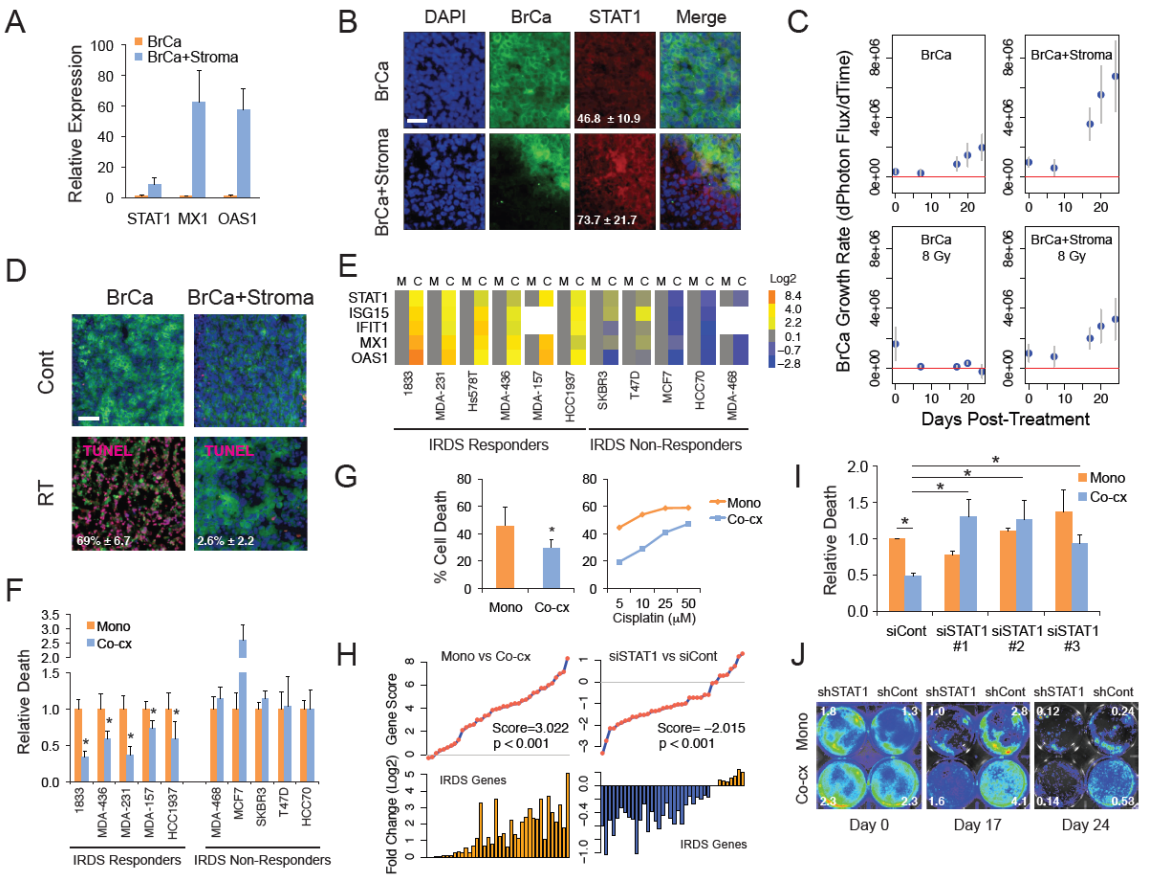

Figure 1. Stromal cells induce ISGs and protect basal-like breast cancer cells against radiation in a STAT1-dependent manner. A) Human MDA-MB-231 metastatic breast cancer cell (BrCa) line (1833) was admixed with or without MRC5 normal human fibroblasts (Stroma) and expression of IRDS genes was determined by qRT-PCR. **B)** GFP-labeled 1833 breast cancer cells with and without MRC5 fibroblasts were xenografted subcutaneously into nude mice and tumors imaged (20X) at day 14. STAT1 intensity in breast cancer cells is quantitated for representative field shown. Scale bar is 100 microns. **C)** Bioluminescence imaging (BLI) response of 1833 breast cancer cells with a luciferase reporter gene after xenografting with and without MRC5 fibroblasts. Tumors were irradiated with 8 Gy (day 0). Shown is change in photon flux over time (first derivative, mean ± SEM, n=5-10). Positive first derivative indicates growth, zero indicates no growth, and negative values denote regression. Data are a separate analysis of the control groups from Figure 9M. **D)** 1833 breast cancer cells were stained with GFP and TUNEL (red) 10 days after RT. Percent TUNEL positive is shown. Scale bar is 100 microns. **E)** Breast cancer cells (Table 1) were classified as IRDS responders (IRDS-Rs) or IRDS non-responders (IRDS-NRs). Heat map and scale shows breast cancer IRDS genes after mono-culture (M) or MRC5 co-culture (C). **F)** Cell death of IRDS-Rs and IRDS-NRs four days after 10 Gy RT in mono- (Mono) and co-culture (Co-cx) (n=3-10). **G)** Cell death of 1833 IRDS-R after cisplatin chemotherapy (n=3) and after dose response. **H)** Gene Set Analysis shows changes in IRDS genes 48 hrs after co-culture vs mono-culture of IRDS-Rs (left, also see Table 1), or after STAT1 knockdown in 1833 IRDS-R in co-culture (right). Top graph plots individual and overall gene scores, and bottom graph shows fold-change. **I)** Cell death of 1833 IRDS-R four days after 10 Gy RT using three independent siRNAs

to STAT1. **J)** BLI-based survival assay after 10 Gy RT (day 0) using luciferase-labeled 1833 cells with shSTAT1 or control knockdown (shCont). Photon flux ($x10^6$) for each well is indicated. Shown is representative experiment (n=5). *$p < 0.05$. Unless noted, all bar plots in figure are mean ± SD of *n* biological replicates.

Stroma-mediated IRDS induction and protection are STAT1-dependent and specific for basal-like breast cancers

To better examine the relationship between IRDS expression and stroma-mediated protection across different breast cancer and stromal cell combinations, we co-cultured both cell types *in vitro* to model stroma-mediated resistance (referred to as co-culture) and discovered that breast cancer cells can be divided into two groups. The first group, called “IRDS responders” (IRDS-Rs), is enriched in the basal-like subtype (Table 1) and upregulated IRDS genes after interaction with MRC5 fibroblasts (Figure 1E). The second group, called “IRDS non-responders” (IRDS-NRs), is comprised of non-basal-like and some basal-like subtypes and failed to induce IRDS genes. Importantly, only IRDS-Rs were protected by fibroblasts after RT (Figure 1F) or after chemotherapy (Figure 1G). Multiple other stromal cell lines (CAFs, bone marrow, fibroblasts) able to induce the IRDS were also able to promote resistance against RT (Figure 2A); however, not all stromal cells were protective, as illustrated by a macrophage cell line that neither induced the IRDS nor protected (Figure 2B). Genome-wide transcriptomic analysis from co-culture of IRDS-R compared to mono-culture (Table 1) demonstrated upregulation of nearly all IRDS genes in breast cancer (Figure 1H, Figure 2C, Table 2). Stroma-mediated induction of IRDS was specific to IRDS-R breast cancer (Table 3). Knockdown of STAT1 in 1833 IRDS-R prior to co-culture with MRC5 fibroblasts depressed nearly all IRDS genes compared to control (Figure 1H) and also inhibited stroma-mediated resistance (Figure 1I), a result observed with multiple different siRNAs targeting STAT1 (Figure 2D-E). Stable STAT1 knockdown (Figure 2D-E) also selectively inhibited the protective effects of MRC5 fibroblasts as measured by an *in vitro* luciferase-based assay (Figure 1J). In the absence

of RT, disruption of STAT1 had negligible effects on growth with or without fibroblasts (Figure 2F). Thus, a subset of basal subtype breast cancers can interact with multiple stromal cell types to increase IRDS genes and RT/chemo resistance in a STAT1-dependent manner.

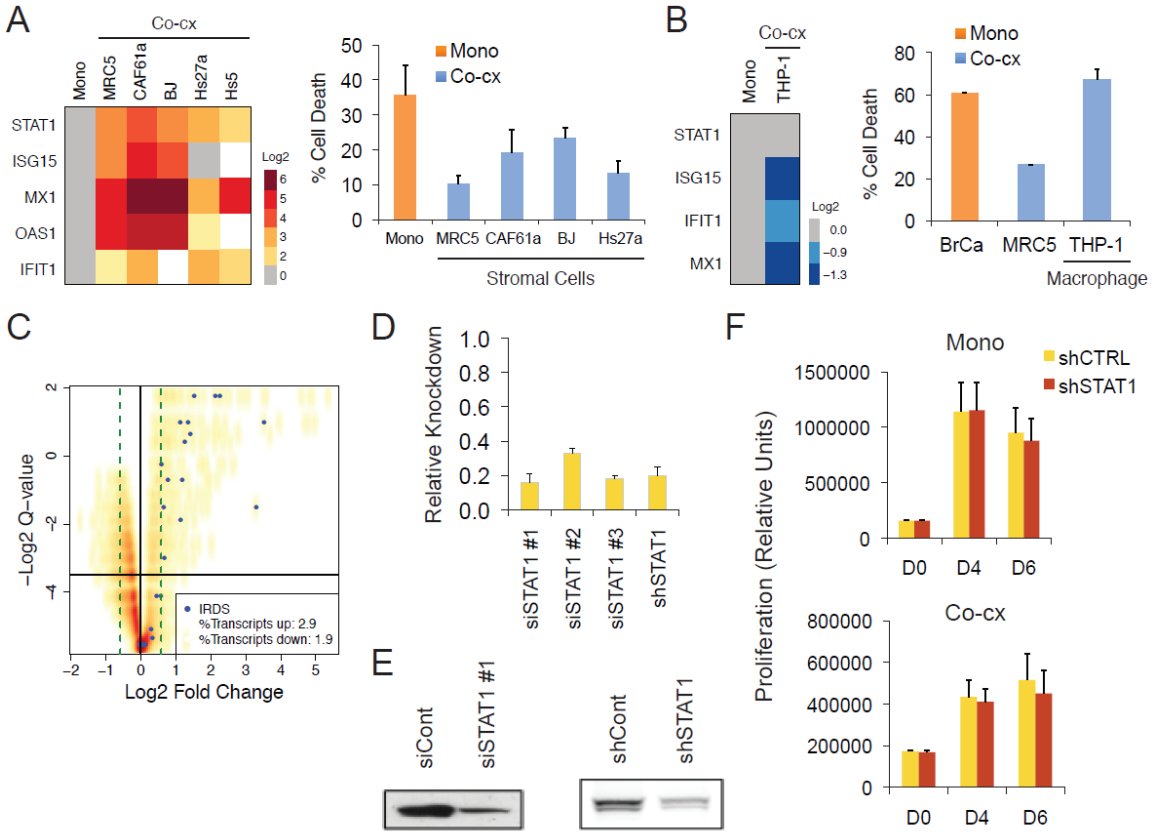

Figure 2. The ability of stromal cells to protect breast cancer cells against radiation is coupled to upregulation of IRDS genes. A) The 1833 IRDS-R cell line was grown in mono-culture (Mono) or co-cultured (Co-cx) with the indicated stromal cell line or with **B)** the macrophage cell line THP-1. CAF61a is a carcinoma-associated fibroblast cell line. Shown is a heat map of IRDS genes showing relative upregulation (red shades) or downregulation (blue shades). Grey is expression in mono-culture, which was used to normalize each gene. White indicates no data. On the right of each heat map is cell death four days after treatment with 10 Gy RT in either mono-culture or co-culture with the indicated cell lines (n=2). H10 stromal cells were not tested for stroma-mediated protection but is shown to allow for comparison in Figure 4K. **C)** Transcriptomic changes in breast cancer after co-culture with MRC5 fibroblasts reveal induction of IRDS genes. After co-culture, breast cancer and MRC5 stromal cells were sorted by flow cytometry. Volcano plot shows microarray gene expression changes (x-axis) versus significance by q-value (y-axis). Horizontal black line represents a false discovery rate of 10%. Orange is high density of genes and yellow is low. Blue dots are IRDS genes. Green dashed line represents 1.5-fold change. See Table 2. **D)** Multiple independent siRNAs and an shRNA

to STAT1 were each introduced into the 1833 IRDS-R breast cancer cell line and analyzed for knockdown by qRT-PCR. Shown are knockdown levels compared to cells transfected with a control si/shRNA. **E)** Knockdown was also confirmed by immunoblotting for STAT1 after transfection with siSTAT1 or shSTAT1. **F)** 1833 IRDS-R transfected with shSTAT1 or control shRNA (shCont) were seeded in either mono-culture or co-culture with MRC5 fibroblasts. At days 0, 4 and 6, cell growth was measured by luciferase-based luminescence. All bar plots in figure are mean ± SD. All gene expression assays were performed after 24-48 hrs of culture.

Table 2: Genes Upregulated in IRDS-R Breast Cancer Cells after Co-culture

Gene ID	Score(d)	Fold Change
TNFSF10	9.51175075	2.39654789
PAPPA	9.50811651	1.73625789
EGR1	9.15391015	2.33440593
EDNRA	8.929463	5.42601126
PAPPA	8.72827447	7.87175655
CDH6	8.56804829	8.20739467
CFB	8.55320523	2.11443065
IFI44L	7.73843143	34.198318
TMEM176A	7.49882318	2.26668984
NA	7.49831933	2.37487425
STAT2	7.20634429	1.84069078
CCL2	7.19144971	5.28689347
PAMR1	7.17076079	7.80477608
OAS2	6.7050865	9.72737688
MEIS1	6.67907311	5.14952985
LTBP1	6.55554459	2.00106414
MSC	6.5523153	1.8778532
DKK3	6.49077312	7.20767782
MIR21	6.39875367	1.60805803
PIEZO2	6.39867122	5.20369927
HGF	6.39818891	15.3752323
IFI6	6.38646998	8.87480621
IRF9	6.2546392	2.75398143
XAF1	6.22233223	4.34260997
TRIM22	6.13241982	6.31148865
MMP2	6.11930698	10.5044086
IFI16	6.10845758	1.71835165
WNT5A	6.07738868	9.22868664
STAT1	6.05976298	3.39204979
SLFN11	6.02630643	3.49634883
TCF21	6.01469106	2.76236241
CFB	6.00374702	3.0328043
ANGPTL2	5.98683165	4.1110645
LRP1	5.98262926	2.76064673
TRPA1	5.96005598	16.6919472
TCF4	5.92808361	4.2274197
ECM1	5.91936933	1.52084958
GPC6	5.903451	1.85379347
BDKRB1	5.89985196	10.3602752
IFITM1	5.87899966	4.34361694
VCAN	5.87813333	14.6981149
CD248	5.75363674	3.9813116
SGIP1	5.7515508	6.1586101
FAP	5.74804294	5.72581044
PARP9	5.73893329	5.19915479
JAM3	5.71704795	3.30444238

IRDS induction is controlled by RIG-I

Stroma-mediated IRDS induction and resistance requires live stromal cells and does not associate with expression and/or function of interferons or interferon receptors (Figure 4A-E). To explore alternative pathways to IRDS induction, we examined the transcriptome of IRDS-R breast cancer cells in MRC5 co-culture compared to mono-culture. Among the upregulated genes (Table 2) were several PRRs known to activate ISGs. Random forest (RF) multivariable regression analysis[114] of these and other similar PRRs demonstrated that increasing expression of RIG-I best explains the upregulation of IRDS genes by fibroblasts (Figure 3A). Accordingly, knockdown of RIG-I in 1833 IRDS-R inhibited IRDS gene induction after co-culture, while disruption of MYD88, which is required for signaling by multiple TLRs not predicted to regulate the IRDS, had no effect (Figure 3B, Figure 4F). Disruption of RIG-I by shRNA (Figure 4F) also partially reversed stroma-mediated resistance, as measured by short- and long-term survival (Figure 3C), without influencing general cell proliferation (Figure 4G). Concomitant disruption of the type one interferon receptor with RIG-I had no additive effect. Thus, STAT1/IRDS induction and stromal protection are primarily initiated through RIG-I rather than interferon receptors.

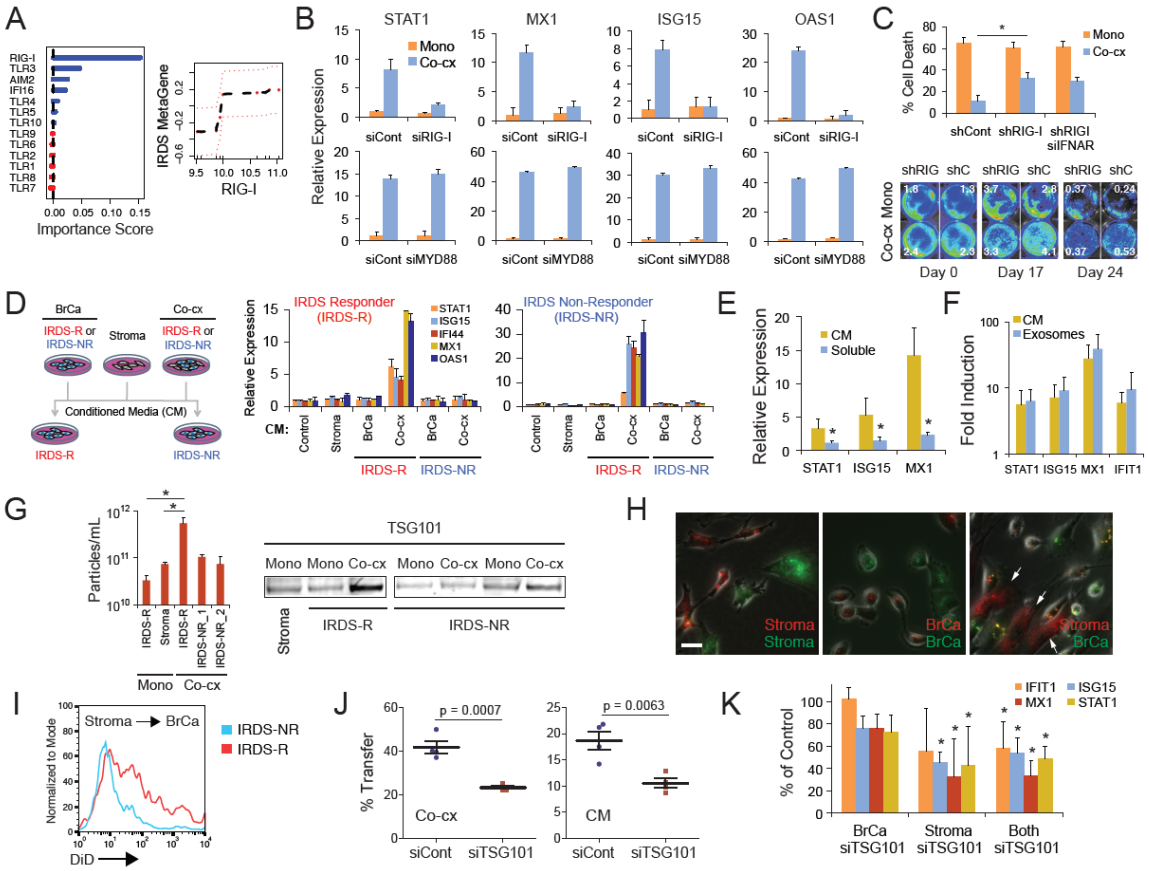

Figure 3. Stromal cell interaction increases exosomes that upregulate ISGs through a RIG-I anti-viral pathway. A) Importance scores (higher is more predictive) of PRRs from a multivariable random forest (RF) regression model to predict induction of IRDS after MRC5 co-culture with IRDS-Rs. The model explains 60.8% of the total variance. Adjusted effect of *RIG-I* on IRDS metagene expression is shown on right (red dashes are ± two SE). **B)** Expression of IRDS genes after siRNA to RIG-I (top row) or MYD88 (bottom row) in 1833 IRDS-R. Shown is a representative experiment (n=3). **C)** Cell death of 1833 IRDS-R after RT (n=4) and a representative BLI-based survival assay (n=2) after the indicated knockdown (RT on day 0). Photon flux (x10^6) for each well is shown. The control is same as Fig. 1J. **D)** Expression of IRDS genes in 1833 IRDS-R (middle) or MCF7 IRDS-NR (right) after addition of conditioned media (CM) from MRC5 fibroblasts (Stroma), IRDS-R or IRDS-NR (BrCa), or MRC5 co-culture with IRDS-Rs or IRDS-NRs (Co-cx). See schematic (left). **E)** CM collected after 48 hrs or the soluble fraction from CM (Soluble) was applied to 1833 IRDS-R and expression of IRDS genes was examined (n=4). **F)** Fold induction of IRDS genes in 1833 IRDS-R after addition of co-culture CM or purified exosomes (n=5). **G)** NanoSight quantification of exosomes (left) from 1833 IRDS-R, MRC5 fibroblasts (Stroma), and MRC5 co-culture using either 1833 IRDS-R or IRDS-NR (MDA-MB-468 or MCF7). Immunoblot for TSG101 (right) using 1833 IRDS-NR and MDA-MB-468 IRDS-NR. **H)** MRC5 fibroblasts (Stroma) or 1833 IRDS-R were labeled with green or red lipophilic dye in mono-culture (left and middle). For co-culture (right), MRC5 (arrows) were labeled red and breast cancer cells green. Scale bar is 40 microns. **I)** Representative flow cytometry of DiD dye transfer from MRC5 stroma to 1833 IRDS-R or MDA-MB-468 IRDS-NR. **J)** Exosome transfer from co-culture after TSG101 knockdown

(left) and after addition of the co-culture CM cleared of debris and apoptotic bodies (right) (n=4). **K)** IRDS gene induction by co-culture CM after TSG101 knockdown in 1833 IRDS-R, MRC5 stroma, or both (n=3). Gene expression and significance levels are relative to siControl. *p < 0.05. Unless noted, all bar plots in figure are mean ± SD of *n* biological replicates.

Exosomes are transferred from stromal cells to breast cancer to increase IRDS

Conditioned media (CM) from co-culture of IRDS-Rs with stromal fibroblasts, but not from stromal co-culture of IRDS-NRs or from mono-culture, upregulates IRDS genes when applied to mono-cultured IRDS-Rs (Figure 3D). Interestingly, CM from co-culture of IRDS-Rs also upregulates IRDS when applied to IRDS-NRs. These results suggest that stromal cell interaction with IRDS-Rs produces a secreted factor capable of activating RIG-I. Recent evidence suggests that some PRRs can be activated by exosomes. Consistent with a role for exosomes in IRDS activation, the exosome-depleted soluble fraction of CM poorly induced the IRDS (Figure 3E). Conversely, addition of purified exosomes, which were confirmed by electron microscopy and by analyses of size properties and markers (Figure 4H), was sufficient to induce IRDS genes (Figure 3F).

To examine how co-culture with IRDS-Rs influences exosome secretion and possible transfer to breast cancer cells, exosomes were quantified by particle counting and by the exosome marker TSG101. Both methods indicated that more exosomes were present after co-culture of IRDS-Rs compared to either IRDS-NRs or mono-culture (Figure 3G). To examine exosome transfer, stromal cells and/or breast cancer cells were differentially labeled with either red or green fluorescent lipophilic dye to mark exosomes. For both cell types, dye transfer in mono-culture appeared minimal (Figure 3H). In co-culture, microscopy and flow cytometry revealed an apparent unidirectional transfer of exosomes from fibroblasts preferentially to IRDS-Rs but not to IRDS-NRs (Figure 3H-I, Figure 4I-J). Multiple stromal cell types capable of inducing the IRDS were also able to transfer exosomes to IRDS-Rs (Figure 4K). Transfer was also observed upon addition of co-culture CM cleared of debris and apoptotic bodies (Figure 3J). With both assays,

transfer was mitigated by knockdown of TSG101 (Figure 3J, Figure 6C), which is a regulator of exosome biogenesis. Accordingly, TSG101 disruption in fibroblasts, but not in breast cancer cells, also inhibited IRDS induction without affecting elevation in non-IRDS genes such as *MMP1* and *CXCL1* (Figure 3K, Figure 6D). Thus, IRDS-Rs, but not IRDS-NRs, coerce an increase in secretion of exosomes by stromal cells that results in transfer to breast cancer cells and subsequent IRDS induction.

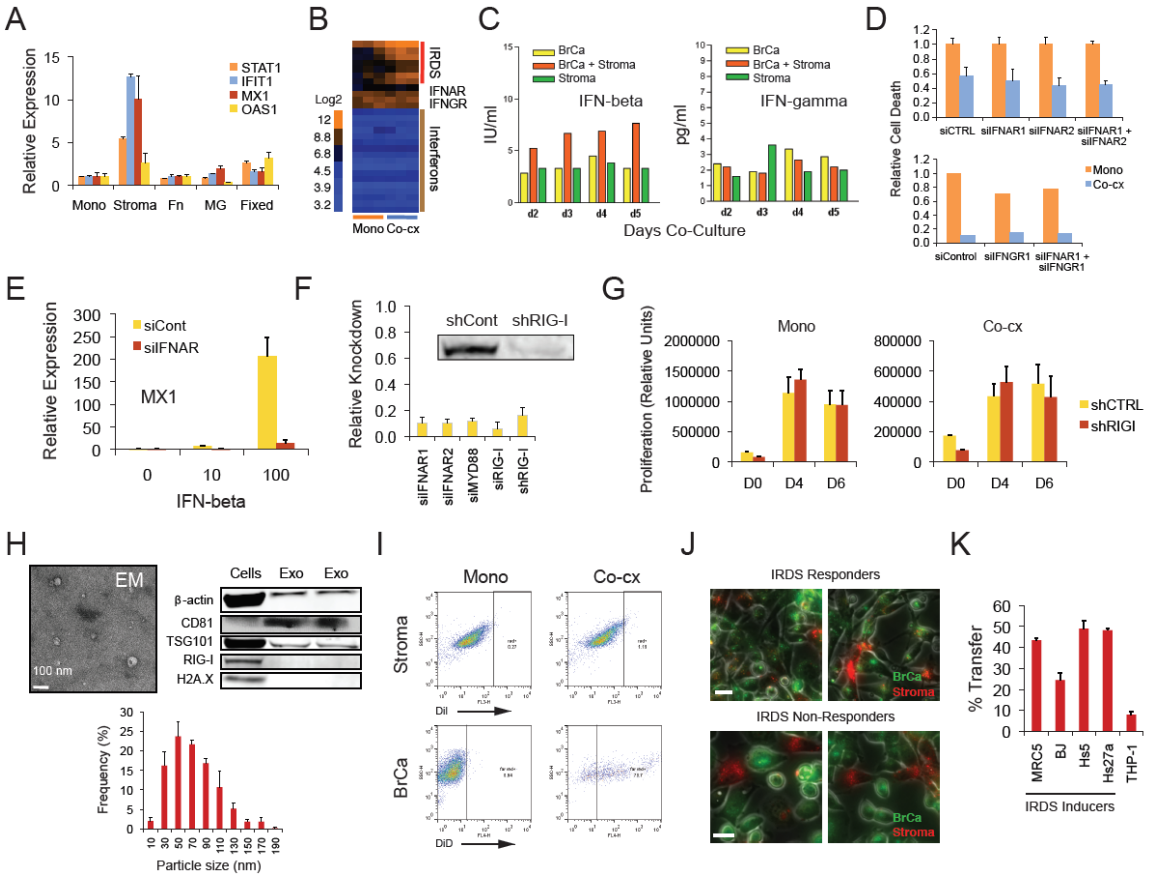

Figure 4. Exosome transfer from stromal to breast cancer cells rather than direct interferon signaling is associated with resistance and IRDS induction in breast cancer. A) Induction of IRDS genes requires live stromal cells. 1833 IRDS-R breast cancer cells were grown in mono-culture (Mono) or cultured with MRC5 fibroblasts (Stroma), fibronectin (Fn), MatriGel (MG), or fixed MRC5 stromal cells (Fixed). Shown is expression of the indicated IRDS genes. **B)** Expression of interferons and IFN receptor genes do not change after stromal cell interaction. Shown is a heat map of microarray data from IRDS-R in mono- or co-culture. **C)** Type one and two interferons are not significantly increased after co-culture. Conditioned media from mono-culture of either 1833 IRDS-R (BrCa), mono-culture of MRC5 cells (Stroma), or co-culture of both cells (BrCa + Stroma) was collected at the indicated days. Shown is protein concentration by ELISA for IFN-beta or IFN-gamma. **D)** Type one and type two interferon receptors are not

necessary for stroma-mediated protection. Shown is relative cell death four days after 10 Gy RT for 1833 IRDS-R grown in either mono-culture or co-culture with MRC5 stromal cells. Either the type one (IFNAR1 or IFNAR2, top), type two (IFNGR1, bottom), or combination of receptors were disrupted by siRNA. **E)** Knockdown of type one interferon receptor inhibits *MX1* gene induction by exogenous IFN-beta. Indicated units of IFN-beta were added to mono-culture of 1833 IRDS-R and *MX1* expression was measured. **F)** Knockdown levels for IFN receptors, *MYD88*, and *RIG-I*. Shown are knockdown levels by qRT-PCR for each si/shRNA relative to cells transfected with a control si/shRNA. Knockdown of RIG-I by shRNA was confirmed by protein (inset). **G)** 1833 IRDS-R transfected with shRIG-I or control shRNA (shCont) were seeded in either mono-culture or co-culture with MRC5 stromal cells. At days 0, 4 and 6, cell growth was measured by luciferase-based luminescence. **H)** Purified exosomes (Exo) from co-culture conditioned media were confirmed by electron microscopy (EM), the presence of exosome markers (β-actin, CD81, TSG101), and the absence of cytoplasmic (RIG-I) and nuclear (H2A.X) markers (top right). Total cell lysates (Cells) were used as comparison. Size distribution of exosomes from co-culture as measured from electron microscopy (bottom). **I)** Exosomes are primarily unidirectionally transferred from stromal cells to breast cancer. MRC5 stromal cells were labeled with DiD and 1833 IRDS-R were labeled with DiI lipid dyes. Shown is transfer from breast cancer to stromal cells (top row) and stromal to breast cancer cells (bottom row) in co-culture as measured by flow cytometry. Gates are based on fluorescence intensity in mono-culture. **J)** Exosomes are preferentially transferred to IRDS-R breast cancer cells. Breast cancer cells labeled with green lipid dye and stromal cells labeled with red dye were co-cultured. Shown are representative fluorescent microscopy images of the IRDS-R cell lines 1833 (top left) and MDA-MB-436 (top right), and the IRDS-NR cell lines SKBR3 (bottom left) and T47D (bottom right). White scale is 40 microns. **K)** Transfer of exosomes from stromal to breast cancer cells is associated with stromal cells capable of inducing IRDS in breast cancer cells (IRDS Inducers). Conditioned media from co-cultures of 1833 IRDS-R with the indicated dye-labeled stromal cells was added to 1833 IRDS-R. Transfer was measured by percent dye positive cells using flow cytometry. All bar plots in figure are mean ± SD. Unless indicated, gene expression and exosome assays were performed after 24-48 hrs of culture or stimulation.

Table 3: Genes Upregulated in IRDS-NR Breast Cancer Cells after Co-culture

Gene ID	Score(d)	Fold Change
PLAC8	14.5431909	28.09085581
PRKCDBP	9.221590661	10.49678396
XAF1	9.159420594	13.45391224
IFI44L	8.630966681	52.79939189
ADAMTS12	8.547922704	6.182649282
SHC3	8.391804719	6.000001542
HERC6	8.122650409	5.840422724
ETV5	7.578174981	5.279498594
GSTT2	7.445394817	5.44163875
MX2	7.428942679	22.31605842

HERC5	7.021381942	8.603379553
SLCO1B3	7.014907663	44.95708011
CD68	6.801351721	8.175324573
IFIT1	6.532348154	19.99911081
STEAP1	6.396327872	13.63207023
GFPT2	6.325927538	6.596892255
VEGFC	6.062694438	7.596177013
ACSL5	6.056073217	25.66990472
TOX	5.911402089	3.777452313
IRAK2	5.795246	4.7055435
ITGA2	5.671427672	4.184668772
OAS2	5.627284315	25.60423273
CAPRIN2	5.607531074	6.306708439
PTPRM	5.542675403	7.712387813
EPSTI1	5.518995316	4.742798949
IFI44	5.391417455	22.67533361
DDX58	5.369773655	6.200664535
IFIT2	5.352961567	11.83396763
LY96	5.330794588	5.867075852
SEMA7A	5.229840311	4.422835934
MX1	5.189096757	14.92523243
LARP6	5.143833741	2.879853859
PLOD1	5.13750488	2.498201037
IFI35	5.130687365	4.925987347
TGM2	5.129137707	9.920706701
EREG	5.084580087	11.83108307
NDRG1	5.070357658	3.781942991
BST2	5.037302933	11.83570251
RAB34	5.029463527	4.773447437
MYEOV	5.026889174	3.876167147
CD22	5.012080297	3.640705892
FLNB	4.972676373	2.248621915
CDA	4.939545817	8.832433405
PAQR5	4.912789473	4.724677753
EPHA2	4.867721559	4.229377246
CHST11	4.839302013	5.026698939

Exosome transfer is regulated by stromal RAB27B

To determine whether the increased production of exosomes in co-culture primarily originated from stromal or breast cancer cells, we used a protein array of well-known exosome markers. This revealed that co-culture exosomes were much more similar to exosomes from fibroblasts compared to those from breast cancer cells (Figure 5A), arguing that enhanced exosome production in co-culture is primarily from stromal cells. Interrogation of stromal RAB GTPases commonly implicated in exosome secretion[115] revealed that stromal RAB27B transcript and protein were consistently induced after fibroblasts were co-cultured with IRDS-Rs but not with IRDS-NRs (Figure 5B, Figure 6A). Indeed, of all RAB GTPases on the microarray, RAB27B was elevated the most in fibroblasts after interaction specifically with IRDS-Rs (Figure 6B). Knockdown of RAB27B in fibroblasts (Figure 6C) inhibited the ability of CM from co-culture to stimulate IRDS genes (Figure 5C) but had no effect on non-IRDS genes such as *MMP1* and *CXCL1* (Figure 6D). Accordingly, knockdown of RAB27B also interfered with exosome transfer from fibroblasts to IRDS-Rs (Figure 5D), a result observed with multiple siRNAs to RAB27B (Figure 6E). In contrast, inhibition of RAB27A, which was not differentially expressed in fibroblasts, had no effect (Figure 6F). In total, these data argue that exosome transfer from stromal to breast cancer cells and subsequent IRDS induction is regulated by stromal RAB27B.

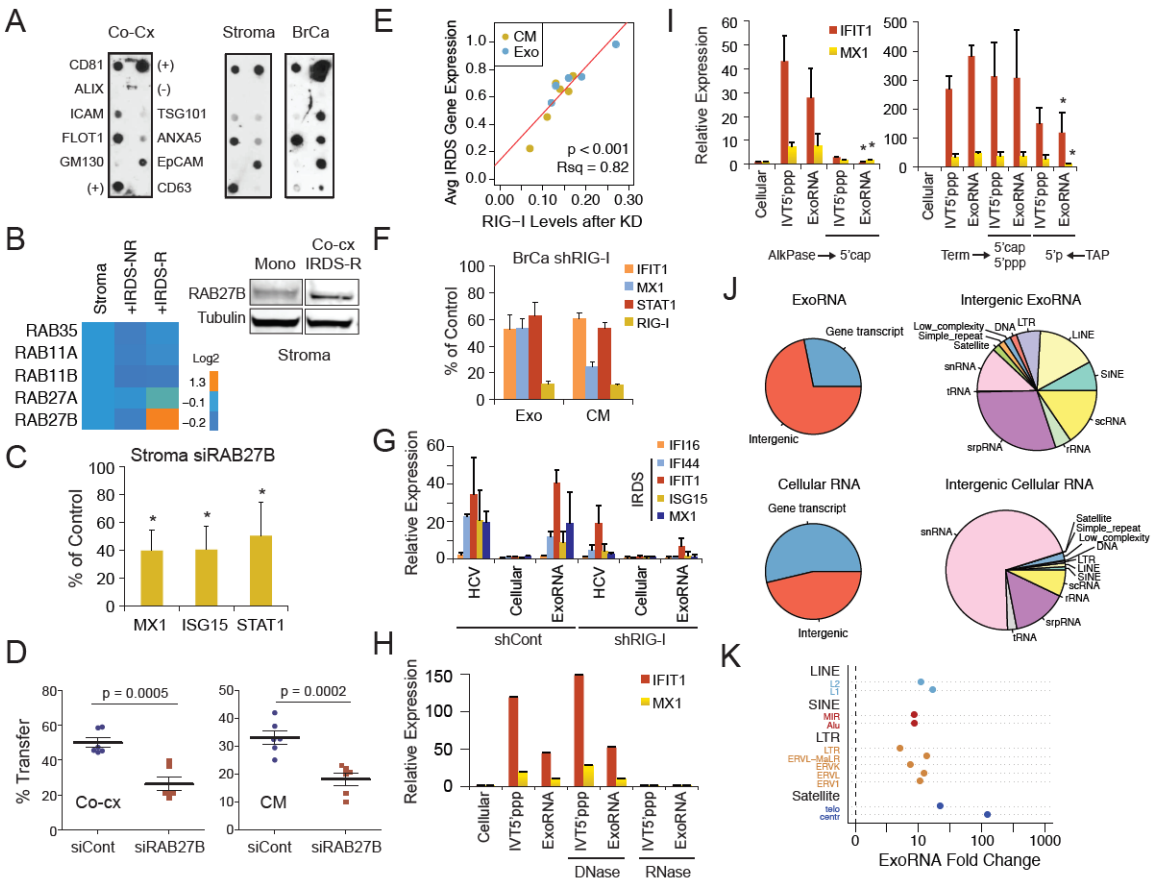

Figure 5. Stromal exosomes are regulated by RAB27B and transfer 5'-triphosphate RNA to activate RIG-I in breast cancer cells. A) Exosomes were isolated from mono-culture of MRC5 fibroblasts (Stroma) or 1833 IRDS-R (right) or from co-culture (left) and profiled by antibody array for the indicated exosome markers. GM130 is a check for cellular contamination. Positive (+) and negative (-) controls are labeled. **B)** Averaged microarray expression of the indicated RABs from MRC5 in mono-culture (Stroma) or after co-culture with IRDS-R or IRDS-NR are shown as a heat map. Immunoblot (right) for RAB27B protein expression in MRC5 after co-culture with MDA-MB-157 or 1833 IRDS-R (Figure 6A) compared to MRC5 mono-culture. **C)** IRDS expression in 1833 IRDS-R after addition of CM isolated from co-culture using MRC5 transfected with siRAB27B compared to siControl (n=3). **D)** Exosome transfer to 1833 IRDS-R after co-culture with or without RAB27B knockdown (left) or addition of co-culture CM cleared of debris and apoptotic bodies (right). **E)** Average IRDS gene expression (mean expression of *IFIT1*, *MX1*, and *STAT1*) in response to exosomes (Exo, n=5) or co-culture CM (n=6) plotted against *RIG-I* levels after knockdown in 1833 IRDS-R. **F)** IRDS gene expression from two representative data points used to generate plot in Figure 3E are shown relative to siControl. **G)** IRDS gene expression after RNA from exosomes (ExoRNA), cellular RNA, or a positive control HCV RNA was transfected into 1833 IRDS-R with or without RIG-I knockdown (n=4). *IFI16* is a non-IRDS gene used as a negative control. **H)** Expression of IRDS genes *IFIT1* and *MX1* resulting from transfection of ExoRNA after RNase treatment, or **I)** removal of 5'-monophosphate (5'-p) and/or 5'-triphosphate (5'-ppp) (n=3). An *in vitro* transcribed 5'-ppp RNA (IVT5'ppp) is used as a positive control. Shown are RNA motifs remaining after enzyme modification with alkaline phosphatase (AlkPase), Terminator

exonuclease (Term), and tobacco acid pyrophosphatase (TAP). IVT5'ppp serves as a control for RNA enzyme modification by AlkPase and TAP. **J)** Distribution of known gene transcripts and intergenic transcripts from rRNA-depleted exoRNA and cellular RNA from 1833 IRDS-R co-culture (left). Distribution of major repetitive elements and transposable element classes for intergenic transcripts are shown on right. K) ExoRNA enrichment for major subfamilies of transposable elements and satellite sequences compared to cellular RNA. *$p < 0.05$. Unless noted, all bar plots in figure are mean ± SD of *n* biological replicates.

5'-triphosphate exosome RNA activates RIG-I to induce the IRDS

Since exosomes and RIG-I both influence the effects of stromal cells, we focused on a potential relationship between the two. When RIG-I was disrupted in 1833 IRDS-R, IRDS gene induction by co-culture CM and by purified exosomes was similarly inhibited (Figure 5E-F). RIG-I activation typically results from binding to viral RNA through recognition of specific motifs such as 5'-triphosphates rather than through sequence specificity[45]. To investigate if exosome RNA (exoRNA) can induce IRDS through RIG-I, exoRNA from co-culture exosomes was re-encapsulated into synthetic lipid vesicles and transfected into mono-culture 1833 IRDS-R. While total cellular RNA from co-culture failed to induce IRDS genes, exoRNA upregulated IRDS genes in a RIG-I-dependent manner to levels that were comparable to a viral HCV RNA used as a positive control (Figure 5G). In contrast, HCV RNA or exoRNA did not significantly increase non-IRDS genes such as *IFI16*, which normally responds to cytosolic DNA. Treatment with RNase but not DNase eliminated the ability of exoRNA, as well as an *in vitro* transcribed 5'-triphosphate control RNA (IVT5'ppp), to elevate IRDS genes (Figure 5H). Removal of 5'-phosphates revealed that the active RNA contains exposed 5'-phosphate ends and is not a typical protein-coding mRNA with a 5'-cap (Figure 5I). Consistent with the known specificity of RIG-I for 5'-triphosphates, IRDS induction was inhibited after specific removal of 5'-triphosphate from exoRNA or from the IVT5'ppp, while digestion of RNA containing 5'-monosphosphates had no effect. Thus, exoRNA containing 5'-triphosphate activates RIG-I to induce IRDS genes.

Sequencing of exoRNA isolated from co-culture of 1833 IRDS-R revealed no apparent match to viral genomes from 19 different viruses known to activate RIG-I. Instead, enrichment for human intergenic and non-coding transcripts was observed in exoRNA compared to total cellular RNA from co-culture (Figure 5J). In both cellular RNA and exoRNA, repetitive sequences accounted for a significant fraction of these intergenic transcripts; however, while snRNA-like repeats were the predominant class of repetitive elements in cellular RNA, transposable elements represented the largest class within exoRNA. Specifically, SINEs, LINEs, and LTR retrotransposons were markedly enriched among exoRNA repetitive elements, with the most prevalent subclasses augmented by 10-fold or more (Figure 5K). Other repetitive sequences such as telomeric and centromeric satellite sequences were present at lower frequencies but demonstrated 100 to 1000-fold enrichment in exoRNA. Since transposable elements are one category of RNA polymerase III transcripts, which can have 5'-triphosphate motifs[116,117], their enrichment suggests that they may contribute to exoRNAs capable of stimulating RIG-I.

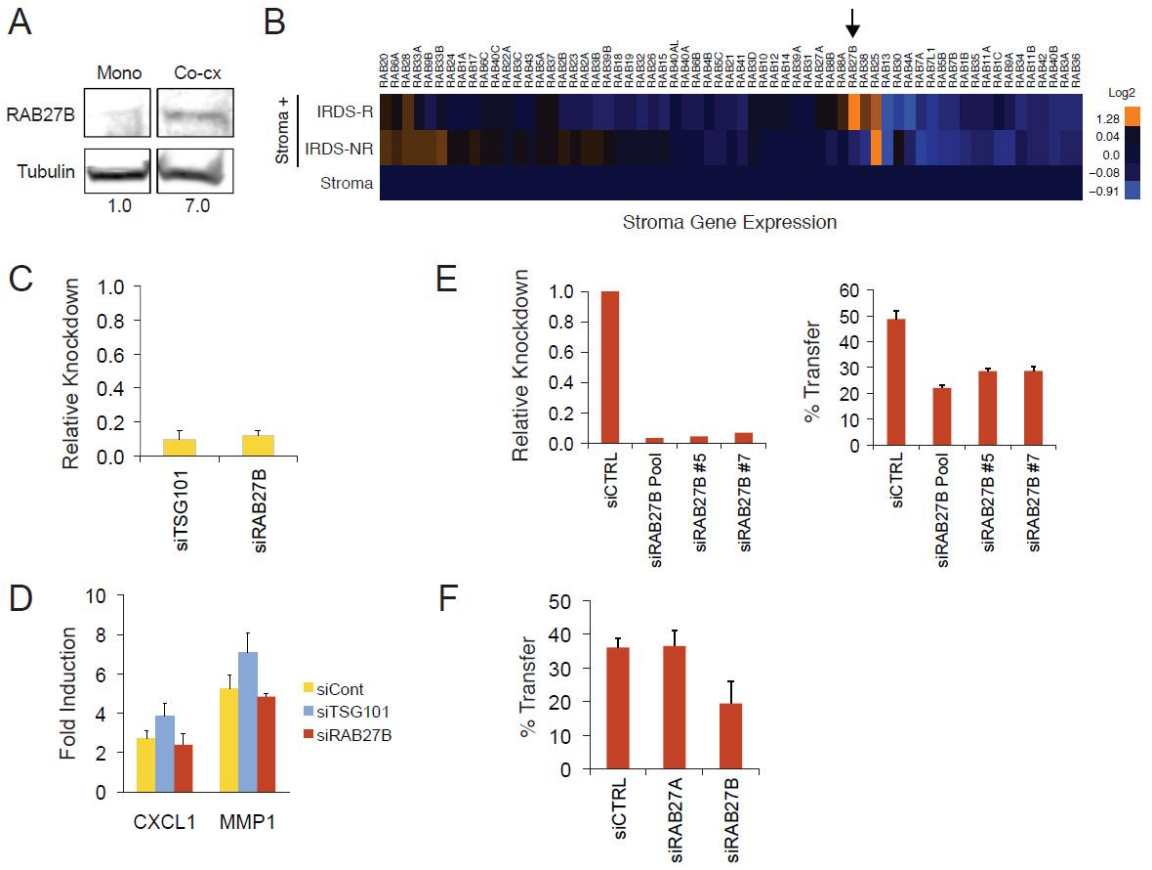

Figure 6. Stromal cells capable of inducing breast cancer IRDS specifically upregulate RAB27B to control exosome transfer. A) RAB27B is increased in stromal cells after co-culture with IRDS-R breast cancer cells. Shown is a representative immunoblot for RAB27B expression in either MRC5 mono-culture (Mono) or co-culture with 1833 IRDS-R (Co-cx). Numbers indicate fold increase determined by densitometry. **B)** *RAB27B* is preferentially increased in MRC5 fibroblasts (Stroma) after co-culture with IRDS-R but not IRDS-NR breast cancer cells. Shown is heat map of relative expression of all RAB GTPases and similarly related RABs annotated on the microarray. Scale is shown. Values are normalized to mono-culture of MRC5. *RAB27B* is marked by the arrow. **C)** Knockdown levels of *TSG101* and *RAB27B* are shown by qRT-PCR relative to cells transfected with a control siRNA. **D)** Knockdown of TSG101 and RAB27B do not influence the ability of co-culture conditioned media to induce metastasis genes. Co-culture conditioned collected after knockdown of either TSG101 or RAB27B by siRNA was used to induce expression of *CXCL1* or *MMP1* in 1833 IRDS-R mono-culture. **E)** Knockdown levels of various siRNAs for RAB27B are shown by qRT-PCR relative to cells transfected with a control siRNA. On the right is exosome transfer using conditioned media from 1833 IRDS-R co-cultured with dye-labeled MRC5 fibroblasts transfected with the indicated siRNAs to RAB27B. Conditioned media was added to 1833 IRDS-R and transfer measured flow cytometry. **F)** Knockdown of RAB27A does not affect exosome transfer to 1833 IRDS-R.

Stroma-mediated paracrine anti-viral signaling and juxtracrine NOTCH3 signaling enhance transcription of NOTCH target genes

Although RIG-I and STAT1 are necessary for stroma-mediated resistance, separation of breast cancer cells from stromal fibroblasts using a transwell filter large enough for exosome passage resulted in retained IRDS induction but loss of RT resistance (Figure 7A). This suggests that the anti-viral pathway may work with an additional juxtacrine pathway to control stroma-mediated protection. To explore this, we computationally constructed a juxtacrine interactome between IRDS-Rs and fibroblasts using differentially expressed genes from each cell type combined with protein-protein interaction data (Figure 8A). This revealed that NOTCH3 expression was increased in IRDS-R breast cancer cells after co-culture, and its membrane-bound ligand JAG1 was both induced in fibroblasts and constitutively elevated in IRDS-Rs. Protein analysis confirmed that NOTCH3 was expressed at low levels in 1833 IRDS-R, but both its expression and its cleaved intracellular domain increased after fibroblast interaction (Figure 7B). In contrast, expression of NOTCH1, 2, and 4 did not change.

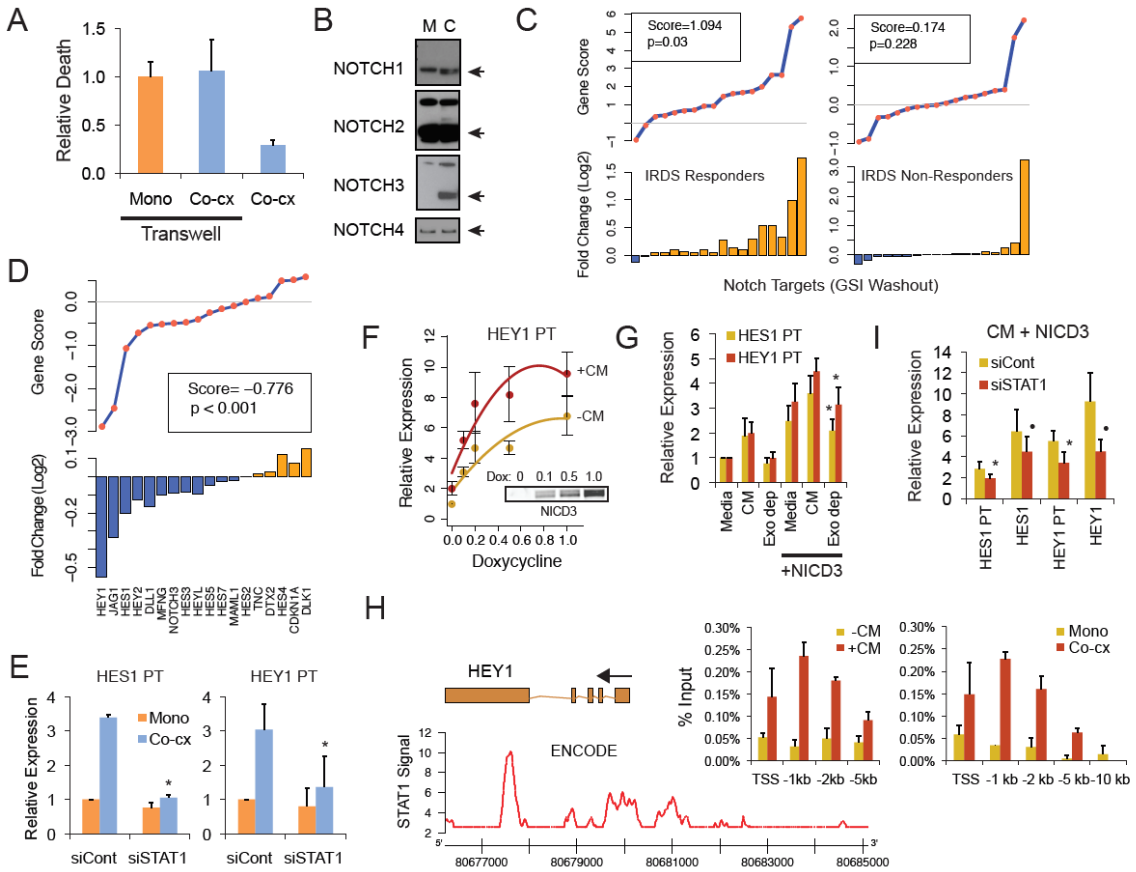

Figure 7. STAT1 enhances the transcriptional response to juxtacrine NOTCH3 signaling that is required for stroma-mediated protection. A) Cell death of 1833 IRDS-R in co-culture after RT. MRC5 fibroblasts were separated by a transwell filter large enough to allow exosome passage (n=3). **B)** Immunoblot of the indicated NOTCH family members in 1833 IRDS-R after mono-culture (M) or co-culture (C). Arrow indicates cleaved intracellular domain. **C)** Expression of NOTCH target genes in IRDS-R and IRDS-NR after co-culture, and **D)** after STAT1 knockdown in 1833 IRDS-R after co-culture. NOTCH targets were experimentally defined by GSI washout (Table 4) and used in Gene Set Analysis. **E)** Expression of the indicated NOTCH target gene primary transcript (PT) in 1833 IRDS-R (n=3). **F)** Expression of *HEY1* PT in response to doxcycyline (Dox) induced NICD3 in 1833 IRDS-R with or without addition of co-culture CM (mean ± SEM, n=6-8). Inset shows NICD3 levels after Dox addition (µg/ml). **G)** Expression of the indicated primary transcripts to NICD3 after addition of co-culture CM or CM depleted of exosomes (Exo dep). CM compared to CM depleted of exosomes is used for significance levels (mean ± SEM, n=4-6). **H)** ENCODE ChIP data for STAT1 occupancy of the *HEY1* proximal promoter region is shown along the indicated genomic coordinates. Bar plots show STAT1 ChIP from 1833 IRDS-R with and without addition of CM (left) and after mono- or co-culture (right). Relative position upstream of the transcriptional start site (TSS) is labeled on the x-axis for each bar plot. Shown are two representative experiments (mean ± SD) out of four total. **I)** Expression of *HEY1* and *HES1* mRNA or primary transcripts in response to NICD3 and co-culture CM in 1833 IRDS-R with and without STAT1 knockdown (mean ± SEM, n=4-7). •p<0.10, *p < 0.05. Unless noted, all bar plots in figure are mean ± SD of *n* biological replicates.

To investigate how anti-viral signaling and NOTCH3 might interact, we explored whether STAT1 facilitates transcription of NOTCH-dependent genes. Gene set enrichment analysis of NOTCH target genes, which we defined by GSI washout experiments (Table 4), confirmed upregulation of NOTCH targets in IRDS-Rs but not IRDS-NRs after co-culture (Figure 7C). Knockdown of STAT1 not only inhibited stroma-mediated upregulation of NOTCH target mRNAs (Figure 7D) but also blunted the primary transcripts for canonical NOTCH targets *HE2* and *HEY1* (Figure 7E), consistent with STAT1 exerting transcriptional control over these genes. To better characterize this, we utilized doxycycline inducible NOTCH3 intracellular domain (NICD3) to constitutively activate NOTCH3 in 1833 IRDS-R and added exosome-containing CM to initiate anti-viral signaling. As measured by the *HEY1* primary transcript, CM augmented responsiveness to NICD3 (Figure 7F). Depletion of exosomes from CM inhibited this effect on the *HEY1* primary transcript (Figure 7G) and mRNA (Figure 8B), and similar results were noted for *HE2*. The exosome-dependent increase in *HEY1* and *HE2* transcripts in the absence of NICD3 induction is likely due to baseline NOTCH and/or leakiness of the inducible system.

Table 4: Notch Target Genes Defined by GSI Washout

Gene Symbol	Average Fold Change
HES1	17.46
NOTCH3	10.94
HEY2	5.86
CDKN1A	3.53
HES7	3.21
HEYL	3.19
HEY1	3.07
MFNG	2.84
DLL1	2.78
HES2	2.55
HES3	2.49
DLK1	2.39
JAG1	2.29
HES4	1.75
MAML1	1.61
HES5	1.55
DTX2	1.44

Interrogation of ENCODE data revealed STAT1 occupancy at several locations within active proximal promoters of multiple NOTCH targets, including *HEY1* and *HE2* (Figure 7H, Figure 8C). Chromatin immunoprecipitation (ChIP) for STAT1 demonstrated that activation of anti-viral signaling by CM or by co-culture increased STAT1 occupancy in the *HEY1* promoter, particularly between the TSS and -2kB where the ENCODE data were the most significant (Figure 7H). STAT1 ChIP analysis for *HE2* was similar (Figure 8C). Despite high constitutive NICD3, knockdown of STAT1 in 1833 IRDS-R decreased primary transcript and mRNA levels for *HE2* and *HEY1* after activation of anti-viral signaling, consistent with the functional importance of at least some of the STAT1 sites in cooperating with NICD3 (Figure 7I). In contrast, although *NOTCH3* itself is a NOTCH target (Table 4), the proximal promoter of *NOTCH3* appears devoid of STAT1 sites by ENCODE. Accordingly, CM had no effect on the *NOTCH3* primary transcript (Figure 8D), suggesting that STAT1 affects transcription of NOTCH targets, rather than the *NOTCH3* gene. Thus, paracrine-activated STAT1 can cooperate with juxtacrine-activated NOTCH3 to augment the transcriptional response of multiple NOTCH targets.

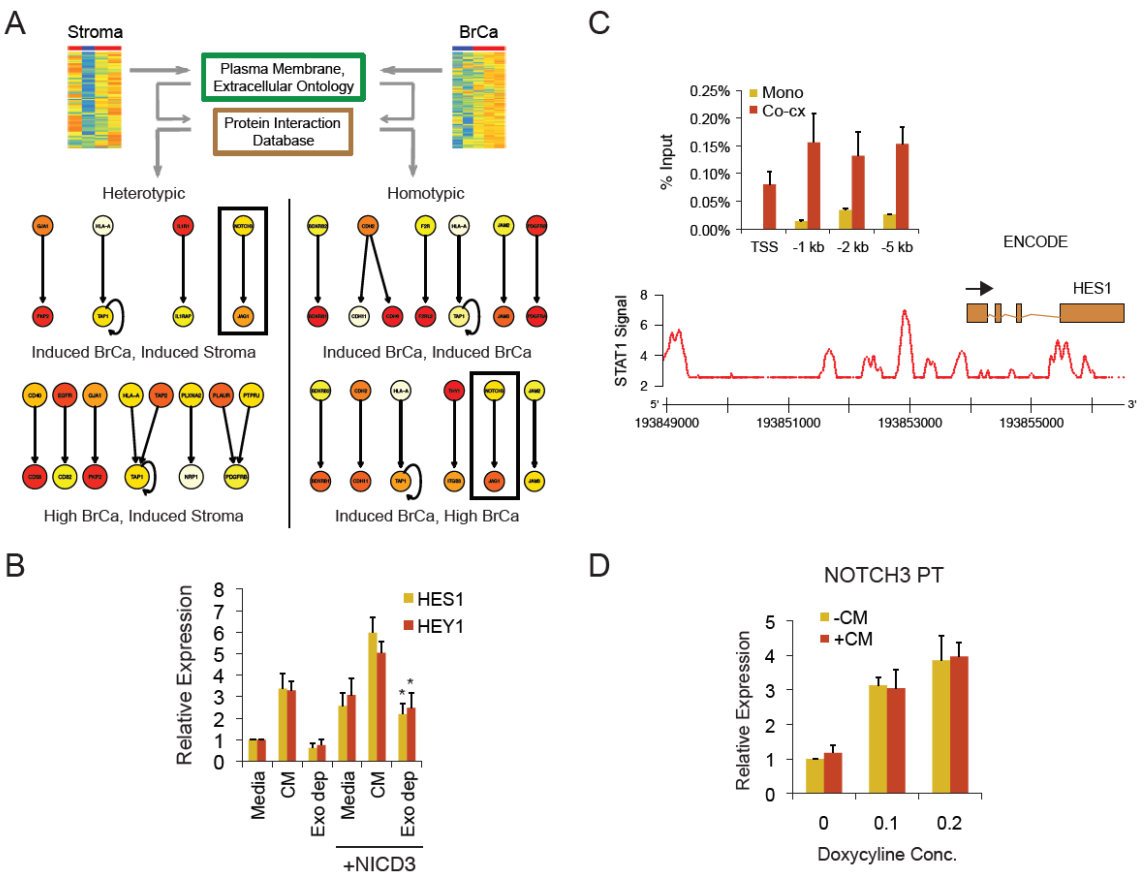

Figure 8. Juxtacrine NOTCH3-JAG1 cooperates with STAT1 to transcriptionally enhance NOTCH target genes in breast cancer. A) Computational construction of extracellular interactome between IRDS-R breast cancer and MRC5 stromal cells identifies NOTCH3 and JAG1. See Extended Experimental Procedures for details. Degree of gene expression after co-culture is color-coded (increasing shade of red is higher) in the directed interaction graph that displays either heterotypic or homotypic interactions. Black box shows NOTCH3/JAG1 interaction. Breast cancer and MRC5 genes can be either induced or expressed at higher levels in IRDS-R vs. IRDS-NR breast cancer cells in co-culture, as indicated in the label below each directed graph. Arrows go from genes expressed in cell listed first in the label to cell listed second. **B)** Depletion of exosomes inhibits the ability of co-culture conditioned media (CM) to enhance *HEY1* and *HES1* after NICD3 induction in 1833 IRDS-R. Relative expression of the indicated mRNA is shown (n=4-6, mean ± SEM). CM compared to CM depleted of exosomes (Exo dep) is used for significance levels (*p < 0.05, two-sample, one-tailed, t-test). **C)** STAT1 binds to the proximal promoter of *HES1* after activation of anti-viral signaling. ENCODE ChIP data for STAT1 occupancy of the *HES1* proximal promoter region is shown along the indicated genomic coordinates. Bar plots show STAT1 ChIP from 1833 IRDS-R with and without addition of co-culture CM. Relative position upstream of the transcriptional start site (TSS) is labeled on the x-axis. **D)** Anti-viral signaling does not influence the transcriptional response of *NOTCH3* to NICD3. Relative expression of *NOTCH3* primary transcript (PT) in response to increasing levels of NICD3 by doxycycline induction (µg/ml) with or without co-culture CM (n=6). Unless noted, all bar plots in figure are mean ± SD. Gene expression and ChIP assays were performed after 24-48 hrs of culture or stimulation.

STAT1 and NOTCH3 control stroma-mediated resistance through the expansion of therapy resistant breast cancer cells

Both anti-viral and NOTCH signaling have roles in controlling normal and cancer stem cells[109,118]. Indeed, NOTCH and its target genes were previously shown to help maintain a subpopulation of $CD44^{+}CD24^{low+}$ cells that have tumor-initiating properties (e.g., increased mammosphere and tumor formation)[110]. Since tumor-initiating cells (TICs) are known to be resistant to RT/chemo, we investigated if stromal cell interaction might lead to the expansion of such therapy resistant cells (TRCs). Indeed, co-culture resulted in the upregulation of a gene signature associated with TICs[119] (Figure 9A) and in the expansion of the $CD44^{+}CD24^{low+}$ subpopulation of 1833 IRDS-R (Figure 9B). This $CD44^{+}CD24^{low+}$ population is resistant to both RT and chemotherapy compared to $CD44^{+}CD24^{neg}$ counterparts (Figure 9C) and enriches after genotoxic damage (Figure 10A). Co-culture with fibroblasts prior to seeding increased mammosphere formation (Figure 9D), and knockdown of STAT1 or inhibition of NOTCH3 with either RNAi or GSI inhibited both mammosphere formation (Figure 9E) and enhancement of the TIC gene signature (Figure 9A). Similar STAT1-dependent stromal cell activation of NOTCH3 and expansion of mammospheres were observed in other IRDS-Rs as well (Figure 10B-D). Constitutive activation of NOTCH3 in mono-culture also led to modest expansion of both mammospheres and $CD44^{+}CD24^{low+}$ cells (Figure 9F, Figure 10E). In accordance with an expansion of $CD44^{+}CD24^{low+}$ TRCs, the proportion of surviving mammospheres was higher after irradiation of cells seeded from co-culture compared to mono-culture (Figure 9G). Thus, these results suggest that STAT1 and NOTCH3 can drive expansion of breast cancer TRCs.

Like with STAT1, knockdown of NOTCH3 with multiple different siRNAs inhibited both stroma-mediated expansion of breast cancer TRCs and resistance (Figure 9H, Figure

10F-G). Inhibiting JAG1 also inhibited RT resistance after co-culture with the greatest effect occurring after disruption in both 1833 IRDS-R and fibroblasts (Figure 9I, Figure 10H), consistent with the interactome results showing JAG1 upregulation in both cell types. Expression of NICD3 in mono-culture 1833 IRDS-R partially recapitulated the protective effect of stromal cells (Figure 9J). Similarly, ectopic NICD3 partially rescued the effect of STAT1 knockdown on stromal cell protection (Figure 9K). These partial effects on resistance parallel the partial transcriptional responses of NOTCH target genes when only STAT1 or NOTCH3 were fully engaged. Together, these data suggest that stroma-mediated resistance results from cooperation between STAT1 and NOTCH3 to expand and/or maintain breast cancer TRCs.

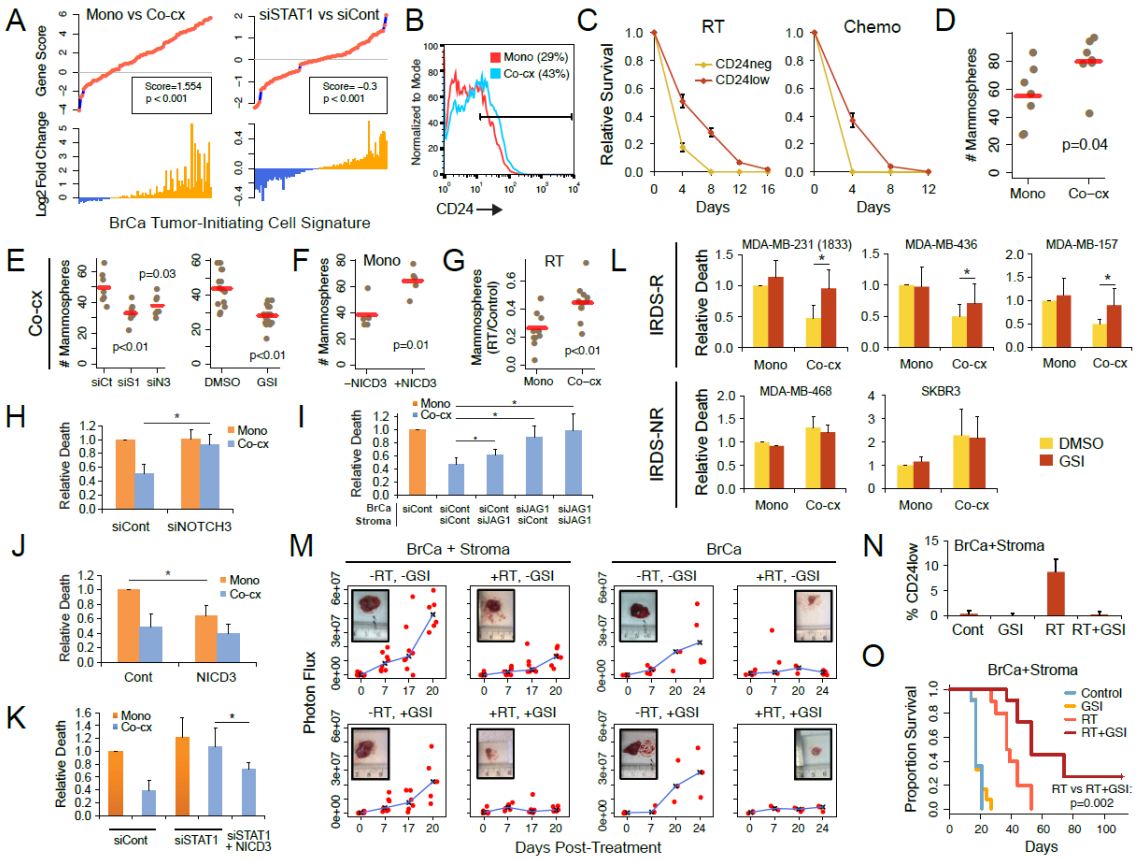

Figure 9. Stromal cells drive the expansion of a subpopulation of therapy resistant breast cancer cells through anti-viral STAT1 and NOTCH3 signaling. A) Gene Set Analysis comparing IRDS-R in mono-culture versus co-culture with MRC5 fibroblasts, or comparing 1833 IRDS-R in co-culture transfected with siSTAT1 vs. siControl. **B)** Percentage of $CD44^{+}CD24^{low+}$ 1833 IRDS-R after co-culture with MRC5. All $CD24^{low+}$ cells

are also $CD44^+$. **C)** Survival of sorted $CD44^+CD24^{low+}$ and $CD44^+CD24^{neg}$ cells after 10 Gy RT or 4 μM doxorubicin (chemo). Number of mammospheres from 1833 IRDS-R after **D)** co-culture, or **E)** co-culture following knockdown of STAT1 (siS1), NOTCH3 (siN3), or control (siCt), or after treatment with the GSI DAPT. **F)** Number of mammospheres after NICD3 induction by doxycycline in mono-culture. **G)** Proportion of surviving mammospheres relative to untreated control in mono- or co-culture after 3 Gy RT. Cell death after 10 Gy RT following **H)** knockdown of NOTCH3 in 1833 IRDS-R, **I)** knockdown of JAG1 in 1833 IRDS-R, MRC5 (Stroma), or both (n=4), **J)** expression of NICD3 (n=7), or **K)** STAT1 knockdown with and without NICD3 expression (n=3-4). **L)** Cell death of IRDS-Rs and IRDS-NRs after 10 Gy RT and treatment with the GSI DAPT or DMSO (n=5-10). **M)** Photon flux from mice xenografted subcutaneously with luciferase-labeled 1833 IRDS-R with or without MRC5 fibroblasts (Stroma) and treated 7 days later with 8 Gy RT, the GSI DAPT, both, or untreated. Mean values (black "X") are connected by blue line. Representative tumors after treatment are inset. In presence of stroma, tumor response was associated with RT ($p < 0.001$) and GSI ($p=0.004$). Without stroma, RT ($p=0.019$) but not GSI ($p=0.79$) was associated with response. **N)** Percentage of $CD44^+CD24^{low+}$ cells in tumors from mice xenografted with 1833 IRDS-R with and without MRC5 stroma 7 days after the indicated treatment. **O)** Survival of these mice, which are independent cohorts from that used in Fig. 5M. $^*p < 0.05$. Unless noted, all bar plots in figure are mean ± SD of *n* biological replicates.

<u>NOTCH inhibition reverses stroma-mediated resistance of IRDS responders and improves survival *in vivo*</u>

Considering that the NOTCH3 and STAT1 pathways are necessary for stroma-mediated resistance in IRDS-Rs, we investigated whether a GSI could selectivity reverse the protective effects of stromal cells. For IRDS-Rs, treatment with the GSI DAPT completely or partially reversed the protective effects of fibroblasts and had only small effects in mono-culture (Figure 9L). In contrast, for IRDS-NRs neither co-culture nor GSI discernibly affected cytotoxicity after RT. *In vivo*, admixing fibroblasts with luciferase-labeled 1833 IRDS-R resulted in the upregulation of NOTCH targets (Figure 10I). Treatment with GSI alone decreased NOTCH targets (Figure 10J) but had only a mild or insignificant effect on breast cancer growth in the presence ($p=0.083$) or absence ($p=0.67$) of admixed fibroblasts (Figure 9M). With RT, the presence of fibroblasts protected breast cancer ($p=0.026$); however, three consecutive doses of GSI starting from the day of RT reversed this protection. Moreover, GSI prevented the *in vivo* enrichment of $CD44^+CD24^{low+}$ TRCs observed after RT (Figure 9N), and the combination of RT and GSI

rendered nearly 30% of mice tumor-free compared to 0% with RT or GSI alone (Figure 9O). Thus, for IRDS-R basal-like breast cancers the combination of GSI and genotoxic therapy prevents stroma-mediated expansion of TRCs adept at tumor re-initiation.

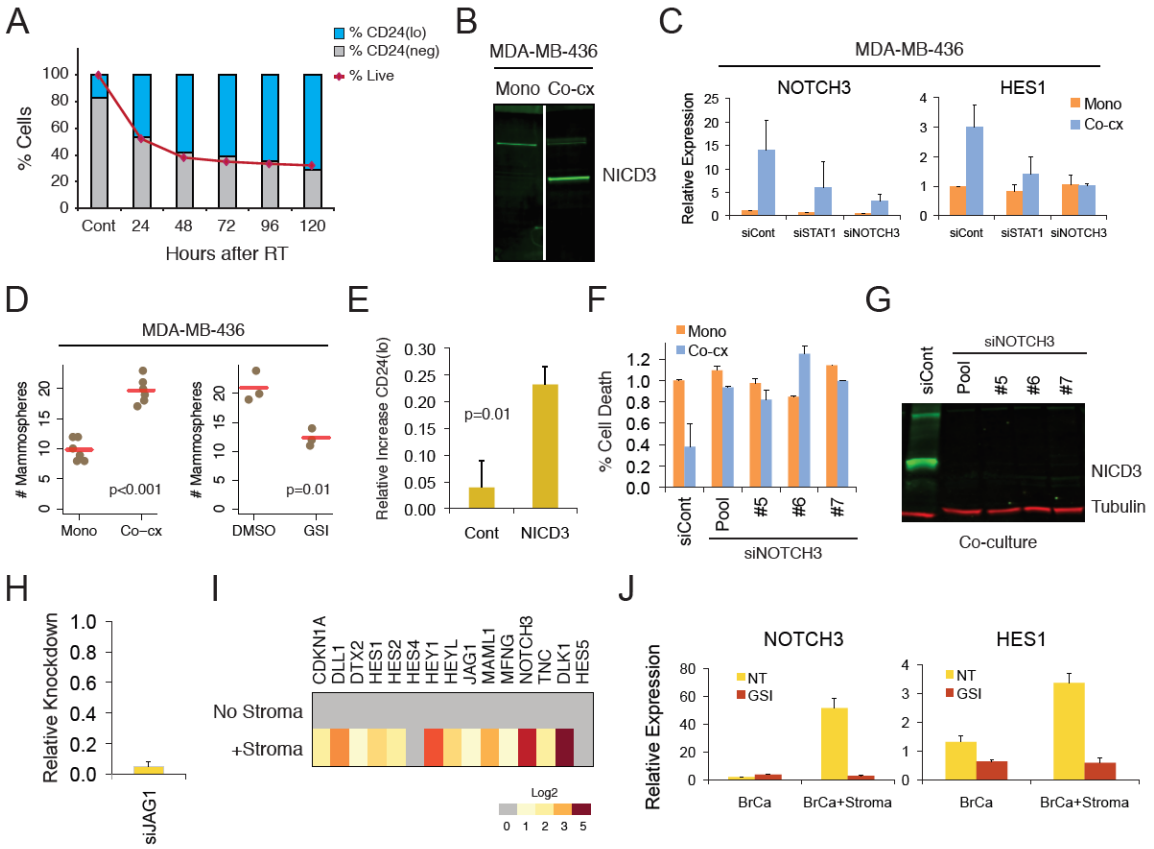

Figure 10. NOTCH3 expands therapy resistant tumor-initiating cells and can be targeted by GSI. A) $CD44^{+}CD24^{low+}$ subpopulation is enriched among surviving cells after RT. The 1833 IRDS-R breast cancer cells were irradiated with 10 Gy and the proportion of $CD44^{+}CD24^{low+}$ cells (blue) and $CD44^{+}CD24^{neg}$ cells (grey) were measured by flow cytometry. The percentage of lives cells relative to an untreated control is also shown (red). **B)** In response to MRC5 stromal cells, MDA-MB-436 IRDS-R breast cancer cells induce NOTCH3 protein, and **C)** upregulate NOTCH target genes in a STAT1- and NOTCH3-dependent manner. Irrelevant lanes in the immunoblot were deleted. Relative expression of indicated NOTCH targets genes with and without knockdown of STAT1 or NOTCH3 is shown (n=3). **D)** Number of mammospheres from MDA-MB-436 IRDS-R after mono- or co-culture (left), or after co-culture following treatment with the GSI DAPT (right). **E)** Increase in $CD44^{+}CD24^{low+}$ subpopulation after ectopic NICD3 expression. Shown are results from flow cytometry using 1833 IRDS-R transfected with a control vector or a doxycycline-inducible NICD3 after addition of doxycycline (n=3). **F)** Knockdown of NOTCH3 using multiple different siRNAs inhibits stroma-mediated protection in co-culture. Knockdown was performed in 1833 IRDS-R. Shown is relative cell death four days after 10 Gy RT (n=2). **G)** Knockdown levels of NOTCH3 using the individual siRNAs are shown

by immunoblot. **H)** Knockdown levels of *JAG1* by qRT-PCR relative to cells transfected with a control siRNA. **I)** NOTCH target genes defined by GSI washout are elevated by MRC5 fibroblasts *in vivo*. Shown is a heat map of relative expression from xenografted 1833 IRDS-R tumors with or without admixed MRC5 stromal cells. Expression is relative to values observed in tumors comprised of 1833 IRDS-R alone. **J)** On-target effects of GSI treatment *in vivo*. 1833 IRDS-R were xenografted with or without MRC5 fibroblasts and mice were treated with or without the GSI DAPT. After 48 hours, tumors were harvested and expression of the indicated genes was examined (n=3). *In vitro* protein and gene expression assays were performed after 48 hrs of culture.

Expression of anti-viral and NOTCH3 pathways in primary human and mouse basal-like breast cancer

To investigate potential disease relevance, we examined whether basal subtype primary human breast cancers show expression and activation of anti-viral/NOTCH3 pathways in ways predicted by our experimental models. We first analyzed protein expression of RAB27B, STAT1 and NOTCH3 in primary human triple-negative breast cancers (TNBC), which overlap with the basal subtype. RAB27B showed strong stromal staining in 71% of TNBC tumors (Figure 11A). By image analysis, the intensity of STAT1 preferentially exhibited a strong tumor-stroma border pattern also in 71% of TNBC samples. For NOTCH3, this tumor-stroma border pattern was more subtle, possibly because NOTCH3 and JAG1 are themselves NOTCH targets, but was discernible in 29% of TNBC cases. Examination of tumors from TNBC patient-derived xenografts (PDX) also demonstrated strong tumor-stroma border patterns for STAT1 and NOTCH3 (Figure 11B). Moreover, breast tumors from the K14cre;BRCA1$^{F/F}$;p53$^{F/F}$ mice, which is a model of basal subtype breast cancer[120], revealed patterns of staining similar to primary human TNBC (Figure 11B). In contrast, a distinct tumor-stroma border pattern was rarely observed in ER+ primary tumors for either STAT1 (14%) or NOTCH3 (0%) and was not observed in ER+ PDX tumors (Figure 12A). Thus, in both human and mouse basal-like tumors, key drivers of anti-viral/NOTCH3 signaling can show preferential localization around sites of tumor-stroma interaction.

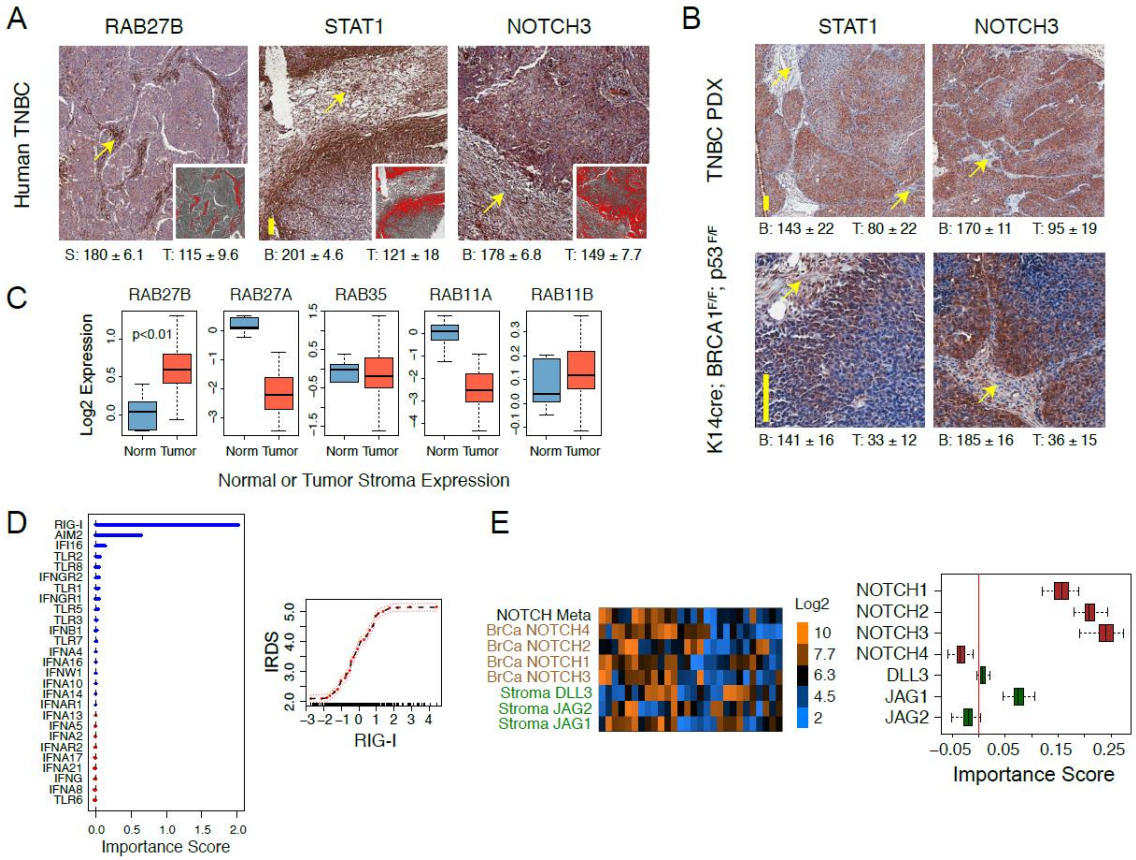

Figure 11. Expression of anti-viral and NOTCH3 pathway predict IRDS and NOTCH target gene expression in primary human and mouse tumors. A) Expression of RAB27B, STAT1, and NOTCH3 in primary human triple negative breast cancer (TNBC), or **B)** in TNBC patient-derived xenografts (PDX) and basal-like tumors from K14Cre;BRCA1$^{F/F}$;p53$^{F/F}$ conditional knockout mice. Arrows show representative areas of stroma. Insets for TNBC images show darker staining regions (red) segmented from lighter regions. Semi-quantitation of expression in stroma (S), tumor (T), or tumor-stroma borders (B) is indicated. Vertical bar is 200 microns. A total of seven primary TNBC tumors were scored. Two out of 2 PDX and 3 out of 3 mouse tumors gave similar results. Shown are representative images and semi-quantitation. **C)** Box-and-whisker plots of expression values for the indicated RABs from primary human breast cancer stroma (Tumor) or normal stroma (Norm) using the Stroma series. **D)** Importance scores (higher is more predictive) from a RF regression model (variance explained: 55.1%) to predict breast cancer IRDS expression using the NKI295 series. Adjusted effect of *RIG-I* on IRDS expression (right). **E)** Heat map and scale showing expression of all available NOTCH receptors in breast cancer (brown) and NOTCH ligands in stroma (green) from the LCMD series. These were used to predict the average expression of NOTCH target genes in breast cancer (variance explained: 30.2 ± 1.1%) defined by GSI washout (NOTCH Meta). On the right are importance scores from Monte Carlo replications.

To investigate whether similarities in localization of anti-viral and NOTCH3 proteins between *in vivo* tumors and *in vitro* models are accompanied by expected gene expression

changes in IRDS and NOTCH target genes, we used three distinct sets of gene expression data from primary human breast cancer. The Stroma series is a 53-sample set of breast cancer stroma and adjacent normal stroma, the NKI295 series is comprised of 295 primary human breast tumors confirmed to be largely cancer cells, and the LCMD series contains 28 paired primary tumor and stroma samples that were separated by laser-capture microdissection. Consistent with breast cancer inducing stromal RAB27B, the Stroma series revealed higher *RAB27B* expression in tumor stroma compared to adjacent normal, while other RABs on average had similar or decreased expression (Figure 11C). Using the NKI295 series, *RIG-I* was the best predictor of IRDS status compared to other PRRs and interferon-related genes (Figure 11D). Of all available NOTCH family receptors and ligands on the LCMD series array (Figure 11E), breast cancer *NOTCH3* and stromal *JAG1* were the best at predicting expression of breast cancer NOTCH targets (Table 4) as measured by their average expression (metagene). Moreover, when breast cancer *NOTCH3* was paired with breast cancer *RIG-I*, and stromal *JAG1* was paired with stromal *RAB27B*, high expression of the two pairs cooperatively predicted high NOTCH metagene expression (Figure 12B-C). In total, these data indicate that gene expression changes attributed to the anti-viral and NOTCH3 pathways can be observed in primary tumors.

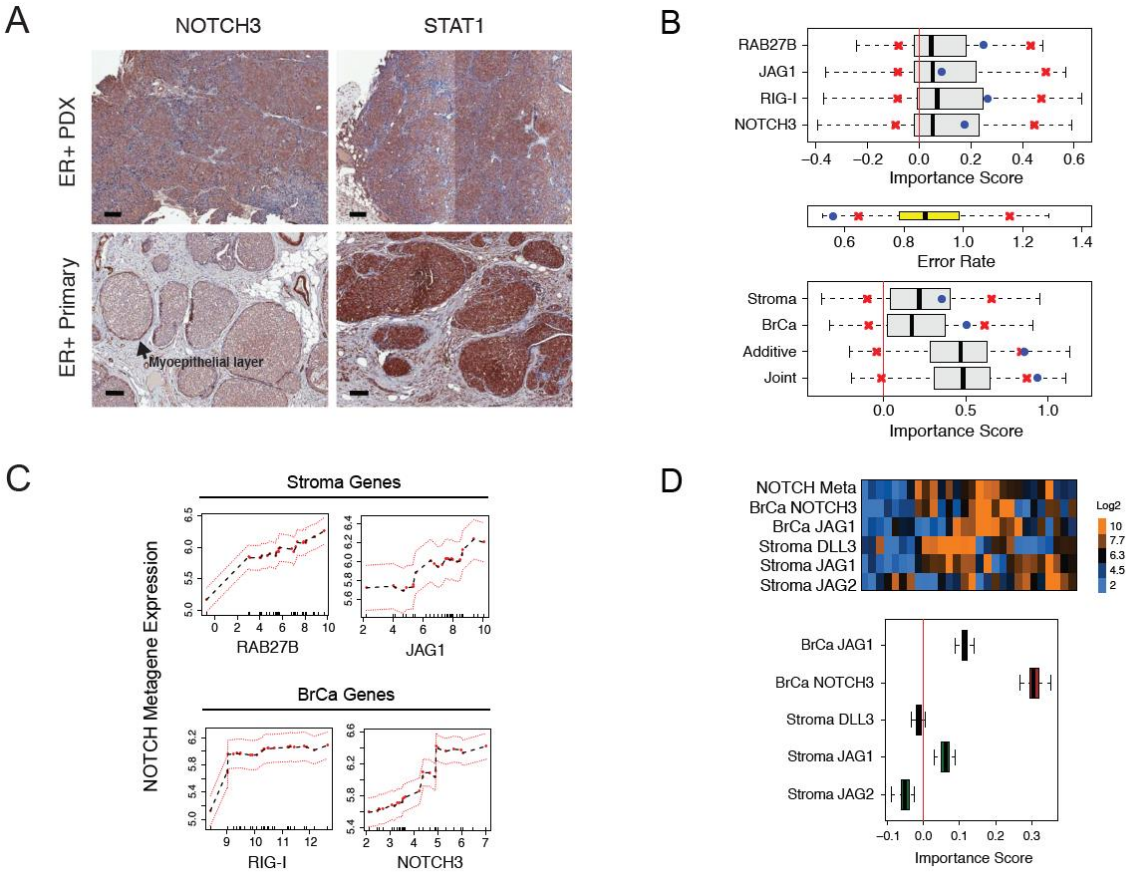

Figure 12. Stromal *RAB27B* and *JAG1*, and breast cancer *RIG-I* and *NOTCH3*, cooperate to predict expression of breast cancer NOTCH target. A) STAT1 and NOTCH3 do not preferentially localize to tumor-stroma borders in ER-positive breast cancer. PDX tumors are on the top row and primary human tumors are on the bottom row. Black arrow marks a myoepithelial layer (non-cancer cells) that shows NOTCH3 staining. Black bar is 200 microns. For primary human tumors, 7 samples were analyzed. Shown are representative images. **B)** The mechanistic interactions between stroma and breast cancer genes can be inferred by statistical interactions. Statistical interactions are detected when the joint importance score of multiple genes is greater than the sum of individual importance scores. Stromal genes, *RAB27B* and *JAG1*, and breast cancer genes, *RIG-I* and *NOTCH3*, were used in a RF regression model to predict breast cancer NOTCH activation (model explains 35.3 ± 1.0% (SD) of the total variance). Top graph shows importance scores of each gene (blue dots). Middle plot shows model error rate (lower is better) for all pathway genes (blue dot). Bottom graph displays importance scores (blue dots) for the stromal genes, breast cancer genes, the sum of these values (Additive), and the joint importance score for all genes (Joint). For comparison, distribution of importance scores (grey) or error rates (yellow) for random genes is shown using box-and-whisker plots with the 5% and 95% quantiles marked (red X). **C**) Adjusted effects of stromal and breast cancer genes on breast cancer NOTCH metagene expression from the RF model. Red dashed lines are ± two standard errors. **D)** *NOTCH3* together with either breast cancer *JAG1* or stromal *JAG1* predicts NOTCH metagene expression. The LCMD series was used to predict breast cancer NOTCH metagene expression. *NOTCH3* and *JAG1* in breast cancer (BrCa) and NOTCH ligands in stroma were used as x-variables

in a RF regression model. Gene expression is displayed in the heat map. Below the heat map is a plot of the distributions of importance scores from 100 Monte Carlo replications (used to obtain better estimates from a small sample size). The RF model explains 26.7 ± 1.2% (SD) of the total variance.

Because STAT1 enhances the transcriptional response to NOTCH3 in IRDS-R breast cancer, high NOTCH target gene expression is expected to associate with high NOTCH3/JAG1 and high STAT1 activity in basal subtype tumors. To examine this, we used the NKI295 series and substituted stromal *JAG1* with breast cancer *JAG1*, as stromal genes cannot be evaluated and breast cancer *JAG1* was comparable to stromal *JAG1* at predicting NOTCH target gene expression (Figure 12D). For STAT1 activity, we used the clinical IRDS classifier since it includes *STAT1*, and STAT1 both regulates (Figure 1H) and correlates with IRDS status (Spearman's correlation coefficient 0.79, $p < 0.001$). As expected, increasing *NOTCH3* resulted in higher likelihood of NOTCH pathway activation (Figure 13A). The probability was highest when *NOTCH3*, *JAG1*, and IRDS were all high, particularly for basal subtype tumors (red dots, upper right plot), a result that was recapitulated in basal-like tumors from the K14cre;BRCA1$^{F/F}$;p53$^{F/F}$ mouse model (Figure 13B). Thus, these results suggest that anti-viral signaling preferentially facilitates the transcriptional response to NOTCH3 in primary human and mouse basal subtype tumors.

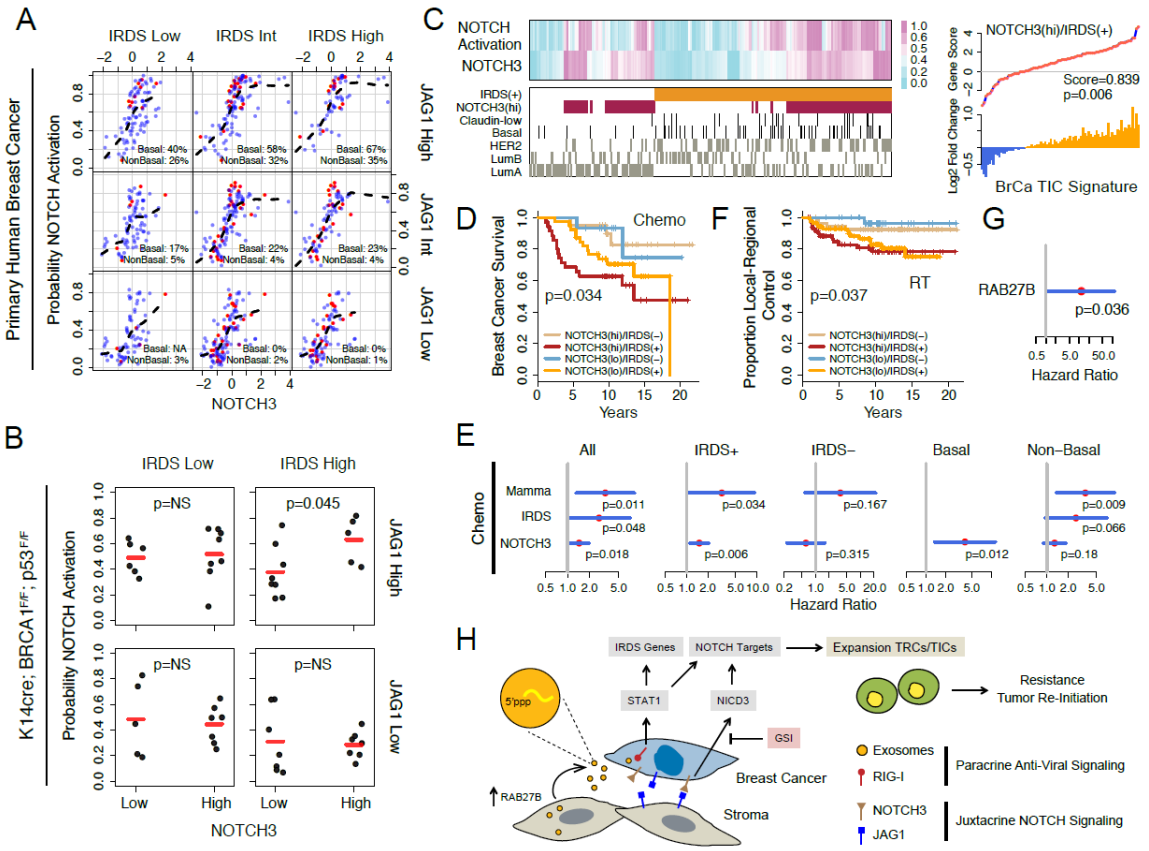

Figure 13. NOTCH3 and STAT1/IRDS cooperate to predict NOTCH target genes and clinical resistance to chemotherapy and RT preferentially in basal-like breast cancers. Prediction of NOTCH target gene expression by IRDS and *NOTCH3*/*JAG1* in **A)** primary human tumors and in **B)** basal-like tumors from the K14Cre;BRCA1$^{F/F}$;p53$^{F/F}$ conditional knockout mice. For human tumor analysis, the NKI295 series was used. The probability of NOTCH pathway activation as measured by the NOTCH metagene is shown on the y-axis with probabilities for basal (red dots) or non-basal (blue dots) tumors displayed separately. The percentage of tumors with greater than 80% probability of NOTCH activation is inset. A LOWESS regression line (black dashed line) is shown. IRDS and *JAG1* were equally divided into low, intermediate, and high values. For mouse tumor analysis, IRDS, *NOTCH3*, and *JAG1* expression were dichotomized into only high and low due to smaller sample size. Mean value is marked by red line. **C)** Heat map showing probabilities of NOTCH activation and *NOTCH3* expression for each patient (columns) in the NKI295 series. All values are scaled between 0 and 1. Hatches below the heat map show status for IRDS(+), *NOTCH3*(hi), and the indicated molecular subtypes. On the right is Gene Set Analysis for the same TIC signature used in Fig. 5A and compares *NOTCH3*(hi)/IRDS(+) tumors to those that are *NOTCH3*(lo) and/or IRDS(-). **D)** Survival after adjuvant chemotherapy of patients from the NKI295 series stratified by *NOTCH3* and IRDS. Overall p-value is shown. **E)** Hazard ratios and 95% confidence intervals from Cox regression analysis for breast cancer survival using *NOTCH3* as a continuous variable, IRDS status (positive vs. negative), and MammaPrint (Mamma) metastasis signature status (positive vs. negative). All patients received adjuvant chemotherapy. Hazard ratio for *NOTCH3* is per unit increase in expression. Analyses are also stratified by IRDS status

and basal vs. non-basal subtype tumors. Values are not shown if there are too few patients in the group. **F)** Relapse in irradiated region (local-regional control) after adjuvant RT. **G)** Hazard ratio from Cox regression for relapse in the Stroma series using stromal *RAB27B* as a continuous variable. **H)** Model of the tumor-stroma anti-viral/NOTH3 pathways controlling RT/chemo resistance.

Anti-viral/NOTCH3 pathway genes predict clinical resistance to chemotherapy and RT

Having shown that *NOTCH3* and the IRDS contribute to predicting NOTCH activation in the NKI295 series, we examined whether both pathways function together to predict clinical resistance to chemotherapy and RT. *NOTCH3* was dichotomized using a mean cut-point, and for consistency, IRDS status was defined using our original seven-gene clinical classifier. Interestingly, 31% of *NOTCH3*(hi)/IRDS(+) tumors belonged to either the basal or claudin-low subtype (Figure 13C; $p < 0.01$ by chi-squared test), two basal-like subtypes that are enriched in cancer stem cell-like features[121]. Consistent with this, *NOTCH3*(hi)/IRDS(+) tumors showed enrichment of the same breast cancer TIC signature upregulated in IRDS-R cells after co-culture (Figure 13C and 9A), suggesting these tumors could also contain TRCs. Indeed, among the patients who received chemotherapy, those with the highest risk of breast cancer-specific death were *NOTCH3*(hi)/IRDS(+) (Figure 13D). Cox regression using continuous values rather than arbitrary cut-offs for *NOTCH3* demonstrated that higher *NOTCH3* augmented risk only among patients with tumors that were IRDS(+) and/or basal subtype (Figure 13E). The effect of both pathways on survival was distinct from metastasis risk as both were independent of the MammaPrint metastasis signature[122], and neither were predictive among patients not receiving chemotherapy (Figure 14A). *NOTCH3*(hi)/IRDS(+) patients were also the most likely to fail RT (Figure 13F). Finally, using the Stroma series, we found that high stromal *RAB27B* predicted poor survival, while other RABs showed no association (Figure 13G and Figure 14B). In total, the anti-viral/NOTCH3 pathways predict clinical resistance, particularly for basal subtype tumors.

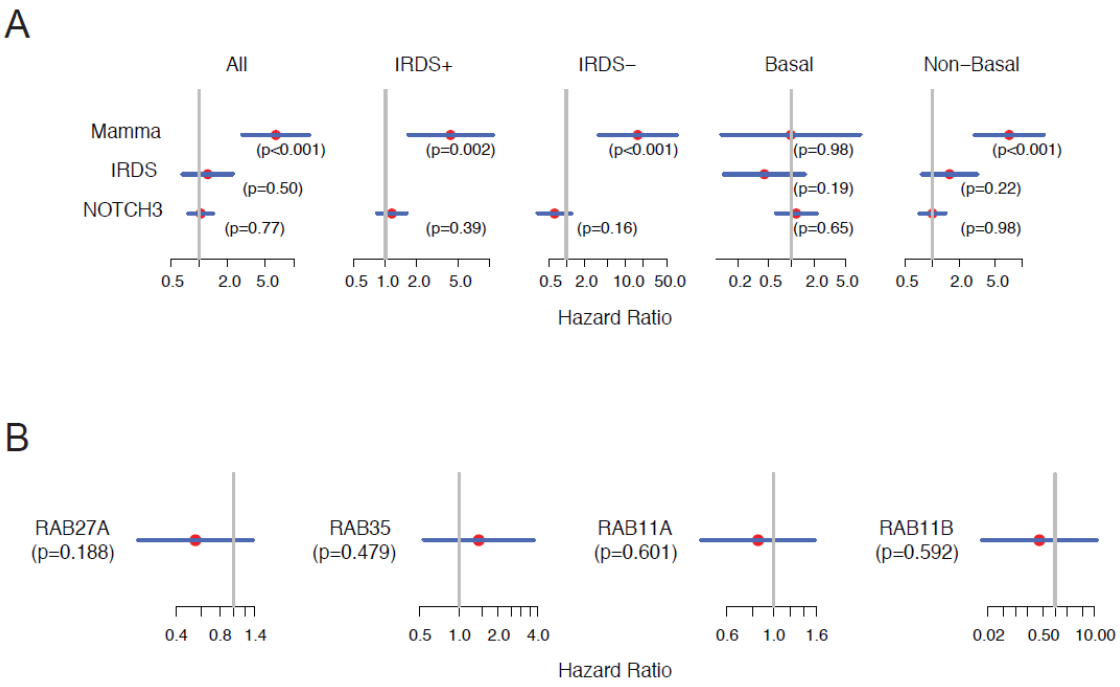

Figure 14. Breast cancer survival is neither predicted by IRDS and *NOTCH3* in the absence of chemotherapy nor by multiple RABs. A) *NOTCH3* and IRDS do not predict survival in patients who do not receive chemotherapy. Cox regression for breast cancer survival using *NOTCH3* as a continuous variable, IRDS status (positive vs. negative), and MammaPrint (Mamma) metastasis signature status (positive vs. negative). Shown are hazard ratios (red dot), 95% confidence intervals (blue line), and p-values for patients who did not receive chemotherapy. Since *NOTCH3* is a continuous variable, its hazard ratio is per unit increase in *NOTCH3* expression. Analyses are also stratified by IRDS status and basal vs. non-basal subtype. **B)** Other RABs besides *RAB27B* that have been implicated in the regulation of exosome secretion do not predict breast cancer relapse. The indicated RAB gene from the Stroma series was used as a continuous variable in Cox regression.

Discussion

We demonstrate that interaction of stromal cells with breast cancer cells results in paracrine and juxtacrine signaling events to drive stroma-mediated resistance (Figure 13H). First, stromal cells increase RAB27B and transfer 5'-triphosphate RNA in exosomes to activate RIG-I anti-viral signaling in breast cancer cells. Second, breast cancer cells induce NOTCH3 to make the receptor available for engagement with JAG1. The paracrine and juxtacrine pathways converge as STAT1 facilitates the transcriptional response to NOTCH3, resulting in the expansion of therapy resistant TICs. Consistent with this, stromal cells mediate both decreased cell death and continued tumor growth after RT. Blocking the NOTCH pathway re-sensitizes tumors to RT, rendering mice tumor-free. These biological interactions between anti-viral and NOTCH3 signaling are mirrored by statistical evidence that they jointly influence NOTCH activation and treatment resistance in primary human basal-like breast cancers.

The role of exosomes in cancer as mediators of cell-cell communication with the microenvironment has gained increasing attention. Functionally, exosomes have intriguing and elaborate roles in cancer progression and can transfer a variety of proteins, DNA, and RNA that can explain some of their effects[84,123]. Our data suggests that RNA contained within exosomes is enriched in non-coding transcripts and can activate RIG-I. Consistent with the known properties of RIG-I stimulatory viral RNA[45], 5'-triphosphates are similarly required for exoRNA to activate RIG-I. Sequencing exoRNA revealed no evidence of viral transcripts, rather exoRNA was enriched in transposable elements and other repetitive sequences, many of which are known or putative RNA polymerase III transcripts. RNA polymerase III transcripts can contain 5'-triphosphates and likely are largely non-coding[117]. Although the quantity and diversity of non-coding human transcripts is large[124] and RIG-I is not known to overtly show sequence-specific binding, the

enrichment for transposable elements and other repetitive elements in exosomes is interesting given the viral origins of some of these sequences[116]. Despite prolific incorporation into the genome, it is notable that these elements are normally transcriptionally silenced but can be de-repressed to high levels in cancer[125]. When expressed, these elements can also exhibit subcellular partitioning into the nucleus and the cytoplasm[126]. Accumulation of transposable elements can result in autoimmunity with elevated ISGs in normal tissue[56]. Thus, our results suggest that non-coding RNA found in exosomes and similar microvesicles[127,128] may coax anti-viral responses to influence treatment resistance, potentially adding to the increasing evidence that atypical RNA transcripts can contribute to human disease.

Both anti-viral/interferon signaling and the NOTCH pathway are known to regulate the maintenance of normal and cancer stem-like cells. Interestingly, inflammatory/stress signaling involving STAT can function with NOTCH signaling in development and in homeostasis to influence self-renewal[35,129] (Kux and Pitsouli, 2014). For example, in Drosophila, inflammation and stress in the midgut leads to compensatory intestinal stem cell proliferation that is regulated by STAT. STAT can be activated non-cell autonomously by damaged cells, while distinct levels of NOTCH controls intestinal stem cell commitment and differentiation. Our findings that stromal fibroblasts can secrete exosomes to induce anti-viral signaling in breast cancer cells, and that STAT1 promotes NOTCH3-driven expansion of therapy resistant TICs, highlight an unexpected way that these two evolutionarily conserved pathways converge to influence cell fate in cancer.

The mechanisms whereby basal-like tumors are preferentially protected by stroma through anti-viral/NOTCH3 signaling require further investigation. One mechanism indicated herein may be the capacity of basal-like breast cancer cells to coerce stromal cells to augment exosome secretion. RAB27B is uniquely induced in stromal cells by IRDS-R but not IRDS-NR breast cancer, and evidence from primary human tumors also

distinguishes it from other RABs. However, alternative methods to either increase exosome production in the microenvironment or instigate similar anti-viral signaling (e.g., immune cells) may also exist. Other factors that might contribute to differences in the way basal-like tumors respond to stroma include defects in the BRCA1 pathway, which have been associated with basal and claudin-low tumors[121]. It is notable that two of the IRDS-R breast cancer cell lines have reported mutations in BRCA1[130], and BRCA1 null mouse mammary tumors show evidence for the anti-viral/NOTCH3 pathway. As a cell extrinsic mechanism of resistance, the protective effect of stroma may be critical for certain breast cancers with intrinsic DNA damage sensitivity.

Extrapolating the relevance of findings from model systems to human disease is often challenging. In this study, extensive statistical modeling of primary tumor expression data was used to support the mechanisms dissected from experimental models. Specifically, primary tumor data suggest that 1) RIG-I is a driver of the IRDS, 2) breast cancer NOTCH3 and stromal JAG1 are important regulators of NOTCH target gene expression, 3) NOTCH3 and STAT1 are localized to sites of tumor-stroma interaction, 4) STAT1 facilitates the transcriptional response to NOTCH3, 5) IRDS/STAT1 and NOTCH3 identify patients with both high NOTCH target genes and chemo/RT resistant tumors, and 6) high IRDS/NOTCH3 is preferentially observed in basal and claudin-low subtype primary tumors, which are known to be enriched in cancer stem cell-like features[121]. These observations, combined with pre-clinical studies showing that GSI can reverse the effects of stromal cells on TRC expansion, tumor growth after genotoxic damage, and survival suggest the disease relevance of our findings. Together, the anti-viral and NOTCH3 pathways may serve as companion biomarkers and druggable targets for stroma-mediated resistance.

CHAPTER 3: VIRUS MIMICRY IN THE TUMOR MICROENVIRONMENT ACTIVATES RIG-I THROUGH UNSHIELDING OF ENDOGENOUS RNA IN EXOSOMES

Sections of this chapter have been adapted from the following manuscript: Nabet, B.Y., Qiu, Y., Shabason, J.E., Wu, T.J., Yoon, T., Kim, B.C., Marcotrigiano, J., and Minn, A.J. Stromal cells utilize viral mimicry to regulate breast cancer therapy resistance through exosomes and non-coding RNA. In revision at *Cell*.

Introduction

The dynamic interaction and co-regulation of critical signaling pathways between cancer cells and stromal cells of the tumor microenvironment can significantly influence tumor progression and therapy response[13]. Through reciprocal signaling between these heterotypic cell types, cancer cell proliferation, cell death, and metabolism can be altered. Paracrine and juxtacrine signaling components that can be employed between cancer and stromal cells include RAS, WNT, NOTCH, STAT, and several others[88,131,132]. The importance of these tumor-stromal signaling cascades may be to help amplify critical oncogenic pathways in cancer cells to promote tumor progression, metastasis, and resistance [15]. However, the mechanisms that govern how cancer and stromal cells interact to accomplish these events are not well understood.

Another pathological condition that favors effective cell-cell communication to amplify critical signaling pathways is viral infection. Upon infection, cells induce an anti-viral response that includes the upregulation of interferon-stimulated genes (ISGs)[48]. This response is driven by the recognition of viral RNA by pattern recognition receptors (PRRs), such as RIG-I [44]. Recent evidence reveals that in addition to cell intrinsic anti-viral responses that occur after viral infection, mechanisms exist to propagate an anti-viral response from infected to uninfected cells. For example, viral RNAs can be packaged into exosomes [62,63], small extracellular vesicles that originate in multivesicular bodies and are also implicated in a myriad of processes related to cancer progression[82,86,133]. Secretion and transfer of exosomes to bystander cells can then result in recognition of exosome-transferred viral RNA by PRRs[78–80]. This culminates in ISG induction within uninfected cells and tissue-level amplification of the anti-viral response.

Across many common human cancers, a large proportion of patients have tumors that unexpectedly express high levels of ISGs[38]. A subset of breast cancer cells, which we

denote as ISG responders (ISG-Rs), can induce ISGs through cell-cell contact with stromal fibroblasts and the subsequent secretion of exosomes[132]. These exosomes contain RNA (exoRNA) that is enriched in non-coding transcripts. Upon transfer to ISG-R breast cancer cells, the exoRNA stimulates RIG-I, resulting in ISG induction and STAT1 activation. STAT1 amplifies the NOTCH3 transcriptional response, resulting in expansion of tumor-initiating cells and therapy resistance. Consistent with these experimental findings, patients with tumors expressing high levels of ISGs are more likely to relapse after chemotherapy or radiation therapy. Thus, a subset of breast cancer cells can amplify oncogenic pathways through anti-viral signaling resulting from stromal cell contact. Activation of breast cancer RIG-I by exoRNA after encountering stromal cells is reminiscent of how viral infection of one cell population can propagate anti-viral responses to neighboring cells. Similar examples of PRRs recognizing exoRNA in the tumor microenvironment have been reported to influence cancer progression[101,102]. However, such potential examples of virus mimicry within a tumor raises questions on the similarities between cancer-associated anti-viral signaling and virus-mediated signaling. Moreover, given that cancer-associated anti-viral signaling is occurring in a sterile microenvironment, the nature of the endogenous RNA and how it activates RIG-I are unanswered questions.

There are multiple properties that RIG-I utilizes to distinguish self from non-self RNA. Typically, RIG-I recognizes cytoplasmic double-stranded RNA that is 5' triphosphorylated, generally short (<300bp), and has a blunt 5' end[45,52]. For viral RNAs, polyuridine motifs can favor recognition (Saito et al., 2008), while RNA modifications such as 2-O-methylation can critically prevent RIG-I binding to 5' capped cellular RNAs[57,58]. However, much of the RNA features and requirements for optimal RIG-I activation are based on synthetic and/or artificial RNAs in vitro. Emerging evidence indicates that endogenous RNA can function as a damage-associated molecular pattern (DAMP) to activate PRRs under a variety of pathological conditions, such as chemotherapy[40–42],

radiation[103,104], and autoimmunity[55,105]. How endogenous RNAs can function as DAMPs to activate PRRs while avoiding recognition under non-pathological conditions is not well understood.

In this study, we investigate the concept of virus mimicry whereby breast cancer cells, like viruses, can provoke an anti-viral response in surrounding stromal cells. We examine how this leads to deployment of endogenous stromal RNA as a RIG-I-activating DAMP, resulting in the propagation of an anti-viral response to enhance tumor progression and therapy resistance.

Results

Stromal activation by breast cancer cell interaction is accompanied by an anti-viral response and stromal exosome transfer

Previously, we demonstrated that breast cancer interaction with stromal fibroblasts increases the production of stromal exosomes. Upon transfer to breast cancer cells, the RNA in the exosomes (exoRNA) stimulates breast cancer RIG-I to initiate an anti-viral response that subsequently promotes resistance to radiation and chemotherapy. In this study, we sought to more closely examine similarities between this anti-viral response initiated by tumor and stromal cell interaction with how viruses instigate an anti-viral response that spreads from infected to uninfected cells. We first investigated major transcriptomic changes resulting from heterotypic interaction between MRC5 normal lung fibroblasts and ISG-R breast cancer cells, which induce ISGs upon co-culture with stromal cells[132]. This revealed that heterotypic cell interaction leads to stromal activation characterized by a transcriptional response dominated by upregulation (Figure 15A, left). Among these transcripts is an enrichment for hallmark gene sets[134] for MYC and RAS oncogenic signaling, glycolysis, and cell cycle progression (Figure 15B, left). Stromal cells additionally induce multiple ISGs, and this was also observed in ISG-R breast cancer cells (Figure 15A). In fact, IFN signaling is among the predominant hallmark gene sets enriched

after co-culture in both cell types (Figure 15B). ISG-R breast cancer cells also show evidence for reciprocal RAS activation and enhanced expression of EMT genes expected to favor invasion, metastasis, and therapy resistance[135]. Thus, these data suggest that besides promoting aggressive features in breast cancer cells, heterotypic interaction leads to stromal activation events accompanied by a reciprocal anti-viral response.

To examine if breast cancer interaction also mimics the ability of viruses to instigate exosome transfer, we labeled stromal cells with a stably expressed CD81-RFP exosome reporter (Figure 15C). This confirmed a high level of exosome transfer from stromal cells to 1833 ISG-R breast cancer cells, which is a metastatic derivative of MDA-MB-231[112]. In contrast, co-culture of stromal cells with breast cancer cells that fail to induce ISGs, which we previously defined as ISG non-responders (ISG-NRs), show only modest transcriptomic changes in stromal cells, no stromal ISG induction (Figure 16A, left), and minimal exosome transfer to breast cancer cells (Figure 15C). Accordingly, no anti-viral response occurs in ISG-NR breast cancer cells after co-culture (Figure 16A, right). Thus, like viruses, ISG-R breast cancer cells not only can coerce an anti-viral response in stromal cells but can also promote exosome transfer to propagate anti-viral signaling.

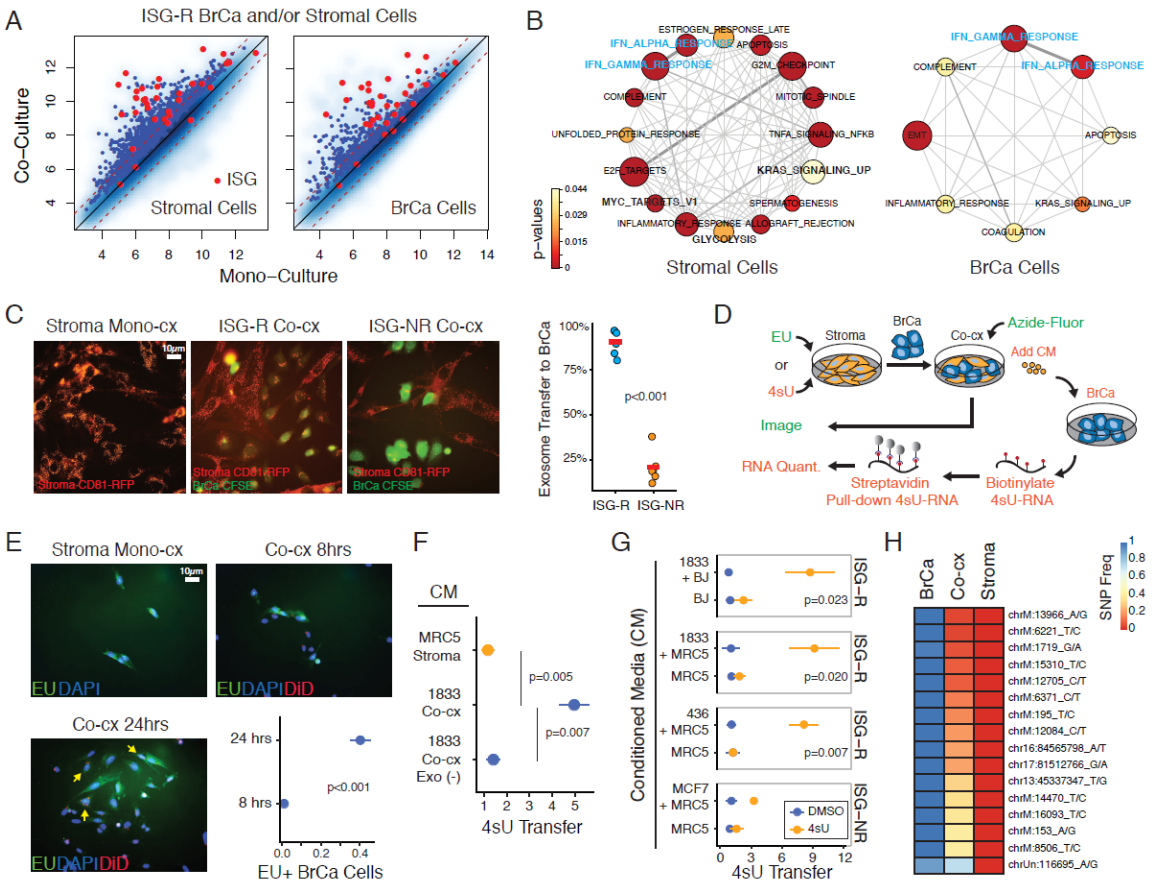

Figure 15. Stromal cell activation and ISG induction occurs upon breast cancer cell interaction and results in stromal RNA transfer via exosomes. A) Gene expression of MRC5 fibroblasts (Stromal Cells) and ISG-R 1833 breast cancer cells (BrCa Cells) after co-culture versus mono-culture. Genes indicated in red are cancer-associated ISGs. Genes in blue are significantly upregulated either in stromal cells (left) or ISG-R breast cancer cells (right) after co-culture. **B)** Gene set analysis showing significantly enriched hallmark gene sets after co-culture versus mono-culture in fibroblasts and ISG-R breast cancer cells. Size of circles is proportional to number of genes, and circles are color-coded by FDR-adjusted p-value as indicated in the legend. Thickness of lines is proportional to genes shared between sets. Anti-viral response pathways (blue) and select stromal activation pathways (bold) are highlighted. **C)** MRC5 fibroblasts transduced with CD81-RFP to track exosome transfer were co-cultured with CFSE-labeled ISG-R 1833 or ISG-NR MCF7 breast cancer cells. Exosome transfer to breast cancer was quantified as percentage of breast cancer cells with RFP foci (right). **D)** Schema for measuring RNA transfer from stromal to breast cancer cells utilizing the uridine analog EU for fluorescence microscopy (green) or 4sU for streptavidin pull-down (orange). **E)** MRC5 fibroblasts were labeled with EU and co-cultured with DiD lipid-labeled 1833 breast cancer cells. Shown are representative images, with yellow arrows indicating EU-positive 1833 cells, and quantitation. **F)** Conditioned media (CM) from 4sU-labeled MRC5 fibroblasts grown in mono-culture (Stroma, orange) or co-cultured with 1833 breast cancer cells (Co-cx, blue) was isolated. Shown is relative 4sU RNA transfer to mono-cultured 1833 breast cancer

cells after addition of CM or exosome depleted CM (Co-cx Exo(-) CM) (n=5). Comparisons are made to DMSO control. **G)** Same as in (F) except CM was isolated from MRC5 or BJ 4sU-labeled fibroblasts left in mono-culture or co-cultured with indicated ISG-R or ISG-NR breast cancer cells. Shown is relative 4sU RNA transfer after CM addition to each of the mono-cultured breast cancer cells (n=3). **H)** Allelic frequency of exoRNA SNPs from exosomes isolated from 1833 breast cancer (BrCa), MRC5 fibroblasts (Stroma), or from co-culture of both cell types (Co-cx). Analysis is based on SNPs present in exoRNA from breast cancer cells and not present in fibroblasts. Unless indicated, error bars are SEM of biological replicates and *p<0.05, **p<0.01, ***p<0.001.

Stromal RNA is transferred to breast cancer cells by exosomes to mediate an anti-viral response

After viral infection, viral RNA from infected cells can be packaged into exosomes for subsequent transfer to uninfected cells. To examine if RNA from stromal cells are similarly transferred to breast cancer cells by exosomes, we metabolically labeled MRC5 stromal RNA with 5-ethynyl uridine (EU) prior to co-culture with ISG-R 1833 breast cancer cells that were fluorescently marked with lipid dye (Figure 15D). After 24 hours, over 40% of breast cancer cells acquired stromal cell RNA as measured by EU-modification by azide-linked fluorescein (Figure 15E). To assess the role of exosomes in this transfer, stromal cell RNA was similarly labeled with 4-thiouridine (4sU) prior to co-culture with breast cancer cells (Figure 15D and 16B). Application of the conditioned media (CM) from these co-cultures to mono-cultured breast cancer cells also resulted in stromal RNA transfer, as determined by streptavidin pull-down of biotinylated 4sU-labeled stromal RNA, but not when exosomes were depleted from the CM (Figure 15F). Exosome-mediated transfer of MRC5 stromal RNA was also observed using another ISG-R breast cancer cell line, MDA-MB-436, and from co-cultures using BJ fibroblast cells (Figure 15G). In contrast, markedly less stromal RNA was transferred by exosomes using CM from co-cultures with the ISG-NR breast cancer cell line MCF7 (Figure 15G).

To corroborate the transfer of stromal RNA by exosomes, we also performed exoRNA SNP analysis using exosomes from mono-cultures of either ISG-R 1833 breast cancer cells or MRC5 stromal cells and compared SNP allelic frequencies to the exoRNA

from co-culture (Figure 15H). Multiple SNPs, primarily from mitochondrial RNA, were discovered to have an allelic frequency of near one in the exoRNA from breast cancer cells but near zero in stromal exoRNA. Examination of exoRNA from co-culture revealed that most of these SNPs maintained a frequency closer to zero, consistent with the exoRNA primarily originating from stromal cells. In total, these results suggest that similar to transfer of viral RNA from infected to uninfected cells, cellular RNAs are transferred from stromal to breast cancer cells in an exosome-dependent manner.

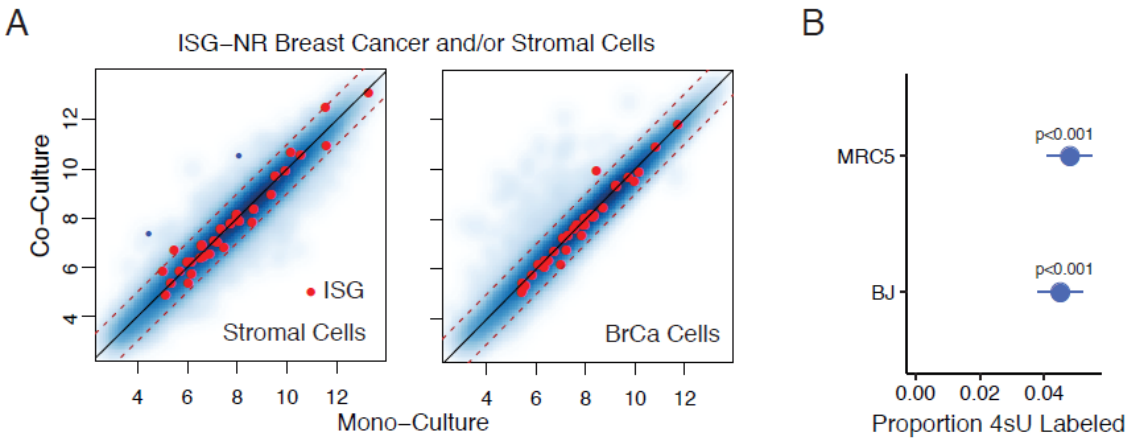

Figure 16. ISG-NR breast cancer cells do not induce ISGs in stromal cells. A) Gene expression of MRC5 fibroblasts (Stromal Cells) and ISG-NR breast cancer cells (BrCa Cells) after co-culture versus mono-culture. Genes indicated in red are ISGs. Genes color-coded blue are significantly upregulated in stromal cells after interaction with ISG-NR breast cancer cells. **B)** Percentage of 4sU-labeled RNA in indicated fibroblasts after 24 hours compared to total RNA (n=3). Error bars are SEM of biological replicates.

5' triphosphate stromal exoRNA activates breast cancer RIG-I

Classification of non-ribosomal exoRNA transcripts from stromal and breast cancer cell co-cultures reveals an enrichment in non-coding RNAs compared to cellular RNA (Figure 17A). These non-coding RNAs include repeat and transposable elements, snRNA, srpRNA, and others, but no viral RNAs were detected. Previously, we demonstrated that upon transfection this exoRNA activates the pattern recognition receptor RIG-I to induce ISGs in recipient breast cancer cells, and this activity requires a

5’ triphosphate (5’ppp) moiety. Thus, although the non-ribosomal portion of exoRNA demonstrates significant complexity, functional studies suggest that exoRNA ligands responsible for the breast cancer anti-viral response are 5’ppp exoRNA that binds to RIG-I. To confirm this notion, we utilized CRISPR/Cas9 to knockout RIG-I in breast cancer cells and re-expressed either wild-type (WT) RIG-I or RIG-I with alanine substitution mutations in key lysine residues (K858 and K861) that make contacts with the 5’ppp motif (RIG-$I^{K858/861A}$)[136] (Figure 18A-B). Co-culture-derived exosomes were purified (Figure 18C-D) and transfection of the exoRNA failed to induce ISGs in RIG-I KO breast cancer cells (Figure 17B). Re-expression of WT RIG-I rescued this defect whereas RIG-$I^{K858/861A}$ was markedly less effective at restoring activity. In contrast, cellular RNA failed to induce ISGs regardless of RIG-I status. Consistent with these findings, addition of exoRNA but not equimolar amounts of cellular RNA to recombinant RIG-I stimulates RIG-I ATP helicase activity as measured by ATP hydrolysis (Figure 17C). Thus, like the recognition of viral 5’ppp RNA, these results provide evidence that 5’ppp exoRNA from stromal cells can directly activate RIG-I to induce an anti-viral response.

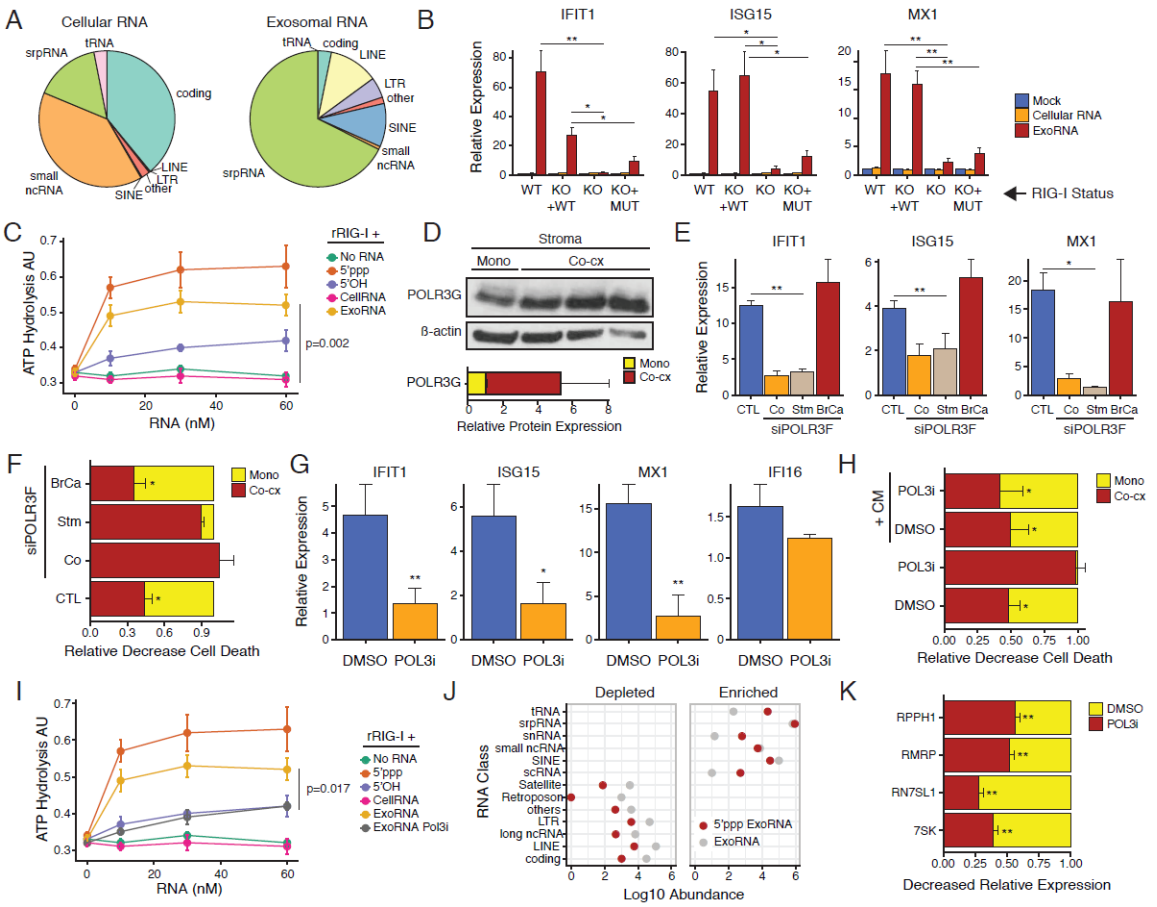

Figure 17. Stromal POL3-derived exoRNA activates breast cancer RIG-I in a 5'triphosphate-dependent manner. A) Distribution of RNA classes found in cellular RNA and exosome RNA by RNA-seq after co-culture of 1833 breast cancer cells with MRC5 stromal cells. Ribosomal RNA counts were removed. **B)** ISG expression after transfection of co-culture exoRNA or co-culture cellular RNA into 1833 control cells (WT), RIG-I knockout 1833 cells (KO), or RIG-I KO 1833 cells restored with either wild-type (KO + WT) or RIG-I$^{K858/861A}$ 5'ppp binding mutant (KO + MUT) (n=5). Baseline was established by mock transfection (see legend). **C)** ATP hydrolysis assay for RIG-I activation in response to increasing amounts of the indicated RNA. ExoRNA and cellular RNA are from co-culture of 1833 and MRC5 cells. 5'OH is a negative control and 5'ppp is a positive control (n=3). **D)** Immunoblot for RPC32 (POLR3G) and β-actin in sorted MRC5 fibroblasts after mono- or co-culture (top). Quantification of POLR3G protein expression relative to β-actin after co-culture (bottom). **E)** Expression of ISGs in sorted 1833 cells or **F)** RT-mediated cell death in 1833 cells after co-culture with MRC5 cells (CTL) or after siRNA knockdown of POLR3F in 1833 (BrCa), MRC5 (Stm), or both cell types (Co). Gene expression values are relative to sorted 1833 cells grown in mono-culture, and cell death was assessed 4 days after 10 Gy RT (n=3). **G)** ISG expression in 1833 cells after addition of CM from DMSO or POL3 inhibitor (POL3i) treated co-cultures. Values are relative to 1833 cells grown in mono-culture (n=3). **H)** RT-mediated cell death of 1833 cells in mono-culture (Mono) or co-culture with MRC5 cells (Co-cx). Cells were grown in the presence of DMSO or POL3i and with (+CM) or without rescue using co-culture CM (n=3). **I)** ATP hydrolysis assay for RIG-I activation as shown in (C) except exoRNA from POL3i-treated co-cultures

was additionally assessed (n=3). **J)** Abundance (Log10) of RNA classes in 5'ppp-seq compared to exoRNA-seq. RNA classes depleted in 5'ppp-seq by approximately 10-fold or greater are shown on the left (n=4)**. K)** Relative RNA polymerase III transcript levels in exosomes harvested from DMSO or POL3i-treated co-cultures (n=3). Unless indicated, error bars are SEM of biological replicates and *p<0.05, **p<0.01.

Stromal RNA polymerase III generates 5'ppp exoRNA that activates the anti-viral response in breast cancer cells

In the absence of viral infection, the main source of endogenous 5'ppp RNA is from RNA polymerase III (POL3) transcription[59]. Moreover, POL3 activity is known to be augmented by MYC activation[137], which appeared specifically enhanced in stromal cells after ISG-R breast cancer cell interaction (Figure 15B, left). Therefore, we sought to examine if stromal POL3 generates the exoRNA that is transferred to breast cancer cells to activate anti-viral signaling. Indeed, the POL3 subunit POLR3G was upregulated in stromal cells after co-culture with breast cancer cells (Figure 17D and 18E). Knockdown of POL3 using an siRNA to the POLR3F subunit (Figure 18F) revealed that inhibiting POL3 in stromal cells, but not breast cancer cells alone, significantly blunted breast cancer ISG induction (Figure 17E). Interrogation of functional consequences revealed that the ability of stromal cells to protect breast cancer cells after radiation was impaired with stromal POL3 knockdown, but unchanged after breast cancer POL3 knockdown (Figure 17F). Consistent with these findings, treatment with a POL3 small-molecule inhibitor[138] also blunted stroma-mediated resistance and ISG induction in breast cancer cells after co-culture (Figure 18G-H). To confirm that exoRNA is responsible for the effects resulting from inhibiting stromal POL3 RNA, we isolated CM from co-cultures treated with or without the POL3 inhibitor. CM isolated from co-cultures both induced ISGs when added to mono-cultured breast cancer cells (Figure 17G) and re-established stroma-mediated radiation resistance that was abrogated by POL3 inhibition (Figure 17H). In contrast, CM from co-cultures treated with POL3 inhibitor failed to induce ISGs, but expression of unrelated genes such as IFI16 was not affected (Figure 17G-H). Accordingly, exoRNA from POL3

inhibitor treated co-cultures also was defective in binding to recombinant RIG-I and stimulating ATP hydrolysis activity (Figure 17I). Thus, these results suggest that stromal POL3 generates exoRNA that activates breast cancer RIG-I to induce anti-viral signaling and stroma-mediated protection against DNA damage.

To characterize the exoRNA generated by stromal POL3, we developed an approach to identify 5'ppp RNA by sequencing. For this, we utilized a set of enzymatic reactions to sequentially modify the 5' end of RNA prior to library construction to deplete RNA lacking a 5'ppp modification (5'ppp-seq) (Figure 18I). Many coding and non-coding RNAs were depleted by approximately 10-fold or greater, consistent with the absence of a 5'ppp (Figure 17J, left). Examination of RNA classes that maintained or increased abundance revealed many exoRNA transcripts known to be under POL3 regulation, including tRNAs, srpRNA, Y RNA/snRNAs, and ALU/SINE RNAs (Figure 17J, right). As expected, inhibiting POL3 resulted in a decrease in the abundance of several of these 5'ppp RNA in exosomes (Figure 17K). Thus, multiple 5'ppp exoRNAs regulated by stromal POL3 are present in exosomes and represent candidate RNA ligands for propagating an anti-viral response from stromal cells to breast cancer cells.

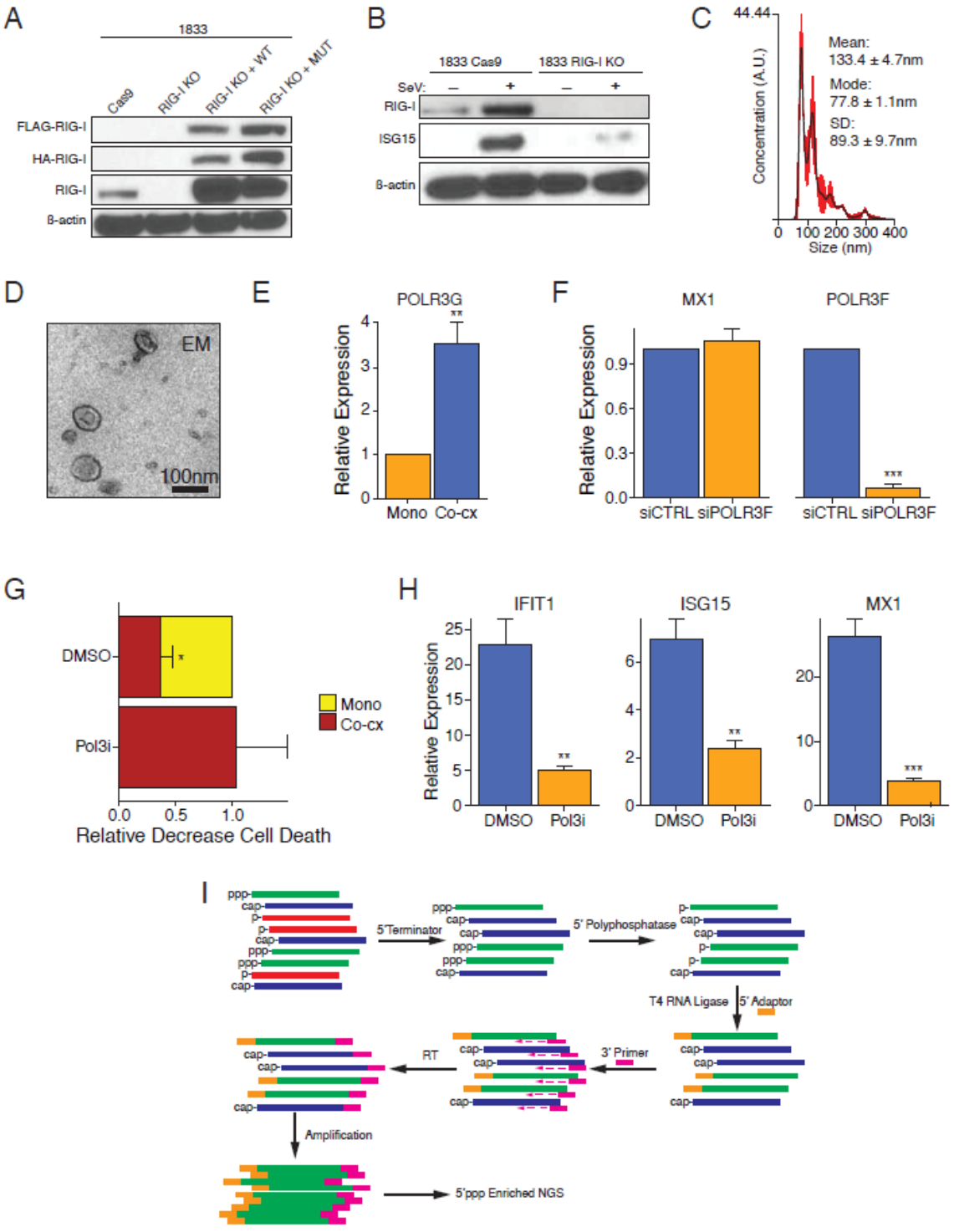

Figure 18. Stromal POL3 is required for maximal ISG induction in breast cancer cells. A) Immunoblot confirmation of Cas9 control (WT), RIG-I knockout (KO), and RIG-I KO 1833 cells restored with either wild-type (KO + WT) or RIG-I$^{K858/861A}$ 5'ppp binding mutant (KO + MUT). **B)** Immunoblot confirmation of RIG-I KO in ISG-R 1833 breast cancer cell line. RIG-I pathway activation was stimulated by Sendai virus (SeV) and assessed by

ISG15 induction. **C)** Nanosight quantification of size and quantity of a representative exosome purification. **D)** Purified exosome confirmation by electron microscopy negative staining. **E)** Gene expression of sorted MRC5 fibroblast RNA polymerase III subunit POLR3G after co-culture with ISG-R 1833 breast cancer. Values are relative to sorted MRC5 cells grown in mono-culture (n=3). **F)** Gene expression after indicated siRNA transfected in MRC5 cells (n=3). **G)** RT-mediated cell death in 1833 cells in mono-culture (Mono) or co-culture with MRC5 cells (Co-cx). Cells were grown in the presence of DMSO or POL3 inhibitor (Pol3i), and cell death was assessed 4 days after 10 Gy RT (n=3). **H)** ISG expression in sorted 1833 after co-culture with MRC5 cells in the presence of DMSO or POL3i. Gene expression values are relative to sorted 1833 cells grown in mono-culture (n=7). **I)** Schema for 5'triphosphate enriched RNA-seq (5'ppp-seq). Unless indicated, error bars are SEM of biological replicates and **p<0.01, ***p<0.001.

RN7SL1 5'ppp exoRNA generated from tumor-stromal interaction demonstrates extensive protein unshielding

As part of a strategy to identify a specific 5'ppp exoRNA from stromal cells that activates breast cancer RIG-I, we sought to examine differences in 5'ppp exoRNA abundance that correlate with differences in the ability of exosomes to induce anti-viral signaling. Toward this end, we took advantage of the observation that exosomes from co-culture, but not stromal cell mono-culture, induce ISGs (Figure 19A). Because 5'ppp-seq may not be quantitative, we first performed RNA-seq from exosomes (exoRNA-seq) isolated from co-culture versus stromal mono-culture. Using these data, we specifically examined transcripts that were also identified by 5'ppp-seq. This revealed that most 5'ppp exoRNA does not or only modestly varies in abundance in exosomes from co-culture compared to stromal mono-culture (Figure 19B). In contrast, RN7SL1, or srpRNA, and RN7SL1 pseudo-genes stood out as abundant transcripts that markedly increase in exosomes from co-culture compared to stromal mono-culture (Figure 19B-C and 20A, Table 5). Accordingly, exoRNA derived from stromal mono-culture was less effective than co-culture exoRNA at eliciting an ISG response in breast cancer cells (Figure 20B).

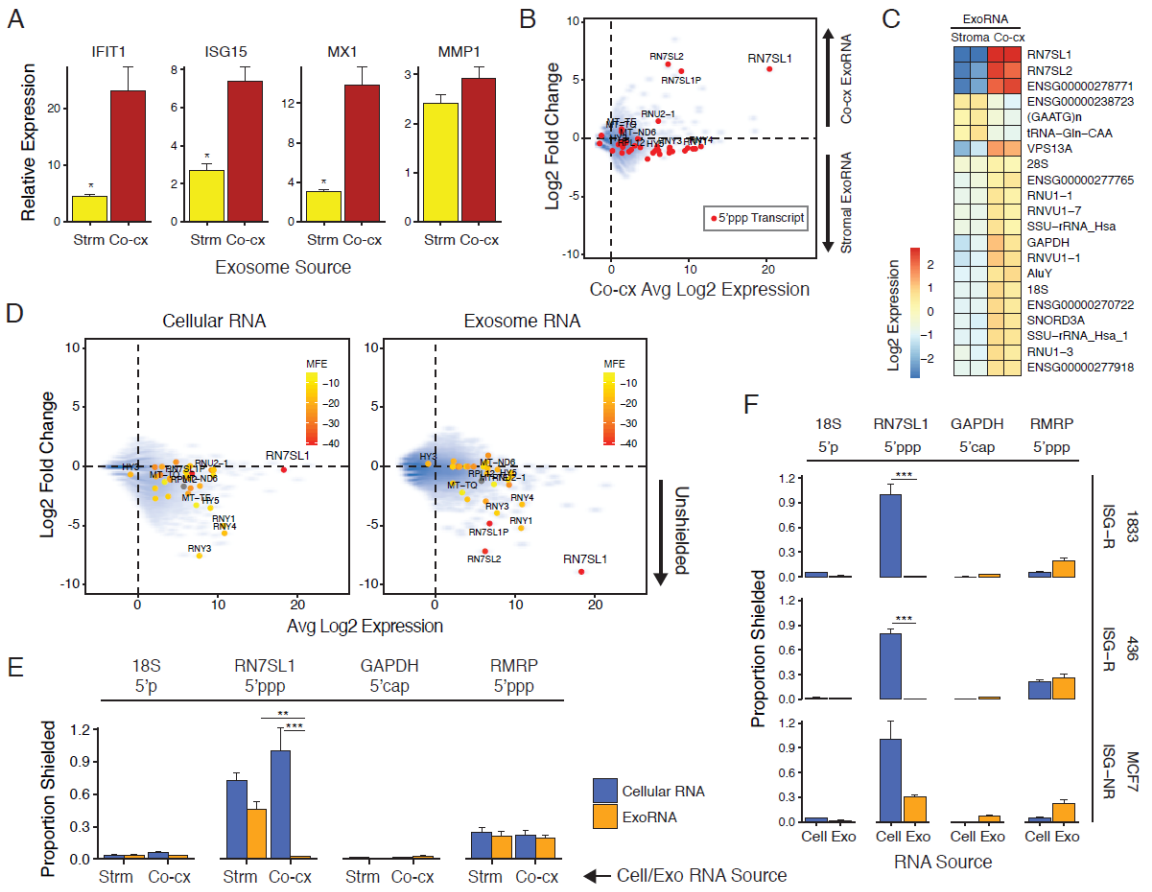

Figure 19. 5'ppp RN7SL1 exoRNA generated by tumor-stromal interaction is unshielded. A) ISG expression in 1833 breast cancer cells after addition of exosomes from MRC5 stromal cell mono-culture (Strm) or co-culture of 1833 and MRC5 cells (Co-cx) (n=3). Values are relative to mock control. **B)** ExoRNA and 5'ppp exoRNA enriched in co-culture exosomes. Shown is average expression (Log2) by exoRNA-seq in co-culture versus fold-change in co-culture compared to MRC5 stromal cell mono-culture (n=2). Transcripts identified by 5'ppp-seq are shown in red. ExoRNA was rRNA-depleted. **C)** Differentially expressed exoRNA from MRC5 mono-culture (Stroma) compared to co-culture of 1833 and MRC5 cells (Co-cx) (n=2). **D)** Expression of co-culture cellular RNA (left) or co-culture exoRNA (right) versus degree of RNA binding protein (RBP) unshielding. RBP unshielding (y-axis) is determined by fold change in RNA expression after MNase treatment with or without detergent (n=2). Smaller y-axis values indicate more unshielding. Transcripts identified by 5'ppp-seq are denoted by solid circles and color-coded based on normalized minimum free energy (MFE) to predict extent of double stranded RNA folding (lower MFE indicates more extensive double-stranded folding). **E)** Extent of RBP-shielding of 5'ppp RN7SL1 in cells (Cellular RNA) or exosomes (ExoRNA) isolated from either MRC5 stromal mono-culture (Strm) or co-culture of 1833 and MRC5 cells (Co-cx). Proportion shielded is determined by MNase treatment with and without detergent followed by qRT-PCR (MNase-qRT-PCR) (n=3). Also shown are other RNAs with the indicated 5' modification. **F)** Extent of RBP-shielding for cellular RNA (Cell) or exoRNA (Exo) isolated from co-cultures of the indicated ISG-R and ISG-NR breast cancer cells (labeled on right) with MRC5 fibroblasts. Proportion shielded is determined by

MNase-qRT-PCR (n=3). Unless indicated, error bars are SEM of biological replicates and *p<0.05, **p<0.01, ***p<0.001.

Although high levels of RN7SL1 in co-culture exosomes appeared to be a candidate RIG-I ligand based on differential expression, it was unclear why the presence of this 5'ppp RNA in the cytoplasm or in exosomes produced by stromal mono-culture would not activate RIG-I. Moreover, RN7SL1 and possibly other 5'ppp exoRNAs contain extensive double-stranded regions, an important feature given that RIG-I efficiently recognizes dsRNA. Based on these considerations, we reasoned that alterations in binding by RNA binding proteins (RBPs) might influence the ability of endogenous RNA to activate anti-viral signaling. To examine this, we treated cells or exosomes with micrococcal nuclease (MNase) with or without membrane permeabilization prior to sequencing (MNase-seq) (Figure 20C). This revealed that exoRNAs are generally less susceptible to MNase-dependent degradation compared to cellular RNAs, suggesting that exoRNA is relatively more "shielded" by RBPs than their cellular counterparts (Figure 19D). However, examination of 5'ppp RNA shielding combined with predicted RNA secondary structure as measured by normalized minimum free energy (MFE), demonstrated that RN7SL1 stands out as a 5'ppp exoRNA with extensive double-stranded structure (low MFE) that is extensively shielded in cells but highly unshielded in co-culture exosomes (Figure 19D and 20D, Table 5). In contrast, most other 5'ppp exoRNA has less predicted double-stranded structure and/or is significantly more shielded in exosomes compared to RN7SL1. Other 5'ppp RNA or RNA without a 5'ppp (i.e., 5' cap mRNA and 5'-monophosphate rRNA) generally are equally unshielded in cells and exosomes (Figure 19D and 20D), while RN7SL1 exoRNA from stromal mono-culture shows comparable shielding compared to cells (Figure 19E). Unshielding of RN7SL1 exoRNA was also observed when other ISG-R breast cancer cells and stromal fibroblasts were co-cultured (Figure 19F), and when primary mouse lung fibroblasts were co-cultured with

K14cre;$p53^{F/F}$;$Brca1^{F/F}$ murine breast cancer cells that also have hallmarks of ISG-R breast cancers (Figure 20E-H). In contrast, exosomes from co-culture of MCF7 ISG-NR breast cancer cells with stromal cells demonstrated significantly less unshielding (Figure 19F). This, along with diminished exosome transfer (Figure 15C), correlates with the relative inability of ISG-NR breast cancer cells to induce anti-viral signaling after co-culture. In total, these results suggest that after interaction with ISG-R breast cancer, stromal cells selectively deploy unshielded RN7SL1 in exosomes, an endogenous 5'ppp RNA with double-stranded structure.

Table 5: Differential Expression of 5'ppp-seq Identified Transcripts in Co-cx ExoRNA-seq vs. Stroma ExoRNA-seq

GeneID	Symbol	log2FoldChange	pvalue
ENSG00000278771		6.36343356	3.40E-32
RN7SL1	RN7SL1	5.954339049	0
ENSG00000274012		5.766305089	4.26E-58
ENSG00000274585	RNU2-1	1.473067514	0.000256183
ENSG00000210194	MT-TE	0.788711237	0.445398803
ENSG00000210107	MT-TQ	0.567573134	0.581029076
ENSG00000200090		0.238632644	0.816585329
ENSG00000198695	MT-ND6	-0.050443096	0.942091596
RMSK1848423	tRNA-Val-GTY	-0.289504941	0.781427256
RMSK4489775	tRNA-Leu-CTA	-0.399615749	0.675564238
RMSK2896852	tRNA-Gly-GGA	-0.451640769	0.661698379
RMSK4094422	HY3	-0.543342632	0.626965648
RMSK1903167	tRNA-Leu-TTG	-0.647165683	0.399143989
RMSK0284494	tRNA-Glu-GAG_	-0.711842908	0.133137812
ENSG00000252316	RNY4	-0.713159963	0.014826978
RMSK1848200	tRNA-Leu-CTY	-0.75997998	0.45907332
RMSK1898352	tRNA-Lys-AAG	-0.786930354	0.235743198
ENSG00000202354	RNY3	-0.788798711	0.019543371
RMSK1900244	tRNA-Asp-GAY	-0.844448884	0.0020408
ENSG00000201098	RNY1	-0.904999318	0.000490539
RMSK0444065	tRNA-Glu-GAG_	-0.907348767	0.002631367
RMSK3874632	tRNA-Asp-GAY	-0.960878858	0.003912964
ENSG00000197958	RPL12	-0.99099727	0.246632743
RMSK3556856	tRNA-Val-GTA	-1.065156761	0.008702102
RMSK1900901	tRNA-Val-GTY	-1.077724916	0.323350684
RMSK4003721	tRNA-Glu-GAG_	-1.078693607	0.202938517
RMSK2406652	HY5	-1.081991716	0.016164226
RMSK0254000	tRNA-Glu-GAG_	-1.138725411	0.071260176
RMSK4629380	tRNA-Lys-AAA	-1.153250435	0.216004512
RMSK4442186	tRNA-Lys-AAG	-1.254216659	0.002243703
RMSK1899770	tRNA-Val-GTG	-1.260921498	0.0174855
RMSK0284470	tRNA-Leu-CTG	-1.27201565	0.23295901
RMSK2705056	tRNA-His-CAY_	-1.377096393	0.176061556
RMSK5186324	tRNA-Gly-GGY	-1.787469268	0.06272545

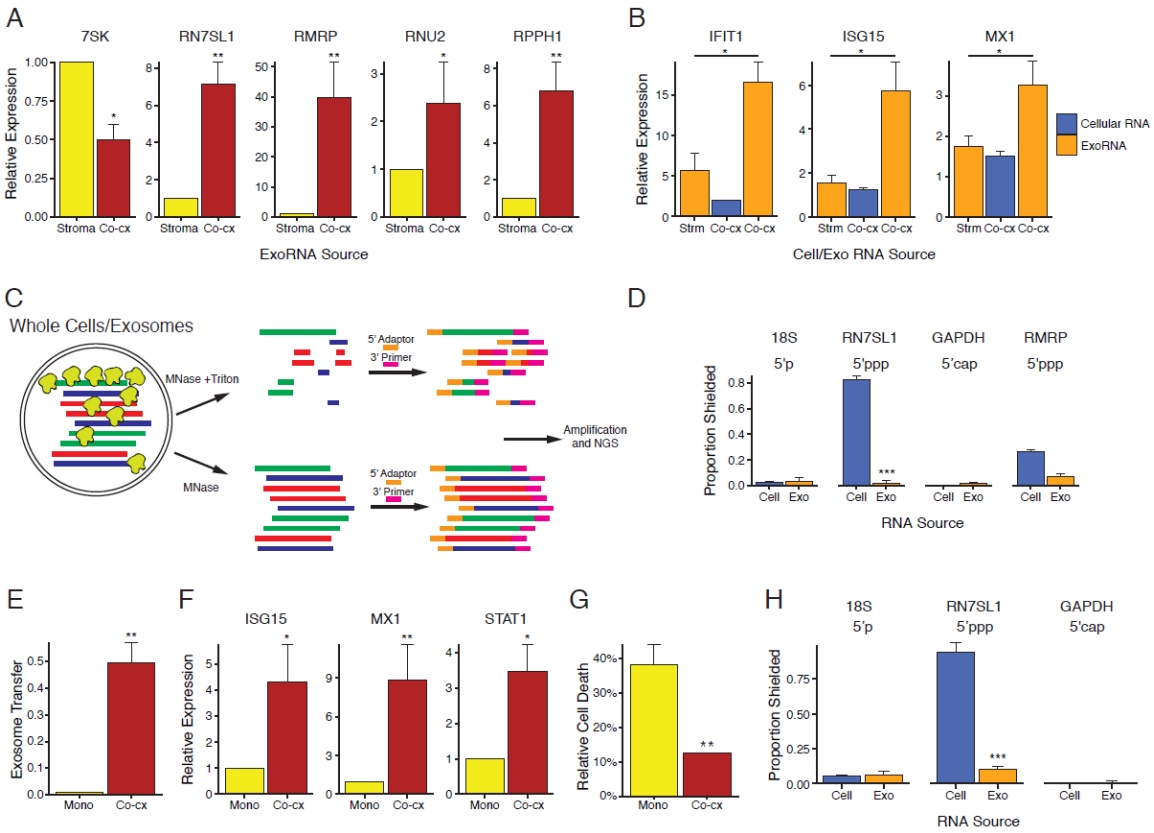

Figure 20. RN7SL1 is unshielded after tumor-stromal interaction. A) Relative expression of transcripts identified by 5'ppp-seq in exosomes from MRC5 mono-culture (Stroma) or MRC5 and 1833 co-culture (Co-cx). Values are relative to exoRNA from MRC5 mono-culture (n=3). **B)** ISG expression in 1833 cells after transfection of exoRNA or cellular RNA from MRC5 mono-culture (Strm) or co-culture of 1833 and MRC5 cells (Co-cx) (n=3). Values are relative to mock transfection. **C)** Schema for MNase-seq or MNase-qRT-PCR to analyze degree of RNA binding protein (RBP) shielding. **D)** Extent of RBP-shielding of 5'ppp RN7SL1 in cells (Cell) or exosomes (Exo) isolated from co-culture of 1833 and MRC5 cells. Proportion shielded is determined by MNase treatment with and without detergent followed by qRT-PCR (MNase-qRT-PCR) (n=3). Also shown are other RNAs with the indicated 5' modification. **E)** Exosome transfer to ISG-R K14cre;p53$^{F/F}$;Brca1$^{F/F}$ (KB1P) mouse breast cancer cells by differential lipid labeling of two populations of KB1P cells (Mono) or co-culture with primary mouse adult lung fibroblasts (ALFs) (Co-cx) (n=3). **F)** ISG expression in sorted ISG-R KB1P cells after co-culture with ALFs. Gene expression values are relative to sorted KB1P cells grown in mono-culture (n=3). **G)** RT-mediated cell death in KB1P cells in mono-culture (Mono) or co-culture with ALFs (Co-cx). Cell death was assessed 4 days after 10 Gy RT (n=3). **H)** Extent of RBP-shielding of cellular RNA (Cell) or exoRNA (Exo) isolated from co-culture of KB1P cells and ALFs. Proportion shielded is determined by MNase-qRT-PCR (n=3). Unless indicated, error bars are SEM of biological replicates and *p<0.05, **p<0.01, ***p<0.001.

Unshielded RN7SL1 exoRNA is transferred by stromal cells and stimulates breast cancer RIG-I

To establish that unshielded RN7SL1 exoRNA generated by stromal cells can serve as a RIG-I ligand, we metabolically labeled stromal cell RNA with 4sU and assayed for transfer to breast cancer cells. This demonstrated that RN7SL1, but not other 5'ppp exoRNAs or exoRNA without 5'ppp, is transferred to breast cancer cells from multiple different stromal cells but only in the context of ISG-R breast cancer cell co-culture (Figure 21A). Moreover, like exoRNA but not cellular RNA, transfection of ribozyme-cleaved in vitro transcribed RN7SL1 induces ISGs in breast cancer cells specifically in a RIG-I-dependent manner (Figure 21B). As expected, the ability of RN7SL1 to stimulate RIG-I requires 5'ppp. Alkaline phosphatase treatment prior to transfection abolished ISG induction (Figure 22), and reconstitution of RIG-I KO cells with WT RIG-I but not RIG-$I^{K858/861A}$, which abolishes amino acid interactions with 5'ppp, restored anti-viral signaling after RN7SL1 transfection (Figure 21B). In vitro RIG-I ATP hydrolysis assay confirmed that RN7SL1, but not equimolar and a similarly sized GAPDH-derived RNA (GAPDH300), directly binds recombinant RIG-I (Figure 21C). Activation of recombinant RIG-I by RN7SL1 was comparable to an equimolar amount of Sendai virus-derived RNA (DVG396). Thus, RN7SL1 is transferred from stromal cells to ISG-R breast cancer and can directly activate RIG-I.

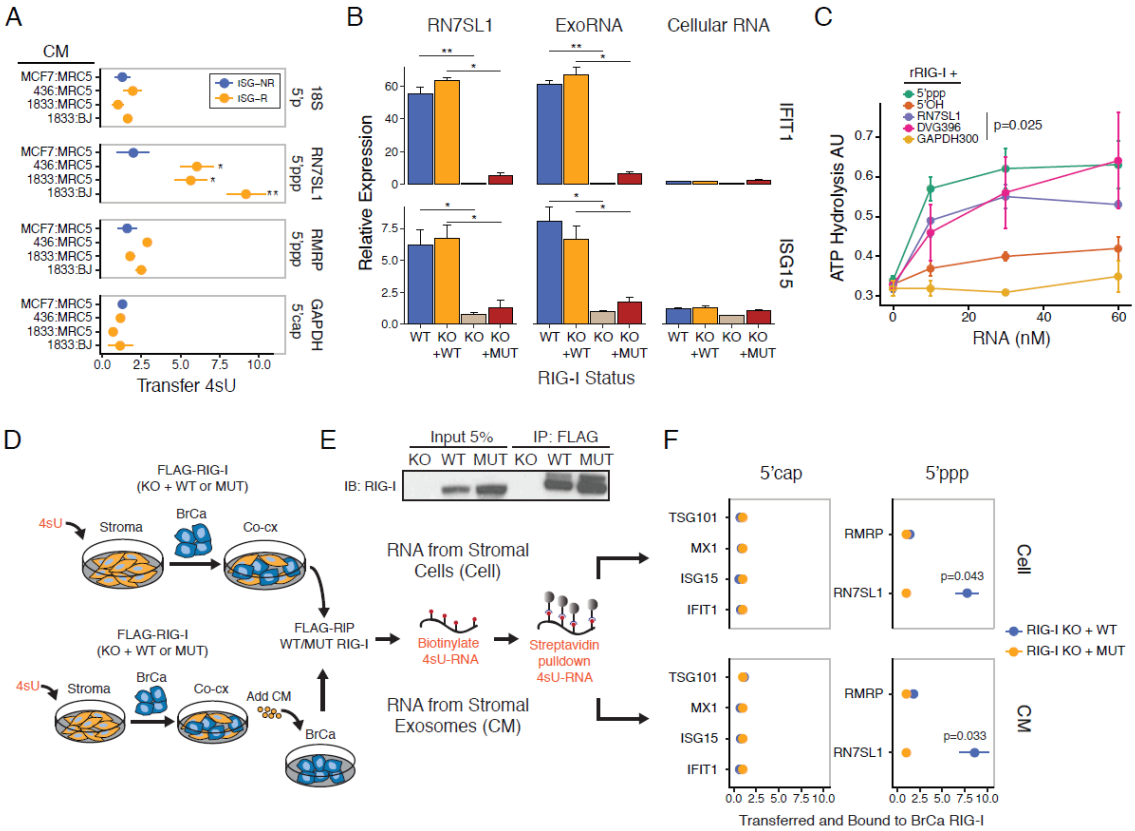

Figure 21. Unshielded RN7SL1 exoRNA is transferred by stromal cells and recognized by breast cancer RIG-I. A) Conditioned media (CM) from 4sU-labeled MRC5 fibroblasts co-cultured with either ISG-R (orange) or ISG-NR (blue) breast cancer cells. Shown is relative 4sU RNA transfer to breast cancer cells in mono-culture after addition of CM (n=3). **B)** ISG expression in 1833 breast cancer cells after transfection of co-culture exoRNA, cellular RNA, or RN7SL1 RNA. RIG-I status of 1833 cells was wild type (WT), knocked out (KO), or knocked out and restored with either wild-type RIG-I (KO + WT) or RIG-I$^{K858/861A}$ (KO + MUT) (n=3). Values are relative to mock control. **C)** ATP hydrolysis assay for RIG-I activation by RN7SL1. Shown are increasing concentrations of RN7SL1 or the indicated RNA ligands. 5'ppp and DVG396 are positive controls. 5'OH and GAPDH300 are negative controls (n=3). **D)** Schema to measure 4sU-labeled stromal RNA bound to breast cancer RIG-I after co-culture (Cell, top schema) or after addition of co-culture conditioned media (CM bottom schema). **E)** Representative immunoprecipitation of FLAG-RIG-I, and **F)** quantitation of indicated 4sU-labeled MRC5 stromal RNA transferred and then bound to 1833 breast cancer RIG-I. Shown is relative binding to reconstituted wild type RIG-I (KO + WT, blue) or RIG-I$^{K858/861A}$ (KO + MUT, orange) after co-culture (Cell) or addition of co-culture CM (CM). Binding of 5'cap mRNAs are shown on the left and 5'ppp RNAs on the right (n=3). Unless indicated, error bars are SEM of biological replicates and *p<0.05, **p<0.01.

To directly examine whether stromal RN7SL1 is transferred by exosomes and binds to breast cancer RIG-I, stromal cells were labeled with 4sU prior to co-culture with breast cancer cells. This was followed by tandem pull-down of stromal RNA bound to

breast cancer RIG-I by first immunoprecipitating FLAG-tagged breast cancer RIG-I and then isolating biotinylated 4sU-labeled stromal RNA with streptavidin beads (Figure 21D, top; Figure 21E). This sequential procedure revealed that stromal-derived RN7SL1, but not RNA without 5'ppp (i.e., capped mRNAs), specifically bound to WT RIG-I compared to RIG-I$^{K858/861A}$ (Figure 21F, top row). Moreover, other 5'ppp RNA found in exosomes such as RMRP showed markedly less binding. To assess if this transfer of stromal RN7SL1 is mediated by exosomes, CM isolated from 4sU-labeled stromal cells co-cultured with breast cancer cells was added to breast cancer cell mono-cultures (Figure 21D, bottom). Again, tandem pull-down demonstrated that stromal-derived RN7SL1, but not capped RNAs or RMRP 5'ppp RNA, specifically bound to breast cancer RIG-I when compared to RIG-I$^{K858/861A}$, consistent with exosome-mediated transfer (Figure 21F, bottom row). Thus, after breast cancer interaction, stromal cells can transfer unshielded RN7SL1 in exosomes to directly activate RIG-I. These results suggest that similar to how viral RNA in exosomes can propagate an anti-viral response from infected to uninfected cells, stromal cells can disseminate an anti-viral response to breast cancer cells by deploying unshielded endogenous RN7SL1 in exosomes.

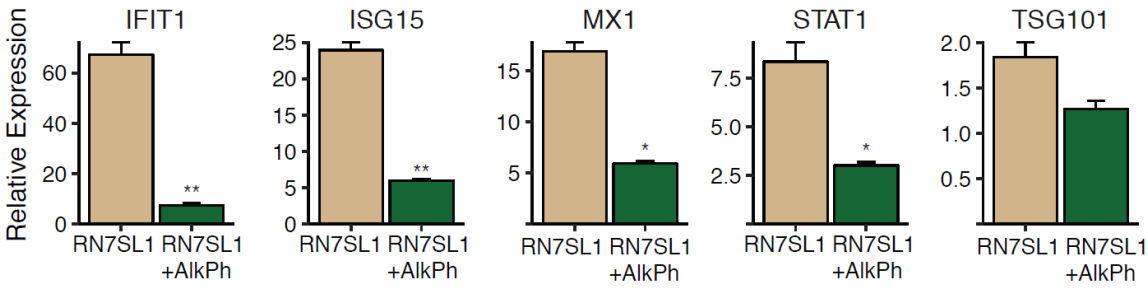

Figure 22. RN7SL1 activity is 5'ppp dependent. ISG expression in 1833 breast cancer cells after transfection of in vitro transcribed RN7SL1 RNA or RN7SL1 RNA treated with alkaline phosphatase (+AlkPh) (n=3). TSG101 is a non-ISG not expected to change. Values are relative to mock control. Error bars are SEM of biological replicates and *p<0.05, **p<0.01.

SRP9 and SRP14 control RN7SL1 shielding and anti-viral stimulatory activity

RN7SL1 is an abundant cellular RNA that complexes with signal recognition particle (SRP) proteins to control co-translational protein translocation[139]. Two SRP proteins, SRP9 and SRP14 normally bind the 5' end of RN7SL1, potentially obscuring the 5'ppp. Thus, to investigate whether SRP9 and/or SRP14 might influence recognition of RN7SL1 by RIG-I through RBP shielding, we examined the expression of SRP9/14 in exosomes. In contrast to cellular extracts, which showed relatively high levels of SRP9 and SRP14, these proteins were not detectable in exosomes (Figure 23A). Therefore, we transiently overexpressed GFP-tagged SRP9 and SRP14 in stromal cells prior to co-culture to determine if this could drive these SRP proteins into exosomes and potentially partially shield exosome RN7SL1 from recognition by breast cancer RIG-I (Figure 23B and 24A-C). Indeed, transiently increasing SRP9 and SRP14 in stromal cells was sufficient to direct expression of both tagged SRP proteins into exosomes (Figure 23C). This led to a significant increase in shielding of RN7SL1 exoRNA but not in 18S rRNA (Figure 23D). Consequently, stroma-mediated ISG induction in breast cancer cells was reduced, while expression of non-ISGs such as MMP1 and TSG101 was not affected (Figure 23E). We were also able to purify recombinant SRP9 (attempts to purify SRP14 were not successful). Addition of SRP9 to in vitro transcribed RN7SL1 partially inhibited ATP hydrolysis by recombinant RIG-I but did not influence Sendai virus-derived RNA (DVG396) or unrelated 5'ppp or 5'OH control RNAs (Figure 23F). These results suggest that RBP shielding of cellular RN7SL1 by its SRP proteins may restrict inappropriate recognition by RIG-I in the cytoplasm. However, the absence of these RBPs in exosomes allows the transfer of unshielded RN7SL1 to neighboring cells, resulting in RIG-I activation. Thus, in a sterile tumor microenvironment, differential RBP shielding in cells

versus exosomes can enable endogenous RNAs to function as DAMPs and propagate anti-viral signaling.

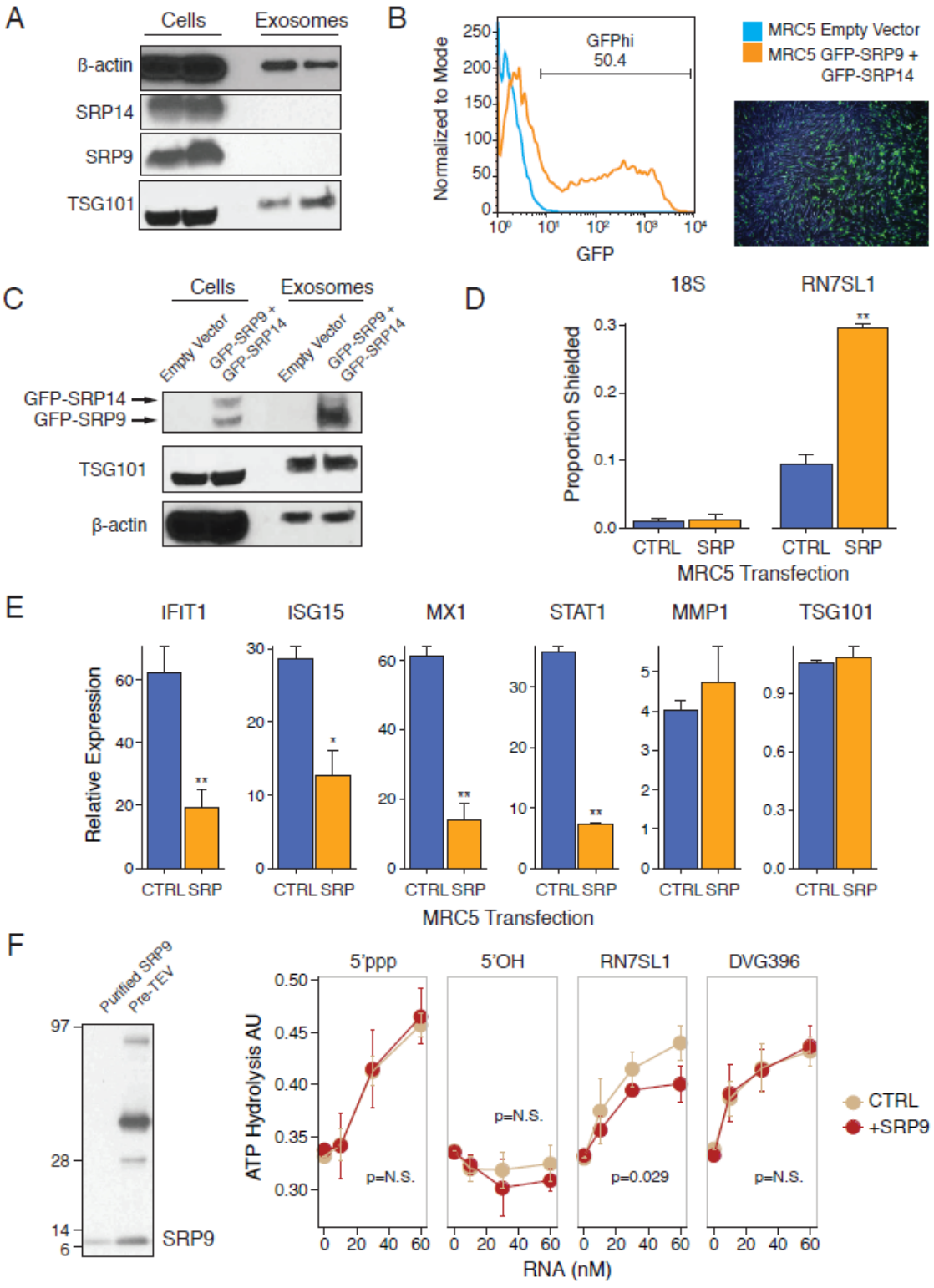

Figure 23. Stromal SRP9 and SRP14 regulate RN7SL1 shielding and activation of breast cancer RIG-I. A) Immunoblot for the indicated proteins in co-culture cells and exosomes. Lysates used were normalized to absolute levels of RN7SL1 RNA. **B)** Flow cytometry (left) and fluorescence microscopy (right) for GFP expression after transfection of GFP-SRP9 and GFP-SRP14 in MRC5 fibroblasts. **C)** Immunoblot for the indicated proteins in co-culture cells and exosomes after GFP-SRP9 and GFP-SRP14 transfection in MRC5 fibroblasts. **D)** Extent of RBP-shielding for the indicated exoRNAs isolated from 1833 breast cancer cells co-cultured with control (CTRL) or GFP-SRP9 and GFP-SRP14 (SRP) transfected MRC5 fibroblasts. Proportion shielded is determined by MNase-qRT-PCR (n=3). **E)** Relative expression of ISGs in sorted 1833 cells after co-culture with MRC5 cells transfected with GFP-SRP9 and GFP-SRP14 (n=3). TSG101 and MMP1 are non-ISGs not expected to change. **F)** Immunoblot for SRP9 pre-cleavage (lane 2) and post-cleavage (lane 1) of the GST tag with TEV protease. RN7SL1 binding to RIG-I was measured by ATP hydrolysis assay with or without addition of equimolar amounts of recombinant SRP9 (n=3). 5'ppp and DVG396 are positive controls. 5'OH is a negative control. Unless indicated, error bars are SEM of biological replicates and *p<0.05, **p<0.01.

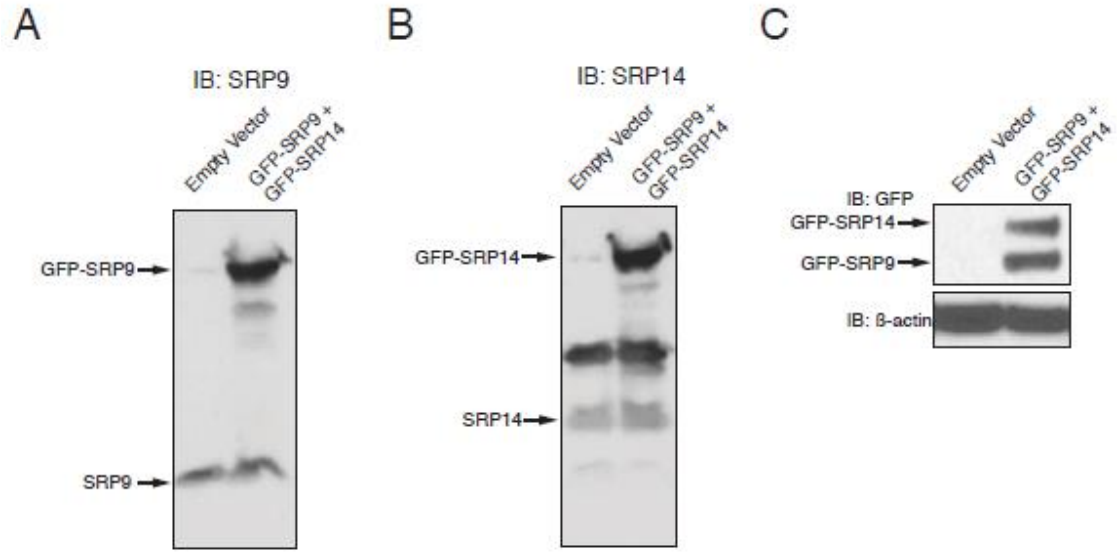

Figure 24. Confirmation of SRP9/14 overexpression in stromal cells. Immunoblot for **A)** SRP9, **B)** SRP14, or **C)** GFP after transfection of GFP-SRP9 and GFP-SRP14 in MRC5 fibroblasts.

RN7SL1 unshielding is regulated by RNA-protein imbalance

SRP9 and SRP14 regulate RN7SL1 shielding; therefore, we hypothesized that excess RN7SL1 RNA produced after tumor-stroma interaction may result in unshielded stromal RN7SL1. To examine if increased stromal POL3 activity after co-culture resulted

in increased RN7SL1, we isolated stromal cells from co-culture and analyzed relative RNA expression. As expected, stromal cells in co-culture with ISG-R breast cancer cells had elevated ISGs and increased levels of several POL3 transcripts, including RN7SL1 (Figure 25A). Further, protein isolated from the same co-cultures showed no concomitant increase in stromal SRP9 or SRP14, suggesting that increase of RN7SL1 without simultaneous increase of SRP proteins could lead to unshielded RN7SL1 (Figure 25B). To assess if the converse was true, we utilized siRNA to knockdown SRP9 and SRP14 levels in stromal cells (Figure 25C). This lead to a specific ISG induction stromal cells with siSRP9/14 (Figure 25C/D). To interrogate whether this knockdown resulted in the production of exosomes with unshielded RN7SL1 and ISG stimulatory activity, we added conditioned media from these stromal cells to breast cancer cells. Conditioned media isolated from siSRP9/14 stromal cells induced ISGs in recipient breast cancer cells (Figure 25E). Exosomes isolated from these same co-cultures were subjected to RN7SL1 unshielding assays and consistent with having lower levels of SRP9 and SRP14, both cellular and exosomal RN7SL1 were largely unshielded (Figure 25F). In total, unshielding of RN7SL1 and its ability to propogate anti-viral signals results from a RNA to protein imbalance.

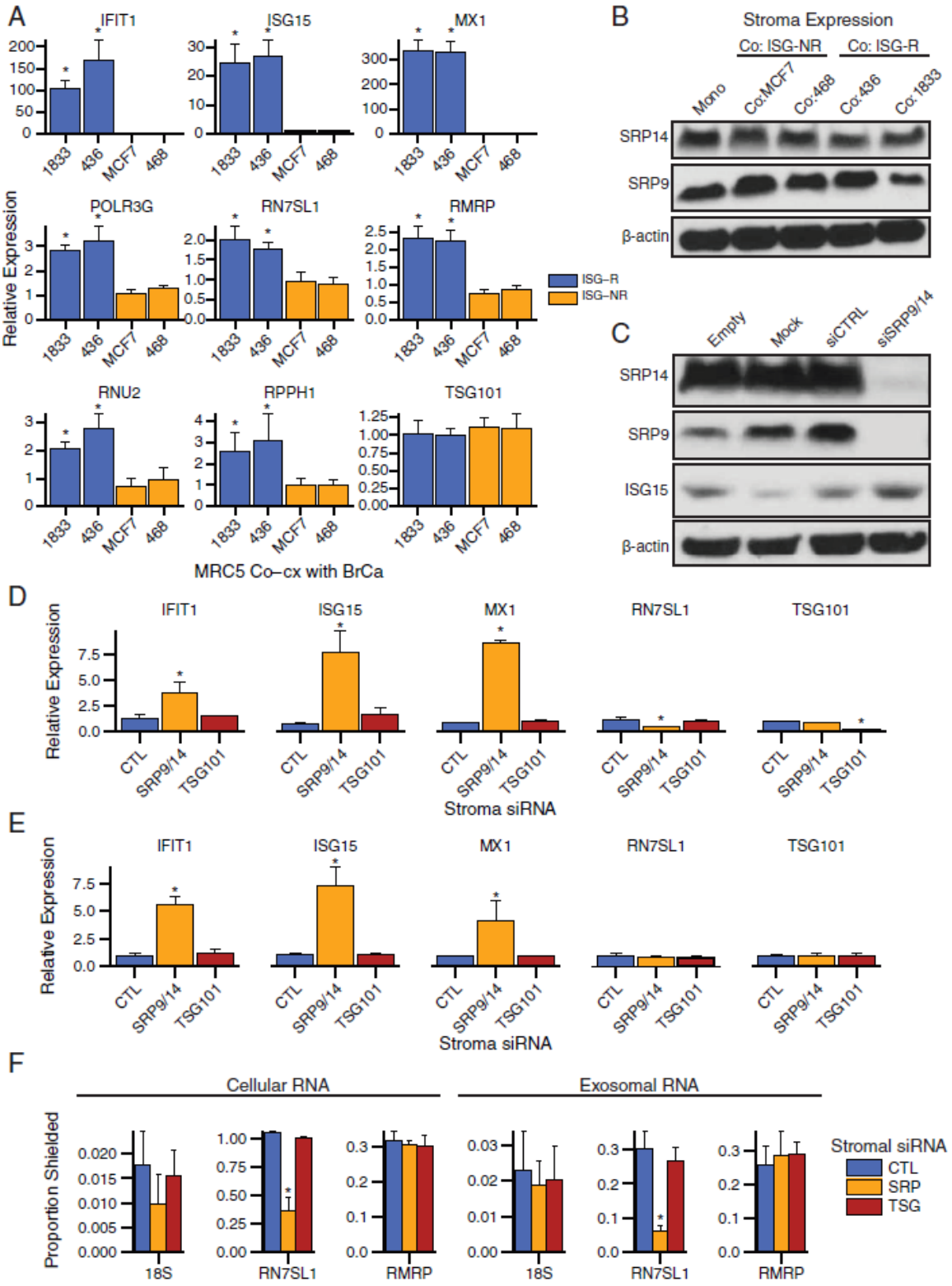

Figure 25. RN7SL1 unshielding is regulated by RNA-protein imbalance. A) Gene expression of MRC5 fibroblasts after co-culture with indicated ISG-R or ISG-NR breast cancer cells. Values are relative to sorted mono-culture MRC5 fibroblasts and TSG101 is a non-ISG not expected to change (n=3). **B)** Immunoblot for the indicated proteins in

MRC5 fibroblasts after co-culture. **C)** Immunoblot for the indicated proteins in MRC5 fibroblasts after the indicated siRNA knockdown. **D)** Gene expression in MRC5 fibroblasts after the indicated siRNA knockdown (n=3). **E)** Gene expression in 1833 breast cancer cells after addition of conditioned media isolated from MRC5 fibroblasts with the indicated siRNA knockdown. TSG101 is a non-ISG not expected to change (n=3). **F)** Extent of RBP-shielding for the indicated cellular and exosomal RNAs isolated from MRC5 fibroblasts after the indicated siRNA knockdown. Proportion shielded is determined by MNase-qRT-PCR (n=3). Error bars are SEM of biological replicates and *p<0.05.

MYC is responsible for POL3 output and subsequent RN7SL1 unshielding.

The POL3 transcriptional machinery relies heavily on MYC for maximal activity[137,140]. Furthermore, it is hypothesized that areas of high POL2 transcriptional output, such as those under MYC control, result in concomitant POL3 output by providing an epigenetically favorable environment[141]. To assess if MYC is activated in stromal cells after interaction with breast cancer cells we co-cultured fibroblasts with GFP-tagged ISG-R breast cancer cells. MYC activation as assessed by nuclear localization demonstrated that upon co-culture MYC is activated in a significant percentage of stromal cells; whereas, there is almost no activation in mono-culture (Figure 26A/B). To assess if RN7SL1 unshielding and ISG stimulating capacity was MYC dependent, we utilized siRNA against MYC (Figure 26C). Addition of conditioned media isolated from co-cultures of ISG-R breast cancer cells and stromal cells with stroma-specific siRNA knockdown of MYC was no longer able to stimulate ISGs in recipient breast cancer cells to the same degree as those with a control siRNA (Figure 26D). Further, exosomes isolated from these experiments demonstrated a significant increase in RN7SL1 shielding after siRNA knockdown of MYC in fibroblasts prior to co-culture (Figure 26E). To assess if activation of MYC alone can result in production of ISG stimulating exosomes containing unshielded RN7SL1, we utilized mouse embryonic fibroblasts stably expressing a MYC-ER construct that allows for 4OHT-inducible activation of MYC (MYC-ER MEFs)[142]. Addition of 4OHT results in robust MYC expression and nuclear localization (Figure 26F). Further, exosomes isolated from MYC-ER MEFs after the addition of 4OHT induce ISGs in

recipient breast cancer cells (Figure 26G). Addition of 4OHT results in a significant increase in unshielded RN7SL1 in exosomes, whereas exosomes isolated from ethanol treated MEFs have significantly more shielded RN7SL1 (Figure 26H). To evaluate if these MYC-dependent changes were also POL3 dependent, MYC was activated in the presence of a POL3 inhibitor. Addition of a POL3 inhibitor to MYC activated MEFs reduced the ISG inducing capacity of equal amounts of exosomes added to recipient breast cancer cells (Figure 26I). As expected, RN7SL1 in exosomes isolated from MYC activated MEFs cultured with a POL3 inhibitor remained largely shielded (Figure 26J). Thus, MYC is both necessary and sufficient to enhance POL3 transcriptional output and produce unshielded RN7SL1 to function an anti-viral signal propagating DAMP.

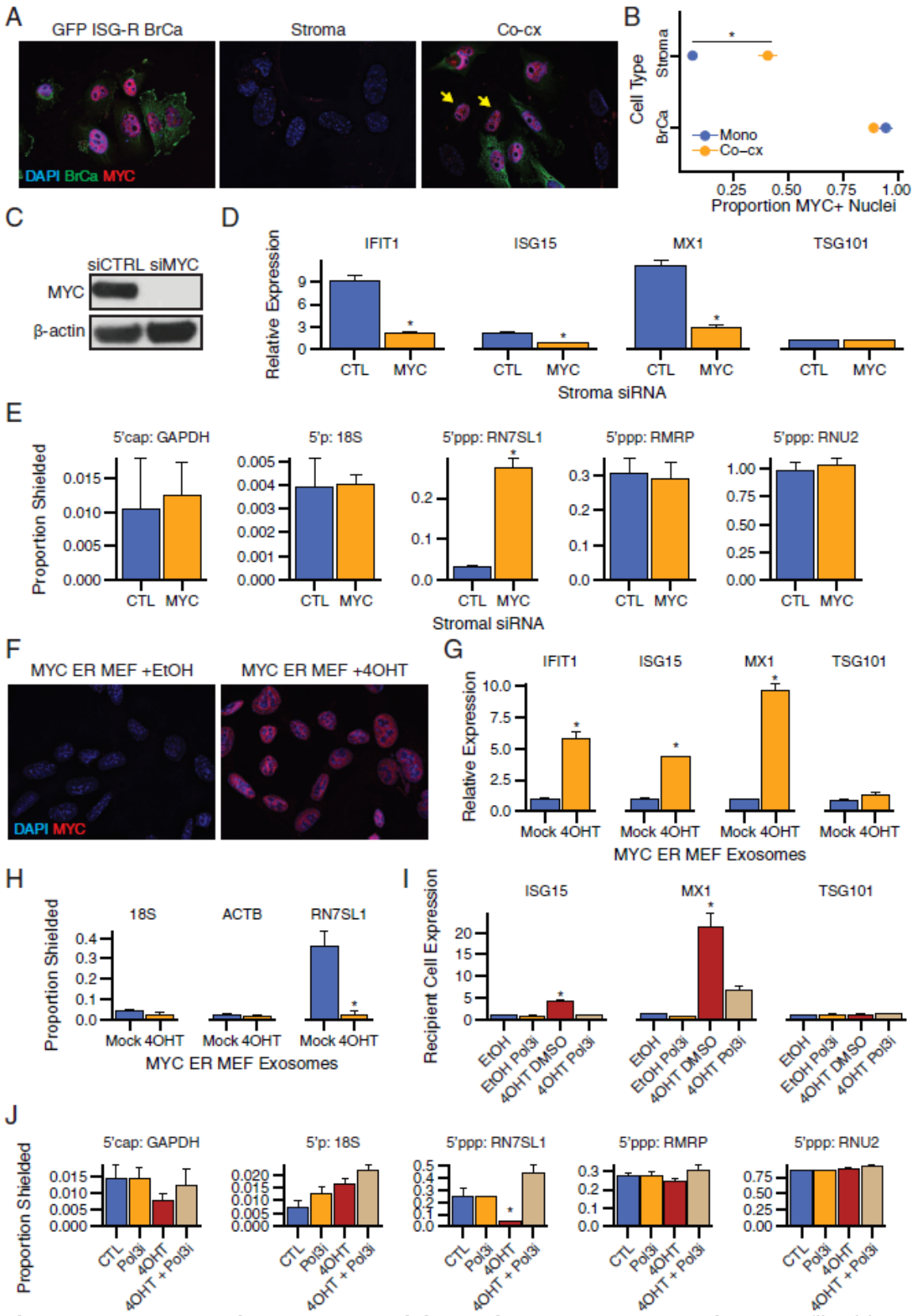

Figure 26. MYC regulates POL3 activity and RN7SL1 output. A) MRC5 fibroblasts were co-cultured with GFP-tagged ISG-R breast cancer cells. Stromal MYC activation is

denoted by strong nuclear staining and absence of GFP signal and designated by the yellow arrows. **B)** Quantification of MYC activation in breast cancer and stromal cells before or after co-culture (n=3). **C)** Immunoblot for the indicated proteins after the indicated siRNA knockdown in MRC5 fibroblasts. **D)** ISG expression after addition of co-culture conditioned media with MRC5 fibroblasts harboring the indicated siRNA knockdown. TSG101 is a non-ISG not expected to change (n=3). **E)** Extent of RBP-shielding for the indicated exosomal RNAs isolated from co-cultures with MRC5 fibroblasts harboring the indicated siRNA knockdown. Proportion shielded is determined by MNase-qRT-PCR (n=3). **F)** MYC expression and localization in MYC-ER MEFs after treatment with 4OHT or vehicle control (ethanol). **G)** ISG expression in recipient breast cancer cells after the addition of purified exosomes from MYC-ER MEFs with or without 4OHT activation. TSG101 is a non-ISG not expected to change (n=3). **H)** Extent of RBP-shielding for the indicated exosomal RNAs isolated from MYC-ER MEFs after 4OHT activation. Proportion shielded is determined by MNase-qRT-PCR (n=3). **I)** ISG expression in recipient breast cancer cells after exosomes from 4OHT-activated MYC-ER MEFs with or without Pol3i were added. TSG101 is a non-ISG not expected to change (n=3). **J)** Extent of RBP-shielding for the indicated exosomal RNAs isolated from MYC-ER MEFs after 4OHT activation with or without Pol3i. Proportion shielded is determined by MNase-qRT-PCR (n=3). Error bars are SEM of biological replicates and *p<0.05.

NOTCH1 regulates stromal MYC expression and activation

Cell-cell contact is required for stromal activation mediated by ISG-R breast cancer cells[132]. Therefore, we interrogated a known cell-cell contact-dependent regulator of MYC signaling, the Notch pathway. NOTCH1 is a strong transcriptional regulator of MYC expression in various cancers[143]. Interestingly, we found that NOTCH1 is specifically activated by release of its Notch intracellular domain (NICD1) in stromal cells after co-culture with ISG-R breast cancer cells, while NOTCH2-4 did not change in their expression or activation (Figure 27A). Moreover, this activation was γ-secretase dependent as treatment with a γ-secretase inhibitor (GSI) completed abrogated this activation (Figure 27A). To assess NOTCH1 activation in human cancers, we utilized a panel of cancer-associated fibroblasts (CAFs) isolated from breast cancer patients. We termed CAFs with the ability to induce ISGs in breast cancer cells 'ISG-inducers' (ISG-I), and those that could not induce ISGs in breast cancer cells 'ISG-noninducers' (ISG-NI). We find that ISG-I breast cancer cells induce NOTCH1 activation (Figure 27B). Moreover, treatment with a GSI to block NOTCH1 activity in co-culture significantly reduces stromal MYC expression

and activation (Figure 27C/D). To evaluate the role of these signaling pathways in breast cancer patients we interrogated breast cancer and stromal gene expression patterns in 28 paired primary tumor and stroma samples that were separated by laser-capture microdissection (LCMD). Strikingly, those patients with highest breast cancer ISG signature expression also had highest stromal ISG signature expression, MYC signature expression, and NOTCH signature expression (Figure 27E). ISG signature expression in both cell types were highly correlated (Figure 27F, left). Stromal NOTCH and MYC signaling were highly correlated, suggesting their co-regulation (Figure 27F, middle). As expected based on our results, expression of the stromal MYC signature was highly correlated with expression of the breast cancer ISG signature (Figure 27F, right). Thus, our results suggest that stromal MYC activation in co-culture and cancer patients in NOTCH1 dependent.

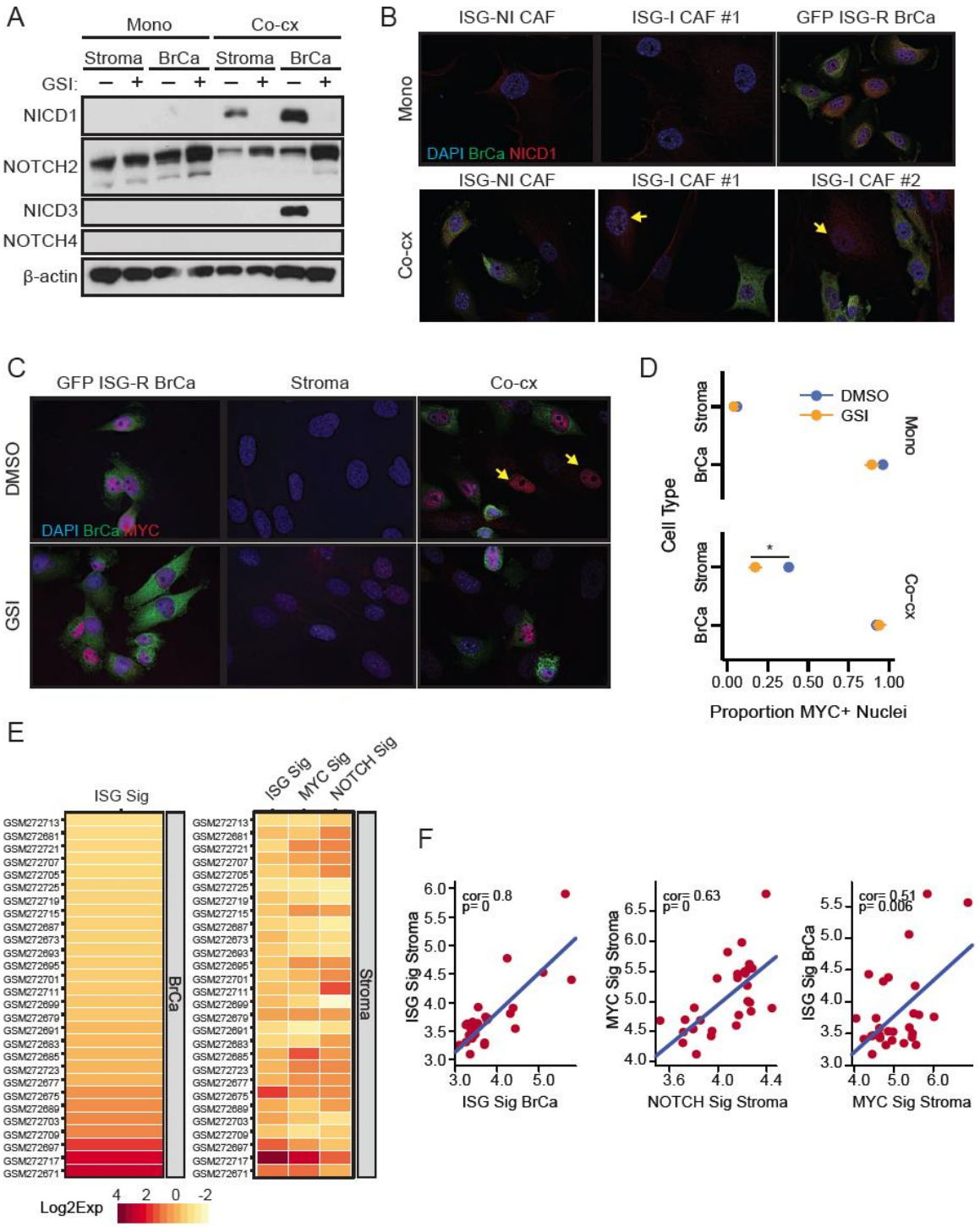

Figure 27. Heterotypic tumor-stroma interaction induces stromal NOTCH1 and subsequent MYC expression and activation. A) Immunoblot of the indicated proteins in MRC5 fibroblasts or 1833 ISG-R breast cancer cells before or after co-culture and with or without GSI. **B)** GFP-tagged 1833 ISG-R breast cancer cells were co-cultured with ISG-I or ISG-NI CAFs and NOTCH1 activation was denoted by increased NICD1 nuclear and cytoplasmic signal and designated by the yellow arrows. **C)** MRC5 fibroblasts were co-cultured with GFP-tagged ISG-R breast cancer cells with or without GSI treatment.

Stromal MYC activation is denoted by strong nuclear staining and absence of GFP signal and designated by the yellow arrows. **D)** Quantification of MYC activation in breast cancer and stromal cells before or after co-culture (n=3). **E)** Expression of a ISG signature, NOTCH signature, or MYC signature primary tumor and stroma samples that were separated by laser-capture microdissection. **F)** Correlation of these signatures in patients from the same data set. Error bars are SEM of biological replicates and *p<0.05.

Unshielded stromal RN7SL1 exoRNA promotes breast cancer progression and is present in the serum of cancer patients

A cardinal feature of stromal fibroblasts in the tumor microenvironment is the ability to promote cancer progression and metastasis. Indeed, the ability of stromal cells to induce anti-viral signaling in breast cancer contributes to metastasis[43] and/or the expansion of tumor-initiating cells[132], which would be expected to favor breast cancer progression. To examine whether unshielded RN7SL1 in exosomes can contribute to tumor growth, we isolated exosomes from co-culture and from stromal mono-culture and performed direct intratumoral injections into subcutaneous 1833 ISG-R breast cancer xenografts. Consistent with having higher levels of unshielded RN7SL1, exosomes from co-culture accelerated tumor growth compared to exosomes isolated from stromal cells alone (Figure 28A). To directly assess if unshielded RN7SL1 can enhance tumor progression, RN7SL1 or GAPDH300 control RNA was encapsulated into liposomes and similarly delivered intratumorally. Only RN7SL1 could enhance tumor growth in a RIG-I-dependent manner as no effect was observed with RIG-I KO or with GAPDH300 control RNA (Figure 28B). Examination of the tumor confirmed an increase in ISG expression, but not in unrelated genes like TSG101, specifically in tumors injected with RN7SL1 and expressing WT RIG-I (Figure 28C). Thus, these results suggest that unshielded RN7SL1 transferred by exosomes can promote breast cancer progression.

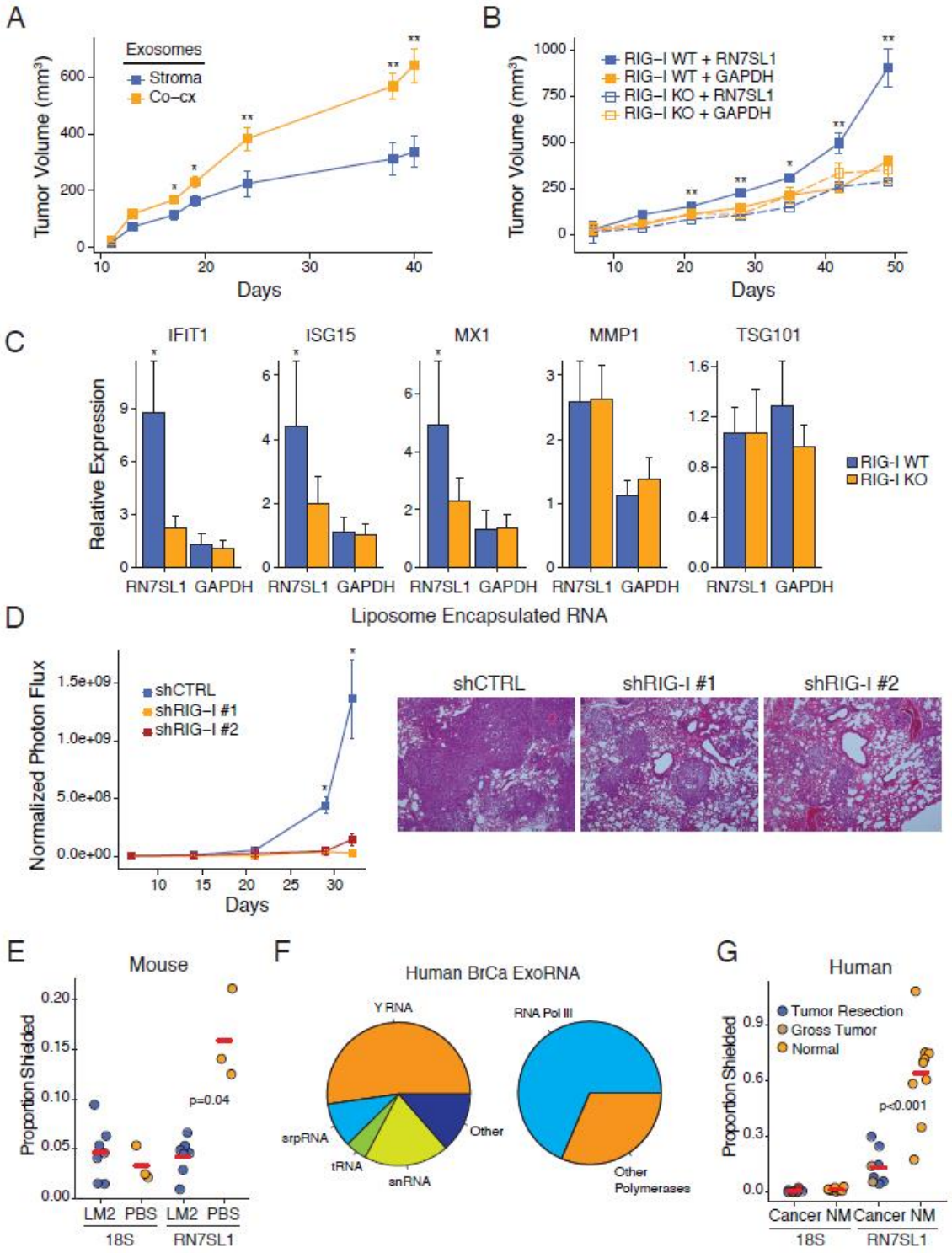

Figure 28. Unshielded stromal RN7SL1 exoRNA promotes breast cancer progression and is present in the serum of cancer patients. A) 1833 breast cancer cells were xenografted subcutaneously into athymic mice and 10µg of exosomes from MRC5 stromal cell mono-culture or 1833 and MRC5 co-culture were injected intratumorally 3 times a week (n=5 per group). Shown are tumor growth curves. **B)** 1833 breast cancer cells with (RIG-I KO) or without (RIG-I WT) knockout of RIG-I were

xenografted subcutaneously into athymic mice and 50ng of the indicated liposome-encapsulated RNA was injected intratumorally 3 times a week (n=5 per group). Shown are tumor growth curves. **C)** Expression of ISGs measured by qRT-PCR with human specific primers from the indicated tumors from (B). TSG101 and MMP1 are non-ISGs not expected to change (n=5). **D)** Normalized photon flux from the lungs of athymic mice (left) tail-vein injected with luciferase-labeled 4175 ISG-R breast cancer cells (LM2) engineered with one of two independent shRNAs to RIG-I or a control shRNA (n=5 per group). Hematoxylin and eosin stain of mouse lung sections at experimental endpoint (right). **E)** Extent of RBP-shielding of mouse RN7SL1 or 18S rRNA from serum exosomes 2 weeks after mice were tail-vein injected for lung metastasis induction with 4175 breast cancer cells (LM2) or injected with PBS. Proportion shielded is determined by MNase-qRT-PCR. Mouse-specific primers were validated for specificity. **F)** Average distribution of exoRNA in each RNA class (left) or by POL3 regulation (right) from serum exosomes of breast cancer patients (n=2). Only the top 200 highest expressed non-ribosomal RNA transcripts were considered. **G)** Extent of RBP-shielding of RN7SL1 or 18S rRNA from serum exosomes of cancer patients or normal volunteers without cancer (NM). Legend indicates samples from normal volunteers and cancer patients with or without tumor resection. Proportion shielded is determined by MNase-qRT-PCR. Unless indicated, error bars are SEM of biological replicates and *p<0.05, **p<0.01.

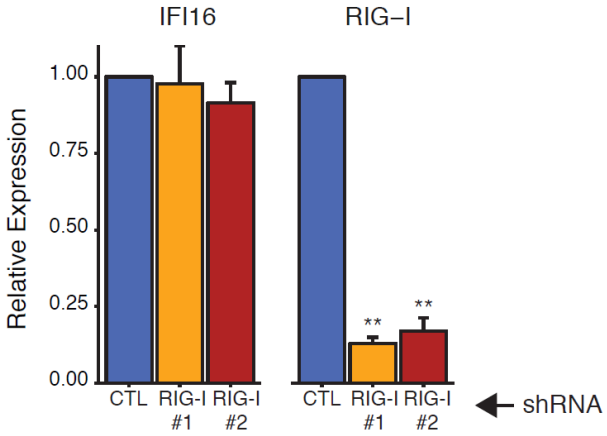

Figure 29. Confirmation of RIG-I shRNA activity. Gene expression in 1833 breast cancer cells after transduction of control shRNA (CTL) or two independent RIG-I targeting shRNA (RIG-I #1 and RIG-I #2) (n=3). Error bars are SEM of biological replicates and **p<0.01.

To study whether metastatic progression is associated with breast cancer RIG-I signaling and unshielded RN7SL1 exoRNA from stromal cells, we utilized 4175 human breast cancer cells, which are an ISG-R lung metastatic derivative of MDA-MB-231[144]. Inhibiting RIG-I expression in 4175 cells using two independent shRNAs (Figure 29)

resulted in a significant defect in lung metastatic colonization, indicating the importance of RIG-I signaling in breast cancer cells (Figure 28D). Compared to non-tumor bearing mice, interrogation of exoRNA from serum of mice with wild-type 4175 lung metastases revealed more unshielding of mouse RN7SL1 but not 18S rRNA as measured using mouse-specific primers (Figure 28E). These data suggest that lung metastases from human breast cancer cells can result in greater amounts of circulating unshielded RN7SL1 in exosomes originating from mouse stromal cells. To corroborate these findings, we also examined exoRNA from the serum of a small cohort of cancer patients (Table 6). To the extent possible, we mimicked the analysis in mice by examining RN7SL1 in patients after tumor resection. This facilitated assessment of RN7SL1 exoRNA from stromal cells and allowed better comparison to normal controls without cancer. ExoRNA-seq from two patients confirmed that RN7SL1 and POL3 transcripts are present at high levels and among the predominant non-rRNA transcripts in exosomes from cancer patients (Figure 28F). Compared to healthy controls, this RN7SL1 exoRNA was significantly less shielded in cancer patients having had tumor resection, suggesting that RN7SL1 from remaining cancerized stroma is more unshielded than from normal cells (Figure 28G). Although cellular origin could not be determined, RN7SL1 exoRNA from two available patients with gross tumors prior to any therapy also showed similar results, arguing that RN7SL1 unshielding was not solely due to confounding factors related to tumor resection. Together, these findings suggest that unshielded stromal RN7SL1 in exosomes can propagate anti-viral signaling in the tumor microenvironment to enhance breast cancer progression or metastasis.

Table 6: Characteristics of patients analyzed for exosome RN7SL1 shielding

ID	Sex	Status	Age	Cancer Type	Resection
H1	Female	Healthy	42	None	N/A
H2	Female	Healthy	77	None	N/A
H3	Female	Healthy	24	None	N/A
H4	Female	Healthy	52	None	N/A
H5	Female	Healthy	27	None	N/A
H6	Male	Healthy	27	None	N/A
H7	Male	Healthy	27	None	N/A
H8	Male	Healthy	44	None	N/A
H9	Male	Healthy	49	None	N/A
H10	Male	Healthy	57	None	N/A
C1	Female	Cancer	52	Breast	Yes
C2	Female	Cancer	49	Breast	Yes
C3	Female	Cancer	49	Breast	Yes
C4	Female	Cancer	72	Breast	Yes
C5	Female	Cancer	55	Breast	Yes
C6	Female	Cancer	49	Breast	Yes
C7	Male	Cancer	82	Pleomorphic undifferentiated sarcoma	No
C8	Female	Cancer	33	Cervical squamous cell carcinoma	No

Discussion

In this study, we describe a phenomenon of virus mimicry whereby the interaction between breast cancer cells and stromal fibroblasts share several similarities with how virus infected cells relay anti-viral signals to surrounding cells. First, upon encounter with breast cancer cells, stromal cells mount an anti-viral response analogous to virally infected cells by upregulating ISGs and other genes associated with anti-viral signaling. In fact, interferon and anti-viral signaling are dominant pathways induced among hundreds of upregulated transcripts. Second, like virally infected cells that can package viral 5'ppp RNA into exosomes to function as pathogen-associated molecular patterns (PAMPs), stromal cells that have encountered breast cancer cells increase the abundance of endogenous POL3-derived and RBP-devoid 5'ppp RN7SL1 in exosomes to function as

DAMPs. Moreover, after interaction between stromal cells and ISG-R breast cancer cells, production of DAMP-laden exosomes can increase ten-fold[132]. After paracrine transfer, the PAMP/DAMPs stimulate PRRs to propagate the anti-viral response. In the case of cancer, RIG-I activation in breast cancer cells by stromal RN7SL1 can result in STAT1-mediated amplification of the NOTCH3 pathway, as previously described[132]. Consequently, this interaction favors tumor progression, resistance to therapy, and tumor-initiation capacity. In total, these data demonstrate how cancers can employ virus mimicry in the tumor microenvironment to coerce stromal cells to disseminate anti-viral signals that amplify oncogenic signaling pathways (Figure 30).

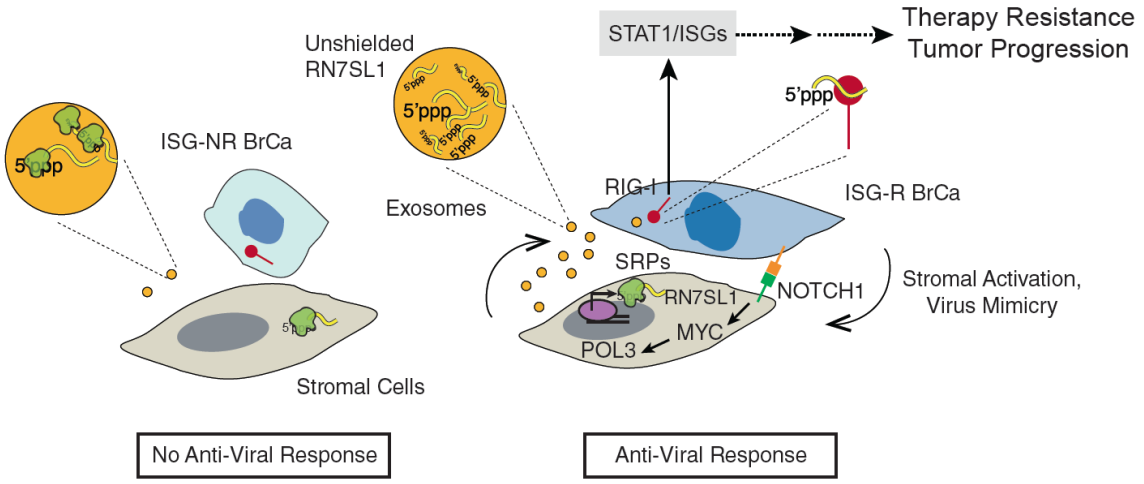

Figure 30. Model of virus mimicry and unshielding of stromal RN7SL1 to activate breast cancer RIG-I through exosome transfer.

Viral PAMPs are under selective pressure to avoid immune recognition, while endogenous RNA DAMPs must avoid recognition by PRRs under non-pathological conditions. Thus, our discovery that RN7SL1 is a cancer-associated DAMP presented a conceptual problem. Specifically, given its abundance in the cytoplasm, it was unclear how RN7SL1 could both function as a DAMP in exosomes but at the same time avoid recognition by RIG-I while in the cytoplasm. Indeed, it has long been recognized that RNA

modification and subcellular localization may be insufficient to prevent inappropriate activation by endogenous and abundant POL3 5'ppp transcripts, arguing that unknown mechanisms must exist[145]. Our findings on how differential RBP shielding of endogenous RN7SL1 can control DAMP activity and PRR activation provide an explanation for how this discrimination can be achieved. In the cytoplasm, RN7SL1 is nearly completely shielded by RBPs, presumably SRP proteins. In particular, SRP9 and SRP14 are known to interact with the 5' end of RN7SL1 and we show that these RBPs interfere with RIG-I recognition and activation. In exosomes generated from stromal activation by ISG-R breast cancer cells, SRP9/14 are absent and results in unshielding of RN7SL1 and recognition by RIG-I in recipient cells. These data also indicate that the stimulatory effects of high affinity RNA ligands for RIG-I measured in vitro, may be superseded in vivo by RBP shielding. Thus, control of RBP shielding may be a critical regulatory layer that prevents inappropriate PRR activation, especially of abundant RNAs, while concurrently allowing for a readily available and rapidly deployable DAMP.

When stromal cells encounter breast cancer cells, the initiating event that mimics viral infection and leads to the deployment of RN7SL1 as a DAMP is currently unknown. Cell-cell contact between stromal and breast cancer cells is required as conditioned media from breast cancer cells does not induce ISGs in stromal cells. Indeed, abnormal cell-cell contact between epithelial cells and fibroblasts, which are often separated by a basement membrane, typically occurs under pathological situations such as wounding or with invasive carcinoma. Thus, one possibility is that this heterotypic interaction itself may represent a "damage" signal that initiates DAMP release by the stromal compartment. Although the mechanism for this potential damage signal is unknown, recent evidence demonstrates that oncogenic signals involved in cell-cell regulation such as the Hippo pathway can lead to the secretion of extracellular vesicles containing RNA DAMPs[146]. Consistent with a role for oncogenic signaling, we show that there is a pronounced

transcriptional upregulation characteristic of cellular activation in stromal cells after contact with ISG-R breast cancer cells, as well as an increase in hallmark genes associated with MYC and RAS activation. Interestingly, POL3 activity is augmented by MYC[137] and by nearby RNA polymerase II (POL2) occupancy[141]. This suggests that high MYC and POL2 transcriptional output resulting from interaction with ISG-R breast cancer cells may enhance POL3-driven RN7SL1 levels in stromal cells. If binding by RBPs such as SRP9/14 are limiting, an ensuing increase in unshielded RN7SL1 may lead to its export into exosomes. We find that NOTCH1-mediated MYC activation is able to enhance RN7SL1 RNA output without a concomitant increase in SRP protein production, resulting in an excess of RN7SL1 that is unbound by RBPs. Thus, unshielded RN7SL1 may be a consequence of stromal activation after inappropriate interaction with epithelial cells. This aberrant stromal activation may be a trigger for virus mimicry.

Besides transferring viral RNA, the ability to horizontally transfer DAMPs may also be an important feature of virus infection, further illustrating how tumor-supporting stromal cells may borrow queues from virally infected cells. Consistent with this, virions have been described to contain not only RN7SL1 in the absence of SRP proteins but multiple other endogenous non-viral RNAs[94–97]. The role of these non-viral RNAs in virions has not been well characterized; however, it has been postulated that they might stimulate innate immune signaling[98]. Our results would support this notion and suggest that RN7SL1 in virions may act as a potent activator of RIG-I like it does in exosomes. Alternatively, in addition to containing viral RNA, exosomes secreted by infected cells may also package unshielded RN7SL1 capable of RIG-I activation. Therefore, whether in virons or in exosomes, cells under viral attack may help to ensure a broad anti-viral response by packaging endogenous DAMPs alongside viral RNA PAMPs. In support of this concept, recent studies show that cells infected by viruses can package the nucleoside second-messenger cGAMP into secreted virions to trigger a STING-dependent interferon

response in recipient cells[99,100]. In total, these observations suggest that horizontal transfer of DAMPs to promulgate anti-viral signaling is a key feature of virus mimicry. Moreover, RBP unshielding of endogenous RNAs may have broad implications for innate immune sensing not only for cancer but also during host-virus interactions.

In the context of cancer, this study, together with previous work, demonstrates that unshielded RN7SL1 activates RIG-I to amplify NOTCH3 signaling, resulting in expansion of tumor-initiating cells. Accordingly, tumor growth, metastasis, and therapy resistance are augmented. Consistent with how horizontal dissemination of DAMP signals can influence metastasis, cell-cell interaction between breast cancer and astrocytes have been shown to facilitate breast cancer brain metastasis through transfer of cGAMP via gap junctions[43]. Other instances of exoRNA activating stromal or host cell PRRs to enhance metastasis have also been described[101,102]. This includes non-coding RNAs such as microRNAs that activate toll-like receptors. In the case of the ISG-R breast cancer cells used in this study, MYD88-dependent TLRs do not have an appreciable role in stromal-mediated anti-viral signaling[132]. Moreover, of all 5'ppp transcripts identified in exosomes, only RN7SL1 was highly abundant, strongly unshielded, and predicted to have extensive double-stranded folding. Nonetheless, we do not rule out contributions from other exoRNAs as DAMPs in our study or in other cellular contexts. Similar to how defense against different viruses may rely on distinct PRRs to optimally engage different viral PAMPs, diverse forms of virus mimicry in cancer may sense different, altered, or inappropriately expressed endogenous RNAs using various innate immune sensors. The extent to which differential RBP shielding impacts these DAMP-PRR combinations remains unknown but is likely an important determinant for activation.

CHAPTER 4: CONCLUSIONS AND FUTURE DIRECTIONS

Exosomes and ncRNA are Mediators of Cell-to-Cell Communication in the Tumor Microenvironment

In these studies, we detail a complex mechanism of breast cancer tumor-stromal interaction that enhances tumor progression and therapy resistance. This interaction is characterized by both paracrine anti-viral signals and juxtacrine Notch pathway activation that converge at various stages. Here, we find that heterotypic interaction of basal-like breast cancer cells and stromal fibroblasts activates NOTCH1 in the stroma, which results in the activation stromal MYC. Consequently, MYC enhances stromal POL3 transcriptional output of RN7SL1, a highly structured, short, 5'ppp ncRNA. This POL3 transcriptional activity in not matched with an upregulation of canonical RN7SL1 RBP binding partners, SRP9 and SRP14, and results in an excess of unbound RN7SL1 transcript. Thus, stromal RN7SL1 is found in its unshielded form in the exosomes produced after tumor-stromal interaction and acts as a DAMP. Recipient breast cancer cells directly recognize unshielded RN7SL1 as a pathogenic nucleic acid through the PRR, RIG-I. This initiates an anti-viral signaling cascade resulting in the upregulation of ISGs.

Concomitantly, paracrine signals originating from presentation of stromal JAG1 to activate breast cancer NOTCH3, result in the release of the NOTCH3 intracellular domain, NICD3. The anti-viral and Notch pathways converge as STAT1 and NICD3 transcriptionally cooperate to maximize Notch pathway output that is responsible for therapy resistance. These seemingly distinct pathways overlap at the initiation and effector stages of tumor-stromal interaction to promote tumorigenicity. *In vivo*, we find that combining radiation therapy with a GSI reverses the breast cancer therapy resistance conferred by stromal cells. Further, breast cancer patients harbor evidence of circulating unshielded RN7SL1, while healthy donor exosomal RN7SL1 is largely shielded.

Expression of these pathways is also predictive of conventional treatment failure, as those patients with high ISGs and high NOTCH pathway expression have significantly worse prognosis. In total, we identify and characterize a conserved pathway by which co-expression networks in breast cancer cells and the surrounding stroma can drastically influence tumor progression, metastasis, and therapy resistance.

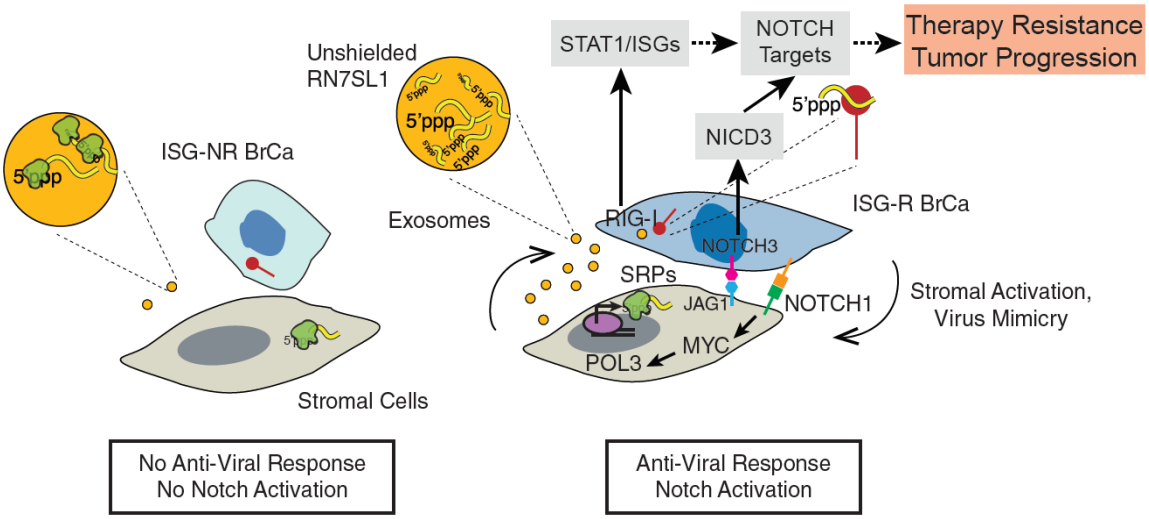

Figure 31. Model of tumor-stromal juxtacrine and paracrine pathway activation in breast cancer.

Shielding of Nucleic Acids Regulates PRR Activation

The characteristics of RNA required for RIG-I activation are well studied[147]. Typically, RIG-I is maximally activated by short, double-stranded, and 5'triphosphorylated RNA. These are all hallmark features of viral RNA that RIG-I is best characterized to bind. Under normal conditions many cellular RNA that match these characteristics are present; however, RIG-I does not bind to them at baseline. The authors of the initial study that identified 5'ppp RNA as a RIG-I ligand highlighted that many cellular RNA species are also 5'ppp and abundant in the cytoplasm; therefore, they speculated these RNA must avoid recognition by unknown mechanisms[145]. Therefore, we hypothesized that protein shielding may be a mechanism of avoiding RIG-I recognition. Viruses often shield their

5’ppp and double-stranded RNA regions with nucleocapsid proteins to avoid RIG-I recognition[148,149]. The largest source of double-stranded, 5’ppp cellular RNA is RNA polymerase III. Much of the POL3 transcriptome functions in RNPs for a variety of essential cellular process and are largely shielded under normal conditions.

We found that if properly presented, a POL3 transcript, RN7SL1, can act as a potent RIG-I ligand. Normally, RN7SL1 is bound by SRP proteins as part of the RNP known as the signal recognition particle. In exosomes originating from tumor-stromal co-culture, SRP proteins are absent and RN7SL1 is unshielded and can act as a DAMP to activate RIG-I and ISGs. We demonstrate this by metabolically labeling stromal RNA and observing its interaction by breast cancer RIG-I upon co-culture and exosome transfer. Unshielded RN7SL1 in exosomes is reminiscent of how many retrovirus virions package unshielded RN7SL1 and other POL3 transcripts[98]. While the function of these host transcripts in virions is unknown, our data suggests that RN7SL1 may also act as a DAMP in these viral infections. This is likely a host defense mechanism to activate ISGs and achieve tissue-level amplification of anti-viral responses. Similar instances of DAMP packaging in virions have been described where the STING activator cGAMP traffics in virions and extracellular vesicles after viral infection[99,100]. It is thought that cGAMP traffics in virions as a specific and potent DAMP to prime uninfected cells of impending infection. We propose that RN7SL1 may function in a similar fashion; however, due to its highly abundant and cytoplasmic nature, it is only available for deployment as a DAMP if it is unshielded. In total, our results suggest that protein shielding is a major determinant of RIG-I recognition of both self and non-self nucleic acids.

Unshielded RN7SL1 as a Regulator and Biomarker of Treatment Resistant Breast Cancer

The clinical management of cancer requires increasingly requires personalized treatment strategies. These treatment strategies often require an understanding of the individual patient's cancer mutational and expression profile. At present, interrogating this complex landscape is achieved by tissue-based methods after surgery or biopsy[150]. These methods have several drawbacks: 1) they are unable to capture the heterogeneity of tumor and tumor microenvironment, 2) they require a detectable tumor in an area that can be biopsied or surgically removed, and 3) they often cannot be obtained repeatedly over the course of disease and treatment progression. Therefore, there is considerable interest in the development of tools to interrogate blood-based biomarkers for cancer detection, prognosis, and monitoring of treatment efficacy[151]. There have been significant advances in developing and implementing technology for the detection of circulating tumor DNA (ctDNA), which, can accurately diagnose and monitor treatment progression in certain cancers[152,153]. Further, enrichment for cancer-derived exosomes with protein markers and identification of KRas mutations can accurately diagnose pancreatic cancer at early stages[75]. While these approaches have extensive capabilities to detect ctDNA with exquisite sensitivity and specificity, they are limited by the assessment of mutational status. In order to further increase the power of liquid biopsy approaches it would be valuable to develop methods that facilitate novel applications, such as identification of therapeutic vulnerabilities not based on mutational status, enumeration of cancer specific mRNA isoforms, and interrogation of cancer gene expression networks.

One potential approach for facilitating these novel applications would be analysis of cell-free RNA. While circulating cell-free RNA has been difficult to assess, exosomal RNA provides a readily available and tractable source of circulating RNA. We identified

unshielded RN7SL1 as both a regulator of breast cancer tumor progression as well as a biomarker of disease. In cancer patients compared to healthy donors we find an abundance of unshielded RN7SL1. In TNBC, where no liquid biomarker has been described, unshielded RN7SL1 provides a potential opportunity for clinical translation[4]. Exosomes and exosomal RNA is readily purified from less than 500µL of serum or plasma in less than four hours. Our MNase-based shielding assays take less than 24 hours from start to finish and produce consistent results. While much work remains to be done to bring these shielding assays to the clinic, it represents a promising avenue to consider.

Tumor-Stroma Co-Expression Networks are a Promising Drug Target

The tumor microenvironment is a driver of cancer initiation, progression, metastasis, and therapy resistance. Therapies that account for these complex interactions must be developed and implemented. Strategies to target the tumor microenvironment have been attempted with varied success. Most prominently, the tumor vasculature can be targeted by blocking the predominant proangiogenic molecule, vascular endothelial growth factor (VEGF), with monoclonal antibodies[154]. Such blocking antibodies were approved by the FDA in for the treatment of metastatic colon cancer in 2004 and subsequently for many other cancers alone or in combination with other therapies. While it presents a mild clinical benefit for many cancers, VEGF blockade in breast cancer is ineffective. The FDA withdrew approval of VEGF blocking antibodies for patients with HER2-negative cancers due to its lack of therapeutic benefit and significant toxicity[155]. Targeting cancer-associated inflammation by inhibition of tumor-associated macrophages (TAM) has found significant preclinical success[156]. Additionally, targeting of microenvironmental signaling pathways such as cyclooxygenase-2 (COX2), transforming growth factor beta (TGFβ), JAK-STAT, TNF-α, and nuclear factor kappa-light-chain-enhancer of activated B cells (NF-κB) have been both preclinically and clinically

successful[157,158]. While these successes are promising, drawbacks include toxicity due to broad targeting of nonpathogenic stroma, acquisition of resistance mechanisms by both the tumor stroma and cancer cells, and lack of sufficient biomarkers to optimally treat patient subsets.

The most clinically beneficial strategies to target the tumor microenvironment may be to target pathways of tumor-stromal crosstalk. Combinatorial therapy in cancer has proven to be an efficacious treatment strategy in most cancers[159,160]. Rational combination of conventional cytotoxic therapies with targeted therapy, immunotherapy, and distinct cytotoxic therapies is the current standard of care in many cancers. Targeting of tumor-stroma interactions provides an opportunity to target both subsets with a single agent. Our data would suggest that specific therapies that target co-expression pathways can serve as a combinatorial single-agent therapy. For example, ISG and NOTCH pathway activation in both stromal and breast cancer cells supports tumorigenesis, progression, and therapy resistance. We have demonstrated that the activation of these pathways is intimately intertwined; therefore, we would predict that targeting of one pathway should cripple the other. Indeed, we find that the combination of radiation therapy and GSI results in remarkable tumor regression in xenograft models of breast cancer. We posit that this is due to simultaneous targeting of tumor and stromal ISG and NOTCH pathways. Therefore, it is imperative to expand these findings to other tumor-stromal interaction networks, such as RAS pathway activation and cGAS/STING pathway activation[43,131].

Exosomal Activation or Suppression of Anti-Tumor Immune Responses

We have identified exosomes and exosomal RNA as a conduit for tumor-fibroblast crosstalk that influence and accelerate various stages of breast cancer tumor progression. While fibroblasts are the predominant stromal subtype in breast cancer, infiltrating myeloid and lymphoid cells may also play a significant role. The immunogenic role of exosomes

are well-characterized[106]. Exosomes can be immune activating by directly and indirectly activating dendritic cells by modulation of antigen presentation. They may also directly activate natural killer (NK) cells, macrophages, B cells, and T cells. Recently, it was also demonstrated that activation of canonically oncogenic signals can result in the release of immune activating exosomes that results in robust tumor clearance[146]. Exosomes can also be immune suppressive by inhibiting cytotoxic activity of effector CD4 and CD8 T cells, and NK cells. They can further suppress immune activation by inhibiting DC differentiation and promotion of myeloid-derived suppressor (MDSC) differentiation. In total, there is a clear interaction with exosomes and the immune system. The role of RNA-sensing pathways in the activation or suppression of innate and adaptive immune system is understudied. It is unclear whether activation of these pathways in the tumor microenvironmental milieu would activate or suppress anti-tumor immune responses. How exosomes contribute to this balance in breast cancer is not yet understood. Generally, fibroblast activation in breast cancer is thought to be immune suppressive[161]; therefore, exosomes containing unshielded RN7SL1 may function to maintain an immunologic environment that is favorable to tumor progression.

Clinical trials utilizing antibody-based blockade of immune checkpoints such as CTLA4 and PD1/PDL1 have resulted in remarkable and durable responses. Unfortunately, the majority of patients do not respond to these therapies alone due to adaptive and acquired resistance mechanisms[162]. Therefore, there is considerable interest in the combination of immunotherapies and targeted or conventional cytotoxic therapies for the treatment of solid cancers[163,164]. Understanding the immune suppressive or activating role of exosomes present in the tumor microenvironment can ultimately lead to the rational combination of therapies. In particular, breast cancer can be largely immunologically silent. If exosomes containing unshielded RN7SL1 are demonstrated to be immunosuppressive, then it would suggest patients harboring evidence of circulating

unshielded RN7SL1 not be treated with immune checkpoint blockade alone, but in combination with GSI to cripple tumor-stroma interactions. If the converse is true, then those patients may be promising candidates for single agent immune checkpoint blockade. Beyond biomarkers, exosomes are emerging as candidates for delivery of therapeutics[165]. RNA lipoplexes have shown promise in activation of antigen presenting cells and mediating rejection of murine tumors in combination with immunotherapy[166]. However, systemic autoimmune responses may result from potent delivery of nonspecific synthetic RNA and liposomes. Therefore, endogenous unshielded RN7SL1 encapsulated into autologous exosomes may result in safer treatment strategies. In total, exosomes provide another opportunity to personalize and adapt conventional and emerging therapies for breast cancer patients.

CHAPTER 5: MATERIALS AND METHODS

Cell Culture and Cell Sorting

Cell culture and cell sorting were completed as previously described[132]. All cell lines were confirmed to be mycoplasma-free with repeated testing. All human breast cancer and stromal cell lines were cultured at 37^{o}C in DMEM supplemented with 10% FBS, 100U/ml penicillin and 100µg/ml streptomycin, and 2mM l-glutamine. The KB1P mouse breast cancer cell lines from K14cre;p53$^{F/F}$;Brca1$^{F/F}$ mice[120] were cultured in RPMI. All co-culture experiments were performed in DMEM with exosome-depleted FBS. Breast cancer cells were labeled with 7.5µM 5-(and-6)-carboxyfluorescein diacetate, succinimidyl ester (CFSE) and mixed 1:1 with stromal cells. Cell populations with a purity of at least 98% were used for RNA or protein isolation.

Cell Death Assays

Sytox cell death assays were completed as previously described[132]. In brief, mono- or co-cultures were irradiated after 48 hours with 10 Gy using a Cs-137 Gammacell 40 EXACTOR. Cell death of CFSE-labeled breast cancer cells was measured at 96 hours post-radiation by flow cytometry using Sytox-Red (Invitrogen). Relative cell death was calculated by comparing mono and co-culture cell death.

Cell Culture Exosome Isolation

Cell cultures used to isolate exosomes were grown in exosome-depleted media prepared by ultracentrifugation of FBS for 3 hours at 100,000xg. Exosomes were isolated from conditioned media collected at 48-72 hours by serial high speed ultracentrifugation as previously described[167] or using 10% final concentration of polyethylene-glycol and low speed centrifugation, as previously described[168]. Purity was examined by electron microscopy by negative staining, protein analysis by immunoblotting, and quantified by NanoSight N1000 analysis. For exosome injection experiments, protein was quantified by

Lowry method, and equivalent volume of 10µg of exosomes were injected. For exosome depletion, conditioned media was ultracentrifuged for 8-16hours.

Serum Exosome Collection

Serum from patients with cancer were obtained through the UPENN RadOnc Biosample Repository. Blood was collected using yellow top Vacutainer (BD) and centrifuged at 3000rpm for 10 minutes. The samples were then frozen at -80^{o}C until use. Serum from healthy donors was obtained commercially (Innovative Research). For exosomes from human or mouse serum, 500µl of serum was spun at 2000xg for 15 minutes, filtered through a 0.22µm filter, and then purified by serial high speed ultracentrifugation.

EU Labeling and Quantification

Stromal cells were labeled with 100µM 5-Ethynyl Uridine (EU) for 24 hours, and breast cancer cells were labeled with DiD (1:200) for 10 minutes at 37^{o}C. Both cells types were then washed and co-cultured for 8 or 24 hours on glass coverslips. EU was then visualized by Alexa Fluor 488 azide (Alexa Fluor® 488 5-carboxamido-(6-azidohexanyl), bis(triethylammonium salt))[169]. Percentage of double positive cells that matched breast cancer cell morphology were scored as EU+ breast cancer cells.

4sU RNA Transfer Quantification

Stromal cells were labeled with 200µM 4sU (4-Thiouracil) for 24 hours, washed, and either left in mono-culture or co-cultured with breast cancer cells. Conditioned media was isolated after 24 hours and added to mono-cultured breast cancer cells. Breast cancer cells were harvested 24 hours later and RNA extracted. 4sU-labeled RNA was specifically biotinylated with HPDP-Biotin and enriched with streptavidin-conjugated magnetic beads, as previously described[170]. Transfer of stromal-derived RNA was determined by quantification of total 4sU-labeled RNA in recipient breast cancer cells compared to total RNA or by qRT-PCR.

4sU-FLAG-RIP

Stromal cells were labeled with 200μM 4sU (4-Thiouracil), washed, and co-cultured with breast cancer cells with RIG-I CRISPR KO, RIG-I KO with re-expression of FLAG-tagged RIG-I or RIG-I$^{K858/861A}$ for 48 hours. Co-cultures were harvested and 100mg of wet cell pellet was lysed by sonication (five, one-second bursts, medium output) in RSB-200 buffer (20mM Tris pH 7.5, 200mM NaCl, 2.5mM $MgCl_2$, 0.5% NP-40, 0.1% Triton X-100, 0.2 U/uL RNase Inhibitor, and one tablet of protease inhibitors). Post-lysis, FLAG-RIG-I was immunoprecipitated with prebound and washed FLAG-M2 beads (Sigma) using 30uL of beads per 100mg of wet cell pellet for 2-3 hours at 4^{o}C. Beads were then washed three times with RSB-200. RNA was extracted with TRIzol reagent utilizing linear acrylamide as a carrier. 4sU-labeled RNA was then enriched as described above.

Gene Targeting and Expression

Gene knockdown by siRNA was completed using SMARTPool siRNAs (Thermo) and transfected using 20nM siRNA and RNAiMax (Invitrogen) transfection reagent. For stable knockdowns, shRNAs were cloned into the pGIPZ vector and transduced by virus using pCMV-VSV-G and pHR8.2ΔR envelope and packaging vectors in HEK293T cells. Transduced cells were selected using 1-2μg/ml of puromycin. Wild-type and K858A/K861A binding mutant of RIG-I was cloned into the pOZ-N vector (a kind gift from Roger Greenberg). Transduced cells were then selected with IL-2 receptor magnetic beads and expression was confirmed by Western blot for FLAG, HA, and RIG-I. RIG-I restoration was functionally confirmed by RIG-I pathway activation in response to Sendai virus infection. SRP9 and SRP14 were transiently transfected with pGFH-9 (Addgene plasmid # 39538) and pGFH-14c (Addgene plasmid # 39541), both gifts from Katharina Strub. Gene knockout by CRISPR was accomplished using pSpCas9(BB)-2A-GFP (PX458), a gift from Feng Zhang (Addgene plasmid # 48138). RIG-I was knocked out utilizing the protocol described[171]. In brief, two distinct guide RNAs cloned into the

pSpCas9(BB)-2A-GFP backbone were transiently transfected into breast cancer cells. After 48 hours, single cells were sorted into 96 well single cell clones based on highest GFP expression. Clones were confirmed to have no RIG-I expression by immunoblot and pooled. RIG-I KO in the pooled clones were functionally confirmed by RIG-I pathway activation in response to Sendai virus infection.

Recombinant Protein Production and Purification

Recombinant SRP9 was produced by subcloning the SRP9 cDNA from pGFH-9 plasmid into the pET Hi12 GST TEV LIC cloning vector (1G), a gift from Scott Gradia (Addgene plasmid # 29655). Recombinant protein was produced in BL21 competent *E. coli* and captured with Glutathione Sepharose beads (GE Healthcare). GST-tagged TEV Protease (Sigma) was used to cleave GST-SRP9.

In Vivo Mouse Studies

All mouse studies were completed in accordance with ULAR and IACUC regulations. For exosome injection studies, 1 x 10^6 1833 breast cancer cells were injected with Matrigel (Corning) into the flanks of 6-8 week old athymic nude mice and 10µg of mono- or co-culture exosomes were directly injected into the tumors 3 times a week. For RNA injection studies, 50ng of 7SL or GAPDH300 RNA encapsulated into RNAiMax liposomes were directly injected into the tumors 3 times a week. Subcutaneous tumor growth was measured by caliper. For lung colonization studies, 2 x 10^5 luciferase-labeled 4175 breast cancer cells were injected in the tail vein. Injections were confirmed by immediate imaging using a Xenogen IVIS 100 system. Serum was isolated from mice by cardiac puncture.

Exosome RNA Sequencing

Exosome RNA was extracted with TRIzol and library preparation was completed using the NEBNext Ultra Directional RNA Library Prep Kit for Illumina (NEB) modified so that the RNA was not fragmented prior to library preparation. ERCC controls (Invitrogen) were

added into all exosome RNA samples. Libraries were sequenced on Illumina HiSeq 2500 with 100 base paired end reads.

Microarray Data Processing and Normalization

Gene expression data for ISG-R and ISG-NR breast cancer cells co-culture with MRC5 fibroblasts have been described[132] and available at the GEO (GSE60998). ISG-R cell lines included: MDA-MB-231, MDA-MB-231 (1833), and HCC1937. ISG-NR cell lines included: MCF7 and MDA-MB-468. Pre-processing, filtering, and differential gene expression analysis were performed as previously described[132]. Gene set analysis was performed using the *piano* R package and Reactome gene sets downloaded from the Molecular Signatures Database v5.1 (http://software.broadinstitute.org/gsea/msigdb). The gene set for upregulated cancer associated ISGs has been previously described [38].

MNase qRT-PCR and RNA Sequencing

Either whole cells or whole exosomes were incubated at 37°C for 30 minutes in MNase Buffer (25mM Tris-HCl, 2.5mM $CaCl_2$, 50mM NaCl, 1X PBS), with or without MNase and with or without 0.1% Triton X-100. Pre-MNase treatment, 10ng of DVG396 RNA was spiked-in to control for differences in MNase activity with or without detergent. Post-MNase treatment, TRIzol LS reagent was used to purify RNA using linear acrylamide as a carrier, and ERCC Controls (Invitrogen) were spiked-in to account for differences in efficiency of RNA extraction. For RNA sequencing studies, libraries were prepared from purified RNA using the NEBNext Ultra Directional RNA Library Prep Kit for Illumina (NEB) without further RNA fragmentation. Libraries were sequenced on Illumina HiSeq 2500 with 100 base paired end reads. For qRT-PCR studies, percent shielded was quantified by ΔΔCt method normalizing to DVG396 spike-in and MNase without detergent.

RNA-seq data analysis

For exosome RNA-seq and MNase RNA-seq analysis, reads were trimmed first using *cutadapt* v1.9[172] with parameters -q 10 -m 30 -O 4. Trimmed reads were then aligned to ERCC controls, rRNAs sequences as well as RN7SL1 by using bowtie2[173]. The remaining reads were aligned to the GRCh38 reference genome using *STAR* v2.4.0k[174] with parameters --outFilterMultimapNmax 100 --outFilterMismatchNmax 999 --outFilterMismatchNoverLmax 0.06. Primary aligned reads were counted against GENCODE annotation v21[175] and RepeatMasker annotation (UCSC Genome Browser) using *Subread* v1.4.6[176] with parameters -s 2 -minReadOverlap 10. The *DESeq2* R package version 1.10[177] was used for differential gene expression analysis. ERCC controls were used for inter-sample normalization.

5' triphosphate RNA Sequencing

To enrich for 5'triphosphate RNA, 0.1-2 µg of exosomal RNA was prepared by first degrading 5'monophosphate RNA with Terminator 5´-Phosphate-Dependent Exonuclease (Epicentre), then converting 5'triphosphate to 5'p with RNA 5' Polyphosphatase (Epicentre), to allow for specific ligation of RNA adaptor P5_RNA to RNAs that originally have 5' triphosphate. Then, cDNAs were synthesized by using a primer with 5' random 9mer (P7_N9), and amplified with NEBNext PCR reagents (NEB) by using the same protocol as other RNA-seq libraries. Libraries were sequenced on Illumina HiSeq 2500 with 100 base paired end reads. Only the first reads of the paired end reads were used in data analysis. Reads were trimmed and aligned the same as RNA-seq analysis. Primary reads that matched the 5' end of annotated features were counted.

In Vitro Transcription

In vitro transcription was performed using of PCR amplified cDNA templates that contained Hepatitis Delta Virus Ribozyme to ensure homogenous 3' ends of the transcripts of interest[178]. In vitro transcription was completed with the MEGAshortscript T7 Transcription Kit (ThermoFisher) according to manufacturer's instructions. RNA was

DNase treated and phenol/chloroform purified. After thermocycling to ensure ribozyme cleavage, correct size transcripts were gel purified.

RIG-I ATPase Assays

RIG-I ATPase assays were performed as previously described[57]. In brief, increasing amounts of RNA (10-60nM) were added to a constant quantity of RIG-I (5nM) in the presence of 1mM ATP. ATP hydrolysis was measured with the EnzChek Phosphate Assay Kit (ThermoFisher) after 60-90 minutes at 37^{o}C. ATP hydrolysis was then measured by absorbance of 360nm compared to background. A 19-mer 5'triphosphate dsRNA (Invivogen) and DVG396 were used as positive controls and a 19-mer 5'OH dsRNA (Invivogen) and an in vitro transcribed 300bp ssRNA stretch of GAPDH (GAPDH300) were used as negative controls.

Protein Analysis

Protein was extracted using 2X SDS lysis buffer, separated by 4%–12% SDS-PAGE, transferred to a PVDF membrane, blocked with 5% nonfat milk in PBS-Tween (0.01%), and probed with the antibodies described. Protein was visualized using ECL (SuperSignal West Pico, Thermo).

qRT-PCR Gene Expression Analysis

Total RNA was isolated and purified from cells using TRIzol reagent (Invitrogen). cDNA was synthesized using the High Capacity RNA-to-cDNA kit (ABI) according to manufacturer's instructions. qRT-PCR was performed using Power SYBR Green PCR MasterMix (ABI) on the TaqMan 7900 (ABI). Relative expression levels were defined using the ΔΔCt method and normalizing to 18S rRNA, β-Actin and GAPDH.

Cell Lines Used in All Studies

The cell lines used are provided in the table below:

Human			Mouse	
ISG-R	ISG-NR	Fibroblast	ISG-R	Fibroblast
MDA-MB-231 (1833)	MCF7	MRC5	KB1P	ALF
MDA-MB-231 (4175)	MDA-MB-468	BJ		
MDA-MB-436				
HCC1937				

Primers Used in qRT-PCR

The primers used in qRT-PCR are provided in the tables below:
Human:

	Forward	Reverse
GAPDH	GCTCAGACACCATGGGGAAGG	TTCCCGTTCTCAGCCTTGAC
18S	GTTCAGCCACCCGAGATTGA	CCCATCACGAATGGGGTTCA
ACTB	GCCCTGAGGCACTCTTCCA	CGGATGTCCACGTCACACTTC
IFIT1	GGCTGCCTAATTTACAGCAACC	GGCATTTCATCGTCATCAATGG
MX1	CGACACGAGTTCCACAAATG	AAGCCTGGCAGCTCTCTACC
ISG15	GAGAGGCAGCGAACTCATCT	CTTCAGCTCTGACACCGACA
RIG-I	CACCTCAGTTGCTGATGAAGGC	GTCAGAAGGAAGCACTTGCTACC
POLR3G	GATGACGATGATGCCGCAGA	GGTTGCCTCATCCATGTTGT
POLR3F	AGGCTCCACCAGTCACAGAC	TGCCATTAACAGAAATCAACAAA
STAT1	TTACTCCAGGCCAAAGGAAG	TTCAGCTGTGATGGCGATAG
7SK	GGGTTGATTCGGCTGATCT	GGGGATGGTCGTCCTCTT
RN7SL1	GTGTCCGCACTAAGTTCGG	TATTCACAGGCGCGATCC
hsRN7SL1	GCTACTCGGGAGGCTGAGGCT	TATTCACAGGCGCGATCC
RMRP	AAAGTCCGCCAAGAAGCGTA	CTGCCTGCGTAACTAGAGGG
RPPH1	AGCTTGGAACAGACTCACGG	AATGGGCGGAGGAGAGTAGT
RNU2	CGTCCTCTATCCGAGGACAAT	CGGAGCAAGCTCCTATTCCA
TSG101	AGAAGGGGCGTGATAGACCT	CACTGAGACCGGCAGTCTTT
MMP1	TGTGGTGTCTCACAGCTTCC	TTTTCAACTTGCCTCCCATC

Mouse:

	Forward	Reverse
GAPDH	AGGTCGGTGTGAACGGATTTG	TGTAGACCATGTAGTTGAGGTCA
18S	CCCCATGAACGAGGGAATT	GGGACTTAATCAACGCAAGCTT
STAT1	ACAACATGCTGGTGACAGAGCC	TGAAAACTGCCAACTCAACACCTC
ISG15	CCAGTCTCTGACTGTGAGAGC	GCATCACTGTGCTGCTGGGAC
MX1	GACCATAGGGGTCTTGACCAA	AGACTTGCTCTTTCTGAAAAGCC
mmRN7SL1	GCTACTCGGGAGGCTGAGACA	TATTCACAGGCGCGATCC

Spike-In Controls

	Forward	Reverse
DVG396	ACTGGGTCATTCCCTGACCA	CCCTCAGGTTCCTGATCTCAC

ERCC04	TGGGGCGAGTATTCCCAATG	TGGGGAAATTTGGGAAGCAGT
ERCC95	CTTGCCTGCTGCATGTTGTG	GAGCGATAGCGGTTAAGCCA
ERCC108	GCCGCTGTTGCGTAAATCAA	AGCCGACTGCTGCTCATATC
ERCC130	GTACTGACCAGCGTCACACA	GCGTGCGGTCAATCATCTTC

Adaptors for 5' Triphosphate RNA Sequencing

P5_RNA	ACACUCUUUCCCUACACGACGCUCUUCCGAUCU
P7_N9	GTGACTGGAGTTCAGACGTGTGCTCTTCCGATCTNNNNNNNNN

Antibodies Used for Immunoblotting

The primers for immunoblotting are provided in the table below:

	Company	Catalog Number	Dilution
β-actin	Cell Signaling	4970	1:10000
SRP9	Proteintech	11195-1-AP	1:500
SRP14	Proteintech	11528-1-AP	1:500
GFP	Abcam	ab6673	1:500
RPC32	Santa Cruz	sc-21754	1:200
RIG-I	Cell Signaling	3743	1:500
ISG15	Santa Cruz	sc-50366	1:200
FLAG	Sigma	F1804	1:2000
HA	Santa Cruz	sc-7392	1:500

Gene Targeting Sequences

The sequences for siRNA, shRNA and CRISPR gRNA are listed in the tables below:

siRNA:

	Sequence	Catalog Number
CTRL	Non-Targeting #1	D-001810-01-20
POLR3F	SMARTpool	L-019240-01-0005

shRNA:

	Sequence	Catalog Number
CTRL	GIPZ Non-Silencing shRNA	RH8346
RIG-I #1	TTAAATTTGTCGCTAATCC	V2LHS-199776
RIG-I #2	TAAAGTCCAGAATAACCTG	V2LHS_197176

CRISPR:

	gRNA Sequence
RIG-I #1	GGGTCTTCCGGATATAATCC
RIG-I #2	GGATTATATCCGGAAGACCC

REFERENCES

1. Siegel, R., Miller, K. & Jemal, A. Cancer Statistics, 2017. *CA Cancer J Clin* **67,** 7–30 (2017).
2. Howlader, N. *et al.* Cancer of the Breast - SEER Stat Fact Sheets. *SEER Cancer Statistics Review* (2013). Available at: http://seer.cancer.gov/csr/1975_2010/.
3. Thariat, J., Hannoun-Levi, J.-M., Sun Myint, A., Vuong, T. & Gérard, J.-P. Past, present, and future of radiotherapy for the benefit of patients. *Nat. Rev. Clin. Oncol.* **10,** 52–60 (2013).
4. Gu, G., Dustin, D. & Fuqua, S. A. Targeted therapy for breast cancer and molecular mechanisms of resistance to treatment. *Curr. Opin. Pharmacol.* **31,** 97–103 (2016).
5. Herrera-Abreu, M. T. *et al.* Early adaptation and acquired resistance to CDK4/6 inhibition in estrogen receptor-positive breast cancer. *Cancer Res.* **76,** 2301–2313 (2016).
6. Arteaga, C. L. *et al.* Treatment of HER2-positive breast cancer: current status and future perspectives. *Nat. Rev. Clin. Oncol.* **9,** 16–32 (2012).
7. Cristofanilli, M. *et al.* Fulvestrant plus palbociclib versus fulvestrant plus placebo for treatment of hormone-receptor-positive, HER2-negative metastatic breast cancer that progressed on previous endocrine therapy (PALOMA-3): final analysis of the multicentre, double-blind, phas. *Lancet Oncol.* **17,** 425–439 (2016).
8. Slamon, D. J. *et al.* Adjuvant Trastuzumab in HER2-Positive Breast Cancer Dennis. *N. Engl. J. Med.* **3365,** 1273–1283 (2011).
9. Swain, S. M. *et al.* Pertuzumab, trastuzumab, and docetaxel in HER2-positive metastatic breast cancer. *N. Engl. J. Med.* **372,** 724–34 (2015).
10. Hanahan, D. & Coussens, L. M. Accessories to the crime: functions of cells recruited to the tumor microenvironment. *Cancer Cell* **21,** 309–22 (2012).
11. Sun, Y. *et al.* Treatment-induced damage to the tumor microenvironment promotes prostate cancer therapy resistance through WNT16B. *Nat. Med.* **18,** 1359–1368 (2012).
12. Wilson, T. R. *et al.* Widespread potential for growth-factor-driven resistance to anticancer kinase inhibitors. *Nature* **487,** 505–9 (2012).
13. McMillin, D. W., Negri, J. M. & Mitsiades, C. S. The role of tumour-stromal interactions in modifying drug response: challenges and opportunities. *Nat. Rev. Drug Discov.* **12,** 217–28 (2013).
14. Obenauf, A. C. *et al.* Therapy-induced tumour secretomes promote resistance and tumour progression. *Nature* (2015). doi:10.1038/nature14336
15. Vanharanta, S. & Massagué, J. Origins of metastatic traits. *Cancer Cell* **24,** 410–21 (2013).
16. Kalluri, R. The biology and function of fibroblasts in cancer. *Nat. Rev. Cancer* **16,** 582–598 (2016).

17. Pickup, M. W., Mouw, J. K. & Weaver, V. M. The extracellular matrix modulates the hallmarks of cancer. *EMBO Rep* **15,** 1243–1253 (2014).

18. Erez, N., Truitt, M., Olson, P., Arron, S. T. & Hanahan, D. Cancer-Associated Fibroblasts Are Activated in Incipient Neoplasia to Orchestrate Tumor-Promoting Inflammation in an NF-kappaB-Dependent Manner. *Cancer Cell* **17,** 135–47 (2010).

19. Scherz-Shouval, R. *et al.* The Reprogramming of Tumor Stroma by HSF1 Is a Potent Enabler of Malignancy. *Cell* **158,** 564–578 (2014).

20. Quail, D. F. & Joyce, J. a. Microenvironmental regulation of tumor progression and metastasis. *Nat. Med.* **19,** 1423–1437 (2013).

21. Özdemir, B. C. *et al.* Depletion of Carcinoma-Associated Fibroblasts and Fibrosis Induces Immunosuppression and Accelerates Pancreas Cancer with Reduced Survival. *Cancer Cell* 1–16 (2014). doi:10.1016/j.ccr.2014.04.005

22. Rhim, A. D. *et al.* Stromal Elements Act to Restrain, Rather Than Support, Pancreatic Ductal Adenocarcinoma. *Cancer Cell* 1–13 (2014). doi:10.1016/j.ccr.2014.04.021

23. Laklai, H. *et al.* Genotype tunes pancreatic ductal adenocarcinoma tissue tension to induce matricellular fibrosis and tumor progression. *Nat. Med.* (2016). doi:10.1038/nm.4082

24. Farmer, P. *et al.* A stroma-related gene signature predicts resistance to neoadjuvant chemotherapy in breast cancer. *Nat. Med.* **15,** 68–74 (2009).

25. Kopan, R. & Ilagan, M. X. G. The Canonical Notch Signaling Pathway: Unfolding the Activation Mechanism. *Cell* **137,** 216–233 (2009).

26. Bray, S. Notch signalling: a simple pathway becomes complex. *Nat. Rev. Mol. Cell Biol.* **7,** 678–689 (2006).

27. Nowell, C. S. & Radtke, F. Notch as a tumour suppressor. *Nat. Rev. Cancer* **17,** 145–159 (2017).

28. Gallahan, D. & Callahan, R. The mouse mammary tumor associated gene INT3 is a unique member of the NOTCH gene family (NOTCH4). *Oncogene* **14,** 1883–90 (1997).

29. Cohen, B. *et al.* Cyclin D1 is a direct target of JAG1-mediated Notch signaling in breast cancer. *Breast Cancer Res. Treat.* **123,** 113–124 (2010).

30. Azzam, D. J. *et al.* Triple negative breast cancer initiating cell subsets differ in functional and molecular characteristics and in γ-secretase inhibitor drug responses. *EMBO Mol. Med.* **5,** 1502–22 (2013).

31. Lawson, D. a *et al.* Single-cell analysis reveals a stem-cell program in human metastatic breast cancer cells. (2015). doi:10.1038/nature15260

32. Osipo, C. *et al.* ErbB-2 inhibition activates Notch-1 and sensitizes breast cancer cells to a gamma-secretase inhibitor. *Oncogene* **27,** 5019–32 (2008).

33. Mittal, S., Subramanyam, D., Dey, D., Kumar, R. V & Rangarajan, A. Cooperation of Notch and Ras/MAPK signaling pathways in human breast carcinogenesis. *Mol. Cancer* **8,** 128 (2009).

34. Meurette, O. *et al.* Notch activation induces Akt signaling via an autocrine loop to prevent apoptosis in breast epithelial cells. *Cancer Res.* **69,** 5015–5022 (2009).

35. Liu, W., Singh, S. R. & Hou, S. X. JAK-STAT is restrained by Notch to control cell proliferation of the drosophila intestinal stem cells. *J. Cell. Biochem.* **109,** 992–999 (2010).

36. van Es, J. H. *et al.* Notch/gamma-secretase inhibition turns proliferative cells in intestinal crypts and adenomas into goblet cells. *Nature* **435,** 959–63 (2005).

37. Aster, J. C. & Blacklow, S. C. Targeting the Notch pathway: Twists and turns on the road to rational therapeutics. *J. Clin. Oncol.* **30,** 2418–2420 (2012).

38. Weichselbaum, R. R. *et al.* An interferon-related gene signature for DNA damage resistance is a predictive marker for chemotherapy and radiation for breast cancer. *Proc. Natl. Acad. Sci. U. S. A.* **105,** 18490–5 (2008).

39. Khodarev, N. N. *et al.* STAT1 is overexpressed in tumors selected for radioresistance and confers protection from radiation in transduced sensitive cells. *Proc. Natl. Acad. Sci. U. S. A.* **101,** 1714–9 (2004).

40. Sistigu, A. *et al.* Cancer cell-autonomous contribution of type I interferon signaling to the efficacy of chemotherapy. *Nat. Med.* **20,** 1301–1309 (2014).

41. Roulois, D. *et al.* DNA-Demethylating Agents Target Colorectal Cancer Cells by Inducing Viral Mimicry by Endogenous Transcripts. *Cell* **162,** 961–973 (2015).

42. Chiappinelli, K. B. *et al.* Inhibiting DNA Methylation Causes an Interferon Response in Cancer via dsRNA Including Endogenous Retroviruses. *Cell* **162,** 974–986 (2015).

43. Chen, Q. *et al.* Carcinoma–astrocyte gap junctions promote brain metastasis by cGAMP transfer. *Nature* **533,** 493–498 (2016).

44. Takeuchi, O. & Akira, S. Pattern recognition receptors and inflammation. *Cell* **140,** 805–20 (2010).

45. Schlee, M. & Hartmann, G. Discriminating self from non-self in nucleic acid sensing. *Nat. Rev. Immunol.* **16,** 566–580 (2016).

46. Ablasser, A. *et al.* RIG-I-dependent sensing of poly(dA:dT) through the induction of an RNA polymerase III-transcribed RNA intermediate. *Nat. Immunol.* **10,** 1065–72 (2009).

47. Chiu, Y.-H., Macmillan, J. B. & Chen, Z. J. RNA polymerase III detects cytosolic DNA and induces type I interferons through the RIG-I pathway. *Cell* **138,** 576–91 (2009).

48. Schneider, W. M., Chevillotte, M. D. & Rice, C. M. Interferon-stimulated genes: a complex web of host defenses. *Annu. Rev. Immunol.* **32,** 513–45 (2014).

49. Sadler, A. J. & Williams, B. R. G. Interferon-inducible antiviral effectors. *Nat. Rev. Immunol.* **8,** 559–568 (2008).

50. Zhao, C., Collins, M. N., Hsiang, T. Y. & Krug, R. M. Interferon-induced ISG15 pathway: An ongoing virus-host battle. *Trends Microbiol.* **21,** 181–186 (2013).

51. Malathi, K., Dong, B., Gale, M. & Silverman, R. H. Small self-RNA generated by RNase L amplifies antiviral innate immunity. *Nature* **448,** 816–9 (2007).

52. Roers, A., Hiller, B. & Hornung, V. Recognition of Endogenous Nucleic Acids by the Innate Immune System. *Immunity* **44,** 739–754 (2016).

53. Cui, X., Imaizumi, T., Yoshida, H., Borden, E. C. & Satoh, K. Retinoic acid-inducible gene-I is induced by interferon and regulates the expression of interferon stimulated gene 15 in MCF-7 cells. **405,** 401–405 (2004).

54. Volkman, H. E. & Stetson, D. B. The enemy within: endogenous retroelements and autoimmune disease. *Nat. Immunol.* **15,** 415–22 (2014).

55. Eckard, S. C. *et al.* The SKIV2L RNA exosome limits activation of the RIG-I-like receptors. *Nat. Immunol.* **15,** 839–845 (2014).

56. Stetson, D. B., Ko, J. S., Heidmann, T. & Medzhitov, R. Trex1 prevents cell-intrinsic initiation of autoimmunity. *Cell* **134,** 587–98 (2008).

57. Devarkar, S. C. *et al.* Structural basis for m7G recognition and 2'-O-methyl discrimination in capped RNAs by the innate immune receptor RIG-I. *Proc. Natl. Acad. Sci.* **113,** 596–601 (2016).

58. Schuberth-Wagner, C. *et al.* A Conserved Histidine in the RNA Sensor RIG-I Controls Immune Tolerance to N1-2′O-Methylated Self RNA. *Immunity* 41–51 (2015). doi:10.1016/j.immuni.2015.06.015

59. Dieci, G., Fiorino, G., Castelnuovo, M., Teichmann, M. & Pagano, A. The expanding RNA polymerase III transcriptome. *Trends Genet.* **23,** 614–22 (2007).

60. Moqtaderi, Z. *et al.* Genomic binding profiles of functionally distinct RNA polymerase III transcription complexes in human cells. *Nat. Struct. Mol. Biol.* **17,** 635–640 (2010).

61. Nikitina, T. V., Tischenko, L. I. & Schulz, W. a. Recent insights into regulation of transcription by RNA polymerase III and the cellular functions of its transcripts. *Biol. Chem.* **392,** 395–404 (2011).

62. Meckes, D. G. & Raab-Traub, N. Microvesicles and viral infection. *J. Virol.* **85,** 12844–54 (2011).

63. Nolte-'t Hoen, E., Cremer, T., Gallo, R. C. & Margolis, L. B. Extracellular vesicles and viruses: Are they close relatives? *Proc. Natl. Acad. Sci. U. S. A.* **113,** 9155–61 (2016).

64. Colombo, M., Raposo, G. & Théry, C. Biogenesis, Secretion, and Intercellular Interactions of Exosomes and Other Extracellular Vesicles. *Annu. Rev. Cell Dev. Biol* **30,** 255–89 (2014).

65. Buschow, S. I. *et al.* MHC II In dendritic cells is targeted to lysosomes or t cell-induced exosomes via distinct multivesicular body pathways. *Traffic* **10,** 1528–1542 (2009).

66. Fauré, J. *et al.* Exosomes are released by cultured cortical neurones. *Mol. Cell. Neurosci.* **31,** 642–648 (2006).

67. Lachenal, G. *et al.* Release of exosomes from differentiated neurons and its regulation by synaptic glutamatergic activity. *Mol. Cell. Neurosci.* **46,** 409–418 (2011).

68. Lespagnol, a *et al.* Exosome secretion, including the DNA damage-induced p53-dependent secretory pathway, is severely compromised in TSAP6/Steap3-null mice. *Cell Death Differ.* **15,** 1723–33 (2008).

69. Lehmann, B. D. *et al.* Senescence-associated exosome release from human

prostate cancer cells. *Cancer Res.* **68,** 7864–71 (2008).

70. Kowal, J., Tkach, M. & Théry, C. Biogenesis and secretion of exosomes. *Curr. Opin. Cell Biol.* **29,** 116–125 (2014).

71. Trajkovic, K. *et al.* Ceramide triggers budding of exosome vesicles into multivesicular endosomes. *Science* **319,** 1244–1247 (2008).

72. Wubbolts, R. *et al.* Proteomic and biochemical analyses of human B cell-derived exosomes: Potential implications for their function and multivesicular body formation. *J. Biol. Chem.* **278,** 10963–10972 (2003).

73. Llorente, A. *et al.* Molecular lipidomics of exosomes released by PC-3 prostate cancer cells. *Biochim. Biophys. Acta - Mol. Cell Biol. Lipids* **1831,** 1302–1309 (2013).

74. Théry, C. *et al.* Cancer: Diagnosis by extracellular vesicles. *Nature* 1–2 (2015). doi:10.1038/nature14626

75. Melo, S. A. *et al.* Glypican-1 identifies cancer exosomes and detects early pancreatic cancer. *Nature* (2015). doi:10.1038/nature14581

76. Thakur, B. K. *et al.* Double-stranded DNA in exosomes: a novel biomarker in cancer detection. *Cell Res.* 1–4 (2014). doi:10.1038/cr.2014.44

77. Kim, K. M., Abdelmohsen, K., Mustapic, M., Kapogiannis, D. & Gorospe, M. RNA in extracellular vesicles. *Wiley Interdiscip. Rev. RNA* e1413 (2017). doi:10.1002/wrna.1413

78. Dreux, M. *et al.* Short-range exosomal transfer of viral RNA from infected cells to plasmacytoid dendritic cells triggers innate immunity. *Cell Host Microbe* **12,** 558–70 (2012).

79. Li, J. *et al.* Exosomes mediate the cell-to-cell transmission of IFN-α-induced antiviral activity. *Nat. Immunol.* **14,** 793–803 (2013).

80. Baglio, S. R. *et al.* Sensing of latent EBV infection through exosomal transfer of 5′pppRNA. *Proc. Natl. Acad. Sci.* **113,** 587–596 (2016).

81. Al-Nedawi, K. *et al.* Intercellular transfer of the oncogenic receptor EGFRvIII by microvesicles derived from tumour cells. *Nat. Cell Biol.* **10,** 619–24 (2008).

82. Melo, S. A. *et al.* Cancer Exosomes Perform Cell-Independent MicroRNA Biogenesis and Promote Tumorigenesis. *Cancer Cell* 1–15 (2014). doi:10.1016/j.ccell.2014.09.005

83. Skog, J. *et al.* Glioblastoma microvesicles transport RNA and proteins that promote tumour growth and provide diagnostic biomarkers. *Nat. Cell Biol.* **10,** 1470–6 (2008).

84. Peinado, H. *et al.* Melanoma exosomes educate bone marrow progenitor cells toward a pro-metastatic phenotype through MET. **18,** (2012).

85. Costa-Silva, B. *et al.* Pancreatic cancer exosomes initiate pre-metastatic niche formation in the liver. *Nat. Cell Biol.* **17,** (2015).

86. Hoshino, A. *et al.* Tumour exosome integrins determine organotropic metastasis. *Nature* 1–19 (2015). doi:10.1038/nature15756

87. Zhou, W. *et al.* Cancer-Secreted miR-105 Destroys Vascular Endothelial Barriers

to Promote Metastasis. *Cancer Cell* **25,** 501–515 (2014).

88. Luga, V. *et al.* Exosomes Mediate Stromal Mobilization of Autocrine Wnt-PCP Signaling in Breast Cancer Cell Migration. *Cell* **151,** 1542–1556 (2012).

89. Zomer, A. *et al.* In Vivo Imaging Reveals Extracellular Vesicle-Mediated Phenocopying of Metastatic Behavior. *Cell* **161,** 1046–1057 (2015).

90. Chen, W.-X. *et al.* Exosomes from Drug-Resistant Breast Cancer Cells Transmit Chemoresistance by a Horizontal Transfer of MicroRNAs. *PLoS One* **9,** e95240 (2014).

91. Hu, Y. *et al.* Fibroblast-Derived Exosomes Contribute to Chemoresistance through Priming Cancer Stem Cells in Colorectal Cancer. *PLoS One* **10,** e0125625 (2015).

92. Federici, C. *et al.* Exosome release and low pH belong to a framework of resistance of human melanoma cells to cisplatin. *PLoS One* **9,** (2014).

93. Shedden, K., Xie, X. T., Chandaroy, P., Chang, Y. T. & Rosania, G. R. Expulsion of Small Molecules in Vesicles Shed by Cancer Cells: Association with Gene Expression and Chemosensitivity Profiles. *Cancer Res.* **63,** 4331–4337 (2003).

94. Garcia, E. L. *et al.* Packaging of host mY RNAs by murine leukemia virus may occur early in Y RNA biogenesis. *J. Virol.* **83,** 12526–34 (2009).

95. Eckwahl, M. J. *et al.* Analysis of the human immunodeficiency virus-1 RNA packageome. *RNA* **22,** 1228–1238 (2016).

96. Eckwahl, M. J., Sim, S., Smith, D., Telesnitsky, A. & Wolin, S. L. A retrovirus packages nascent host noncoding RNAs from a novel surveillance pathway. *Genes Dev.* **29,** 646–657 (2015).

97. Onafuwa-Nuga, A. A., Telesnitsky, A. & King, S. R. 7SL RNA, but not the 54-kd signal recognition particle protein, is an abundant component of both infectious HIV-1 and minimal virus-like particles. *RNA* **12,** 542–6 (2006).

98. Telesnitsky, A. & Wolin, S. L. The host RNAs in retroviral particles. *Viruses* **8,** 1–15 (2016).

99. Gentili, M. *et al.* Transmission of innate immune signaling by packaging of cGAMP in viral particles. *Science* **349,** 1232–1236 (2015).

100. Bridgeman, A. *et al.* Viruses transfer the antiviral second messenger cGAMP between cells. *Science* **349,** 1228–1232 (2015).

101. Fabbri, M. *et al.* MicroRNAs bind to Toll-like receptors to induce prometastatic inflammatory response. *Proc. Natl. Acad. Sci. U. S. A.* **109,** E2110-6 (2012).

102. Liu, Y. *et al.* Tumor Exosomal RNAs Promote Lung Pre-metastatic Niche Formation by Activating Alveolar Epithelial TLR3 to Recruit Neutrophils. *Cancer Cell* **30,** 243–256 (2016).

103. Ranoa, D. R. E. *et al.* Cancer therapies activate RIG-I-like receptor pathway through endogenous non-coding RNAs. *Oncotarget* **7,** 26496–26515 (2016).

104. Bernard, J. J. *et al.* Ultraviolet radiation damages self noncoding RNA and is detected by TLR3. *Nat. Med.* **18,** 1286–90 (2012).

105. Hung, T. *et al.* The Ro60 autoantigen binds endogenous retroelements and regulates inflammatory gene expression. *Science* **350,** 455–459 (2015).

106. Théry, C., Ostrowski, M. & Segura, E. Membrane vesicles as conveyors of immune responses. *Nat. Rev. Immunol.* **9,** 581–93 (2009).

107. Korkaya, H., Liu, S. & Wicha, M. S. Breast cancer stem cells, cytokine networks, and the tumor microenvironment. *J. Clin. Invest.* **121,** 3804–3809 (2011).

108. McAuliffe, S. M. *et al.* Targeting Notch, a key pathway for ovarian cancer stem cells, sensitizes tumors to platinum therapy. *Proc. Natl. Acad. Sci. U. S. A.* **109,** E2939-48 (2012).

109. Ranganathan, P., Weaver, K. L. & Capobianco, A. J. Notch signalling in solid tumours: a little bit of everything but not all the time. *Nat. Publ. Gr.* **11,** 336–351 (2011).

110. Azzam, D. J. *et al.* Triple negative breast cancer initiating cell subsets differ in functional and molecular characteristics and in γ-secretase inhibitor drug responses. *EMBO Mol. Med.* **5,** 1502–1522 (2013).

111. Buess, M. *et al.* Characterization of heterotypic interaction effects in vitro to deconvolute global gene expression profiles in cancer. *Genome Biol.* **8,** R191 (2007).

112. Kang, Y. *et al.* A multigenic program mediating breast cancer metastasis to bone. *Cancer Cell* **3,** 537–49 (2003).

113. Kao, J. *et al.* Molecular profiling of breast cancer cell lines defines relevant tumor models and provides a resource for cancer gene discovery. *PLoS One* **4,** (2009).

114. Chen, X. & Ishwaran, H. Random forests for genomic data analysis. *Genomics* **99,** 323–329 (2012).

115. Raposo, G. & Stoorvogel, W. Extracellular vesicles: Exosomes, microvesicles, and friends. *J. Cell Biol.* **200,** 373–383 (2013).

116. Belancio, V. P., Roy-Engel, A. M. & Deininger, P. L. All y'all need to know 'bout retroelements in cancer. *Semin. Cancer Biol.* **20,** 200–10 (2010).

117. Dieci, G., Conti, A., Pagano, A. & Carnevali, D. Identification of RNA polymerase III-transcribed genes in eukaryotic genomes. *Biochim. Biophys. Acta* **1829,** 296–305 (2013).

118. Baldridge, M. T., King, K. Y., Boles, N. C., Weksberg, D. C. & Goodell, M. A. Quiescent haematopoietic stem cells are activated by IFN-γ in response to chronic infection. *Nature* **465,** 793–797 (2010).

119. Shipitsin, M. *et al.* Molecular Definition of Breast Tumor Heterogeneity. *Cancer Cell* **11,** 259–273 (2007).

120. Liu, X. *et al.* Somatic loss of BRCA1 and p53 in mice induces mammary tumors with features of human BRCA1-mutated basal-like breast cancer. *Proc. Natl. Acad. Sci. U. S. A.* **104,** 12111–12116 (2007).

121. Prat, A. *et al.* Phenotypic and molecular characterization of the claudin-low intrinsic subtype of breast cancer. *Breast Cancer Res.* **12,** R68 (2010).

122. van de Vijver, M. J., He, Y. D., Voskuil, D. W., Rutgers, E. T. & R, B. A gene-expression signature as a predictor of survival in breast cancer. *N. Engl. J. Med.* **347,** 1999–2009 (2002).

123. Valadi, H. *et al.* Exosome-mediated transfer of mRNAs and microRNAs is a novel

mechanism of genetic exchange between cells. *Nat. Cell Biol.* **9,** 654–9 (2007).

124. The ENCODE Project Consoritium. An integrated encyclopedia of DNA elements in the human genome. *Nature* **489,** 57–74 (2012).

125. Ting, D. T. *et al.* Aberrant overexpression of satellite repeats in pancreatic and other epithelial cancers. *Science* **331,** 593–6 (2011).

126. Goodier, J. L., Mandal, P. K., Zhang, L. & Kazazian, H. H. Discrete subcellular partitioning of human retrotransposon RNAs despite a common mechanism of genome insertion. *Hum. Mol. Genet.* **19,** 1712–25 (2010).

127. Balaj, L. *et al.* Tumour microvesicles contain retrotransposon elements and amplified oncogene sequences. *Nat. Commun.* **2,** 180–189 (2011).

128. Li, C. C. Y. *et al.* Glioma microvesicles carry selectively packaged coding and non-coding RNAs which alter gene expression in recipient cells. *RNA Biol.* **10,** 1333–44 (2013).

129. Kux, K. & Pitsouli, C. Tissue communication in regenerative inflammatory signaling: lessons from the fly gut. *Front. Cell. Infect. Microbiol.* **4,** 49 (2014).

130. Elstrodt, F. *et al.* BRCA1 mutation analysis of 41 human breast cancer cell lines reveals three new deleterious mutants. *Cancer Res.* **66,** 41–45 (2006).

131. Tape, C. J. *et al.* Oncogenic KRAS Regulates Tumor Cell Signaling via Stromal Reciprocation. *Cell* **165,** 910–920 (2015).

132. Boelens, M. C. *et al.* Exosome Transfer from Stromal to Breast Cancer Cells Regulates Therapy Resistance Pathways. *Cell* **159,** 499–513 (2014).

133. Becker, A. *et al.* Extracellular Vesicles in Cancer: Cell-to-Cell Mediators of Metastasis. *Cancer Cell* **30,** 836–848 (2016).

134. Liberzon, A. *et al.* The Molecular Signatures Database Hallmark Gene Set Collection. *Cell Syst.* **1,** 417–425 (2015).

135. Kalluri, R. & Weinberg, R. A. The basics of epithelial-mesenchymal transition. *J. Clin. Invest.* **119,** 1420–1428 (2009).

136. Wang, Y. *et al.* Structural and functional insights into 5'-ppp RNA pattern recognition by the innate immune receptor RIG-I. *Nat. Struct. Mol. Biol.* **17,** 781–7 (2010).

137. White, R. J. Transcription by RNA polymerase III: more complex than we thought. *Nat. Rev. Genet.* **12,** 459–463 (2011).

138. Wu, L. *et al.* Novel small-molecule inhibitors of RNA polymerase III. *Eukaryot. Cell* **2,** 256–264 (2003).

139. Akopian, D., Shen, K., Zhang, X. & Shan, S. Signal recognition particle: an essential protein-targeting machine. *Annu. Rev. Biochem.* **82,** 693–721 (2013).

140. White, R. J. Direct activation of RNA polymerase III transcription by c-Myc. *Nature* **421,** 1698–1701 (2003).

141. Oler, A. J. *et al.* Human RNA polymerase III transcriptomes and relationships to Pol II promoter chromatin and enhancer-binding factors. *Nat. Struct. Mol. Biol.* **17,** 620–628 (2010).

142. Hart, L. S. *et al.* ER stress-mediated autophagy promotes Myc-dependent transformation and tumor growth. *J. Clin. Invest.* **122,** 4621–4634 (2012).

143. Sanchez-martin, M., Ferrando, A. & Author, C. The NOTCH1-MYC highway towards T-cell acute lymphoblastic leukemia. (2017). doi:10.1182/blood-2016-09-692582

144. Minn, A. J. *et al.* Genes that mediate breast cancer metastasis to lung. *Nature* **436,** 518–24 (2005).

145. Hornung, V. *et al.* 5'-Triphosphate RNA is the ligand for RIG-I. *Science* **314,** 994–7 (2006).

146. Moroishi, T. *et al.* The Hippo Pathway Kinases LATS1 / 2 Suppress Cancer Immunity. *Cell* **167,** 1525–1539 (2016).

147. Schlee, M. & Hartmann, G. The chase for the RIG-I ligand--recent advances. *Mol. Ther.* **18,** 1254–62 (2010).

148. Weber, F. *et al.* Double-Stranded RNA Is Produced by Positive-Strand RNA Viruses and DNA Viruses but Not in Detectable Amounts by Negative-Strand RNA Viruses Double-Stranded RNA Is Produced by Positive-Strand RNA Viruses and DNA Viruses but Not in Detectable Amounts by Neg. *J. Virol.* **80,** 5059–5064 (2006).

149. Anchisi, S., Guerra, J., Mottet-osman, G. & Garcin, D. Mismatches in the Influenza A Virus RNA Panhandle Prevent Retinoic Acid-Inducible Gene I (RIG-I) Sensing by Impairing RNA /. *J. Virol.* **90,** 1–5 (2016).

150. Siravegna, G., Marsoni, S., Siena, S. & Bardelli, A. Integrating liquid biopsies into the management of cancer. *Nat. Rev. Clin. Oncol.* (2017). doi:10.1038/nrclinonc.2017.14

151. Schwarzenbach, H., Hoon, D. S. . B. & Pantel, K. Cell-free nucleic acids as biomarkers in cancer patients. *Nat. Rev. Cancer* **11,** 426–37 (2011).

152. Newman, A. M. *et al.* An ultrasensitive method for quantitating circulating tumor DNA with broad patient coverage. *Nat. Med.* **20,** 548–54 (2014).

153. Newman, A. M. *et al.* Integrated digital error suppression for improved detection of circulating tumor DNA. *Nat Biotechnol* **34,** (2016).

154. Ferrara, N. & Adamis, A. P. Ten years of anti-vascular endothelial growth factor therapy. *Nat. Rev. Drug Discov.* **15,** 385–403 (2016).

155. Fang, H. & DeClerck, Y. A. Targeting the tumor microenvironment: From understanding pathways to effective clinical trials. *Cancer Res.* **73,** 4965–4977 (2013).

156. Quail, D. F. *et al.* The tumor microenvironment underlies acquired resistance to CSF-1R inhibition in gliomas. doi:10.1126/science.aad3018

157. Hamada, S., Masamune, A. & Shimosegawa, T. Novel therapeutic strategies targeting tumor-stromal interactions in pancreatic cancer. *Front. Physiol.* **4 NOV,** 1–7 (2013).

158. Criscitiello, C., Esposito, A. & Curigliano, G. Tumor–stroma crosstalk. *Curr. Opin. Oncol.* **26,** 551–555 (2014).

159. Bock, C. & Lengauer, T. Managing drug resistance in cancer: lessons from HIV therapy. *Nat Rev Cancer* **12,** 494–501 (2012).

160. DeVita Jr., V. T., Eggermont, A. M., Hellman, S. & Kerr, D. J. Clinical cancer research: the past, present and the future. *Nat Rev Clin Oncol* **11,** 663–669 (2014).

161. Tchou, J. & Conejo-Garcia, J. *Targeting the Tumor Stroma as a Novel Treatment Strategy for Breast Cancer. Shifting from the Neoplastic Cell-Centric to a Stroma-Centric Paradigm*. *Advances in Pharmacology* **65,** (Elsevier Inc., 2012).

162. Minn, A. J. & Wherry, E. J. Combination Cancer Therapies with Immune Checkpoint Blockade: Convergence on Interferon Signaling. *Cell* **165,** 272–275 (2016).

163. Melero, I. *et al.* Evolving synergistic combinations of targeted immunotherapies to combat cancer. *Nat. Rev. Cancer* **15,** 457–72 (2015).

164. Smyth, M. J., Ngiow, S. F., Ribas, A. & Teng, M. W. L. Combination cancer immunotherapies tailored to the tumour microenvironment. *Nat. Rev. Clin. Oncol.* **13,** 1–16 (2015).

165. Moore, C., Kosgodage, U., Lange, S. & Inal, J. M. The emerging role of exosome and microvesicle- (EMV-) based cancer therapeutics and immunotherapy. *Int. J. Cancer* **0,** 1–9 (2017).

166. Kranz, L. M. *et al.* Systemic RNA delivery to dendritic cells exploits antiviral defence for cancer immunotherapy. *Nature* 1–16 (2016). doi:10.1038/nature18300

167. Thery, C. *et al.* Isolation and Characterization of Exosomes from Cell Culture Supernatants. *Curr. Protoc. Cell Biol.* **Chapter 3,** 1–29 (2006).

168. Rider, M. A., Hurwitz, S. N. & Meckes, D. G. ExtraPEG: A Polyethylene Glycol-Based Method for Enrichment of Extracellular Vesicles. *Sci. Rep.* **6,** 23978 (2016).

169. Jao, C. Y. & Salic, A. Exploring RNA transcription and turnover in vivo by using click chemistry. *Proc. Natl. Acad. Sci. U. S. A.* **105,** 15779–84 (2008).

170. Fuchs, G. *et al.* Simultaneous measurement of genome-wide transcription elongation speeds and rates of RNA polymerase II transition into active elongation with 4sUDRB-seq. *Nat. Protoc.* **10,** 605–618 (2015).

171. Ran, F. A. *et al.* Genome engineering using the CRISPR-Cas9 system. *Nat. Protoc.* **8,** 2281–308 (2013).

172. Martin, M. Cutadapt removes adapter sequences from high-throughput sequencing reads. *EMBnet.journal* **17,** 10–12 (2011).

173. Langmead, B. & Salzberg, S. L. Fast gapped-read alignment with Bowtie 2. *Nat Methods* **9,** 357–359 (2012).

174. Dobin, A. *et al.* STAR: Ultrafast universal RNA-seq aligner. *Bioinformatics* **29,** 15–21 (2013).

175. Harrow, J. *et al.* GENCODE: the reference human genome annotation for The ENCODE Project. *Genome Res.* **22,** 1760–74 (2012).

176. Liao, Y., Smyth, G. K. & Shi, W. The Subread aligner: Fast, accurate and scalable read mapping by seed-and-vote. *Nucleic Acids Res.* **41,** 108–125 (2013).

177. Love, M. I., Huber, W. & Anders, S. Moderated estimation of fold change and dispersion for RNA-seq data with DESeq2. *Genome Biol.* **15,** 550–571 (2014).

178. Avis, J. M., Conn, G. L. & Walker, S. C. Cis -Acting Ribozymes for the Production of RNA In Vitro Transcripts with Defined 5’ and 3’ Ends. *Methods Mol. Biol.* **941,** 83–97 (2012).